12-2015

Finite Element Analysis of the Effect of Acoustic Wavelength to Hierarchical Side Length and Facet Area for Elastic Scattering from Polygonal Rings and Geodesic Spheres

Ankit Kumar
Clemson University

Follow this and additional works at: https://tigerprints.clemson.edu/all_theses

FINITE ELEMENT ANALYSIS OF THE EFFECT OF ACOUSTIC WAVELENGTH TO HIERARCHICAL SIDE LENGTH AND FACET AREA FOR ELASTIC SCATTERING FROM POLYGONAL RINGS AND GEODESIC SPHERES

A Thesis
Presented to
the Graduate School of
Clemson University

In Partial Fulfillment
of the Requirements for the Degree
Master of Science
Mechanical Engineering

---

by
Ankit Kumar
December 2015

Accepted by:
Dr. Lonny Thompson, Committee Chair
Dr. Gang Li
Dr. Joshua Summers

ABSTRACT

In this work, the frequency response from two-dimensional polygon and three-dimensional geodesic spheres is numerically simulated using a coupled structural acoustic finite element model. The model is composed of a submerged thin-walled elastic shell structure surrounded by an infinite acoustic air domain. Infinite elements are used to simulate the far-field acoustic radiation condition. Results for the faceted polygon and geodesic sphere are compared to their canonical counterpart viz. a circle/ring and a spherical shell. A unique feature of this study is to compare results as the number of facets in the polygon or geodesic is increased, such that the surface area converges in the limit of a large number of facet sides approaching the geometry of a circle or sphere. In this work the ratio of acoustic wavelength to the local geometric parameter of edge length in 2-D, and facet area in 3-D is proposed and varied to quantify the comparison between the faceted shapes with that of the corresponding reference circle or sphere. A threshold ratio is proposed, up to which scattering response of a polygonal/geodesic spherical scatterer matches the scattering response of a circle/sphere which has the same diameter as the circumscribing circle/sphere of the polygon/geodesic sphere. This ratio is an approximation and can be considered as a guide rule for design. Conversely, this ratio can be used for the inverse scattering problem, where from a known scattering response, the faceted geometry can be predicted without prior knowledge.

The geodesic sphere was invented by Buckminster Fuller in the early 1950's, has been of interest in architecture due to the larger open interior spaces which can be constructed. Of particular interest in this work is the hierarchical geometric structure of the

geodesic sphere which increasingly approximates a spherical surface as the hierarchy (degree) increases. The geodesic sphere has been modelled by taking an icosahedron and projecting the triangular faces onto a surface of the sphere using vector geometry. The scattering response of elastic structures in the mid-frequency resonance band depends strongly on the total mass. For comparisons, the natural frequency of the hierarchical geometries generated in 2-D and 3-D, are designed to have the same total mass. Using this approach, differences in natural frequency and scattering response are driven primarily by changes in overall stiffness and stiffness distribution, and to a lesser degree, by changes in mass distribution. To give a wide range of frequency response, natural vibration frequencies for the different elastic shells have been extracted up to 3000 Hz corresponding to the nondimensional frequency $ka = 55$, where k is the wavenumber defined by the circular frequency over the acoustic wave speed (speed of sound in air), and a is the diameter of the circle/shell which circumscribes the scatterer. Convergence with the natural frequencies of ring/sphere is observed as the hierarchy in polygons (number of sides) and the geodesic sphere (degree) increases.

The target strength is calculated at the important front and back locations on the surface of the elastic scatterer subject to an incoming plane acoustic wave along the major axis aligned with the geometry. More frequency data points near the natural frequencies are used to provide increased resolution needed to capture the peak amplitudes in the response at resonance. Target strength at the same location, calculated for the circle/spherical scatterer is compared and quantified by the ratio of wavelength to facet

dimension. Scattering from rigid bodies has been studied to validate the elastic scattering

response in air.

DEDICATION

I dedicate this thesis to my parents Dr. J.K. Mitra and Mrs. Ujjwala Mitra and my sister Dr.

Ruchi Mitra. This thesis wouldn't have been possible without their support and love.

ACKNOWLEDGEMENT

I would like to thank my advisory committee chair Dr. Lonny Thompson for his invaluable

inputs. It was because of his expert opinions and inputs, this research was made possible. I

have learnt a lot from him and I am extremely grateful for the knowledge he has imparted

onto me. I would also like to thank my advisory committee members Dr. Joshua Summers

and Dr. Gang Li for their support and advice during my time in Clemson.

Last but not the least, I would like to thank all my friends who have supported me and have

been there for me.

TABLE OF CONTENTS

Table of Contents (Continued)   Page

Table of Contents (Continued)   Page

LIST OF FIGURES

List of Figures (Continued)   Page

List of Tables

List of Tables (Continued)   Page

CHAPTER ONE

1   INTRODUCTION

The idea of comparing a polygon domain to a circular domain came from the "polygon-circle paradox". It is well known, that under uniform transverse pressure, flexure of a simply supported n-sided polygon plate inscribed in a circle of radius, a starts to diverge from a simply supported circular plate of the same radius when n tends to infinity. [1]–[3]. H. Uberall predicted the sound-induced resonances of submerged elastic objects (sphere and cylinder) using the phase matching of surface waves, in agreement with the experimental results[4]. Cureton et al related the eigenvalue problem for the Laplacian on regular polygons, with either Dirichlet or Neumann boundary conditions, to the unit circle by conformal mapping. The problem was then equivalent to a weighted eigenvalue problem on the circle with same boundary conditions. [5]

In this thesis, acoustic scattering characteristics of n-sided 2-D polygons are compared with a circle in a similar way. Later comparison of a 3-D faceted model, the geodesic sphere is compared with a sphere. In this case, scattering characteristics are expected to follow the intuition and converge as the model approximates a circle/sphere. It would be of interest to find a parameter which can relate the side/facet length to the wavelength, which can help to predict the scattering characteristics of the faceted geometries. Conversely, inverse scattering can be done with the help of this ratio too. Inverse scattering is reconstruction of a shape from a knowledge of scattered field patterns. Nasit et al [6] studied how the functional representation of the unknown shape affects their inversion algorithm and sample reconstruction of polygons and non-convex profiles. Ivan

et al examined the problem of estimating the geometry of a room from its room impulse response. [7]. Colton et.al developed an inversion scheme for two-dimensional inverse scattering problems in the resonance region which does not use nonlinear optimization methods and is relatively independent of the geometry and physical properties of the scatterer. [8]

1.1   Previous work done in acoustic scattering from 2-D polygons

Researchers have shown interest to study the scattering and other acoustic characteristics from a 2-D convex polygon. Xiaolin et al. compared the sound-absorption capability of 2-D cellular solids. A cellular structure was divided into a tube of a general N-sided polygonal cross section and sound absorption capability of it was studied. Then sound-absorption qualities of those tubes were studied as a whole in cellular structures. They studied the effects of cell shape, shell size and its spatial variation, sample thickness, and cavity depth on sound absorption. [9]. Fawcett presented the time signal scattered from a triangular rigid facet by means of the Kirchhoff/diffraction method. The solutions had some singularity problem for some incident/scattered conditions [10], [11]. Later, Lee et al. using the Kirchoff method, came up with a general acoustic impulse response for a polygon facet which can be used for modelling the high frequency transient scattering from an underwater target or a rough surface, when they are discretized into multiple polygons. [11] A study on the low frequency acoustic scattering of a cube was done to understand scattering from sediment in marine environments [12]. Scattering characteristics of a cube at different orientations were studied and when these are averaged out, the scattering characteristic behaves like a sphere. Later, the average projected area of different polyhedra

2

like icosahedron, dodecahedron, octahedron, cube and tetrahedron were compared to that of a sphere of the same volume. For the low frequency range, the scattered amplitude is expected to be proportional to the average projected area.

For Standard BEM and FEA, degrees of freedom to achieve accuracy increase linearly with the frequency of the incident wave [13][14]. Chandler-Wilde et al. studied the scattering of a time harmonic acoustic incident plane wave by a sound convex polygons and proposed a novel Galerkin Boundary Element method in which the degrees of freedom required to achieve a prescribed level of accuracy grow logarithmically as the frequency of the incident wave increases. This method uses an approximation space consisting of the products of plane waves with piecewise polynomials supported on a graded mesh, with smaller elements closer to the corners of the polygon as the waves diffracted by the corners become more localized near corners especially at higher frequencies [10]. Schmidtke presented a multiparametric gradient method for the iterative solution of systems of linear equations [15].

Research has also been done in marine field on Target detection and classification from exposed rocks, [16] detection and classification of Benthic and planktonic shelled animals for biological and ecological applications [17]. Properties of sound signals by models of Arctic pack ice were studied in [18].

In this thesis, faceted geometries both in 2-D and 3-D which are circumscribed into a circular ring and a spherical shell respectively, are compared with their counterpart canonical shapes viz. ring for 2-D and spherical shell for 3-D. A ratio of wavelength to side/facet length is then proposed which can give a threshold up to which a faceted structure

can have a scattering behaviour as its counterpart canonical structure. An inverse scattering can also be done using that same ratio. For a known scattering behaviour, the dimensions of the facet can be approximated.

1.2   Geodesic Spheres

Figure 1-1 The Montréal Biosphère, formerly the American Pavilion of Expo 67, by R. Buckminster Fuller, on Île Sainte-Hélène, Montreal, Quebec [19]

Geodesic Spheres are R. Buckminster Fuller's trademark. In architecture, the Sphere aimed at maximum efficiency considering the volume to weight, use of materials to useful surface, and assembly time to mobility. As sociocultural alternatives to typical rectangular architecture, the Spheres crystallized society's dreams of a life liberated from constraints. [20]

Ford Rotunda, which was the biggest tourist attraction in the US in 1950's [13], took only 5 weeks to construct. It had 6 different lengths of members and holes were pre punched to a tolerance of $1/1000^{th}$ of an inch. It was mostly made up of triangles combined to form an octahedral – tetrahedral repeated system, which created an open faceted spherical Sphere shape [14]. It was destroyed by fire in 1962. [13]. The Spheres were used as a shelter for helicopters for US Marine Corps in 1959. The lightweight construction concept enabled the Spheres to be flown across by helicopters.

Geodesic Spheres being durable and inexpensive, can be found in places all over the world. In Antarctica they have stood for decades and resisted winds of around 200 miles per hour. Spheres have also withstood hurricanes, earthquakes, and performed better than rectangle-based structures. [21]

In this thesis for 3-D geometries, geodesic Spheres of different degrees are used. These Spheres best approximate a sphere and can effectively give a measure of the difference in scattering response due to the presence of the facets. The construction of geodesic Spheres is discussed in Chapter 2.

1.3   Motivation for present work
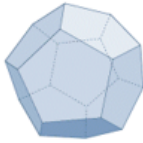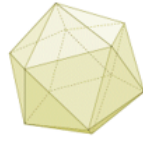
As discussed in Section 1.1, work has been done in scattering from 2-D polygons and facets. Fawcett and Lee et al. found analytical forms of acoustic impulse response from a triangle and later a general polygon [6][7]. New numerical methods have also been proposed Chandler-Wilde et al to reduce the computational time and get more accuracy. In the literature review, no such parameter study has been done, as presented in this thesis. This is a new idea, which can be built upon. As the scattering behaviour of a scatterer

depends upon the wavelength/frequency of the incident wave and the geometry of the scatterer, the ratio of wavelength to some geometrical parameter (facet/side length in this case), seems a valid parameter to compare faceted geometries with their respective canonical counterparts.

For 3-D geometries, the scattering response studies are scarce to find. Chinnery et.al. performed experimental scattering analysis from a cube and gave theoretical predictions of scattering response different polyhedral like icosahedron, dodecahedron, octahedron, hexahedron (cube) and tetrahedron compared to a sphere of the same volume. These solids are known as platonic solids. A platonic solid is a regular, convex polyhedron. It is constructed by congruent regular polygonal faces with the same number of faces meeting at each vertex. [13]. Table 1-1 presents the details of the five platonic solids. These solids have been named after the number of faces they have.

Table 1-1 The platonic solids

Name	Geometry	No. of vertices	No. of edges	No. of faces
Tetrahedron		4	6	4
Hexahedron (Cube)		8	12	6

Name	Geometry	No. of vertices	No. of edges	No. of faces
Octahedron		6	12	8
Dodecahedron		20	30	12
Icosahedron		12	30	20

The tetrahedron, octahedron and the icosahedron have equilateral triangular faces and are approximations to the sphere. The icosahedron fits a sphere the best and has hence been used to model the geodesic sphere.

2-D regular polygons with number of sides n, have been compared to their circumscribing circle under static pressure load subjected to specific boundary conditions, [1] and effects have been studied when n tends to infinity. No such study has been performed in 3-D. The geodesic sphere can be considered analogous to a 2-D regular polygon in this case. The geodesic Sphere can effectively approximate its circumscribing sphere when the degree of the sphere tends to infinity.

In this thesis, faceted geometries both in 2-D and 3-D which are circumscribed into a circular ring and a spherical shell respectively, are compared with their counterpart

canonical shapes viz. ring for 2-D and spherical shell for 3-D. A ratio of wavelength to facet/side length is then proposed which can give a threshold up to which a faceted structure can have a scattering behaviour as its counterpart canonical structure. An inverse scattering can also be done using that same ratio. For a known scattering behaviour, the dimensions of the facet can be approximated.

As the waves diffracted by the corners become more localized near corners especially at higher frequencies, which needs special handling of mesh densities near the corners and edges (in 3-D), a frequency range 1-3000 Hz has been selected ($ka < 55$), where a is the diameter of the circumscribing circle/sphere and $k = \omega / c$ is the wavenumber. ω is the angular frequency and c is the speed of sound in the medium. The parameter ka helps to relate the overall dimension of the elastic sphere to the wavelength of interest as $k = \omega / c = 2\pi / \lambda$. $ka = 55$ corresponds to the smallest wavelength of interest, which gives $\lambda = 0.11423a$. Hence in this case, shortest wavelength is around $1/10^{th}$ of the overall diameter (a) of the circle/sphere.

1.4   Thesis Objectives

1) Develop and compare the structural vibrations and acoustic properties of the geometries in 2-D and 3-D by calculating their natural frequency and exterior scattering response in air.

2) Develop parameters to compare the acoustic properties of the 2D-polygons and the geodesic Spheres with that of a circle and spherical shell respectively. Normalize this parameter such that it relates the frequency to the desired facet variable and is

8

independent of the overall dimensions of the structure. Normalize the frequency range of interest to relate the wavelength to the scatterer size.

3) Develop the 2-D and 3-D geometries for numerical analysis. The 2-D geometry is a straight forward regular polygon. In case of 3-D, use vector geometry to calculate the coordinates of the vertices and then model the Sphere structure.

4) Develop a Finite Element Model in ABAQUS to extract the natural frequency of the structures. Later, use these frequencies and perform structural-acoustic coupling analysis with infinite boundary condition. Perform rigid body scattering to validate the results.

5) Compute the Steady-State dynamic response of the structures to the acoustic incident wave and obtain the target strength plots for 2-D and 3-D.

6) Formulate a ratio of wavelength to edge/facet length and compare the plots obtained from different geometries with a 2D ring/infinite circular cylinder and a 3-D spherical shell.

1.5 Thesis Outline

Chapter 1 gives an introduction of the thesis. The Literature review is done in the first part of this chapter. Then, history of the Geodesic Sphere is discussed. The motivation and objectives are then presented.

Chapter 2 presents details of the construction of geometries under investigation. First construction of the 2-D finite element domain is discussed. The geometrical parameters are calculated and the dimensions are presented. Then the construction of the acoustic domain in 2-D is discussed. In the next section, the 3-D Finite element domain is

discussed. The coordinates of triangular vertices are derived by using vector geometry for geodesic Spheres is presented. The parameters are calculated and the dimensions for the 3-D geometry is presented.

Chapter 3 presents the theory and equations behind the Natural Frequency. Then Natural Frequency of the structures are extracted in ABAQUS. The thickness of the geometries are varied so that the mass is constant. The frequency range of interest is 1-3000 Hz. The natural frequencies of the geometries are then compared. These frequencies are then later used in acoustic scattering response.

Chapter 4 presents the theory and equations relating to acoustics. Then, a finite element formulation for the structural acoustic coupling is presented. The 2-D elastic body scattering response calculation is done in ABAQUS. A step by step guide is presented for setting up the model. Target strength vs ka plots for all the 2D geometries are then plotted, and a parameter study is done comparing the 2D polygons with the circular ring/infinite cylinder. A similar study is done for the 3-D geometries later. A step by step guide for setting up the model in ABAQUS is also presented. In the last section, scattering response from rigid body is calculated in ABAQUS for 2-D and 3-D geometries. The rigid body scattering is done to compare the results obtained from the elastic body scattering.

Chapter 5 The conclusions obtained from the results and the possible future works which can be derived from this work has been discussed.

CHAPTER TWO

2   GEOMETRY MODELLING OF FINITE ELEMENT DOMAINS

The acoustic scattering response due to the effect of facets is studied. Both 2-D and 3-D models have been investigated in comparison to that of a thin-walled circular cylindrical (2D) and a spherical shell (3-D).

2.1   2D Finite Element Domain

The 2D finite element domain has three parts, the structural domain, the acoustic domain and the infinite boundary.

2.1.1   The structural domain

In case of 2-D, the thin walled cylinders, having cross sections as regular polygons are modelled having an exterior air domain. These polygons can be circumscribed by a circle of radius r. Three cases have been investigated against a circular cylinder. These cylinders with regular polygonal cross section are identified by the number of sides of the polygon or angle 'α', which is subtended by the sides of sectional polygon at the centre of the circumcircle inscribing the polygon (Figure 2-1). The side lengths of the polygon L, are given by the cosine law of trigonometry as, $L = r\sqrt{2 - 2\cos\alpha}$. The number of sides n = $360/\alpha$ (where α is in degrees).
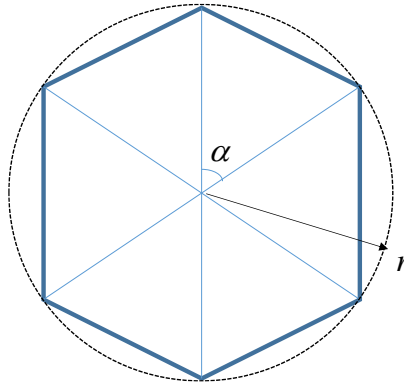
Figure 2-1 Angle subtended at the circumcentre

In the thesis, the 2D polygons are referred to as the angle they subtend at the centre (α) cases investigated are 45^0, 30^0, 15^0 and Ring as shown in figures below
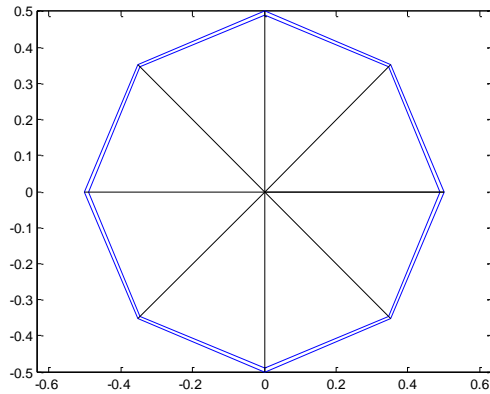
Figure 2-2 n=8 (45^0)

Figure 2-3 n = 12 (30^0)

12
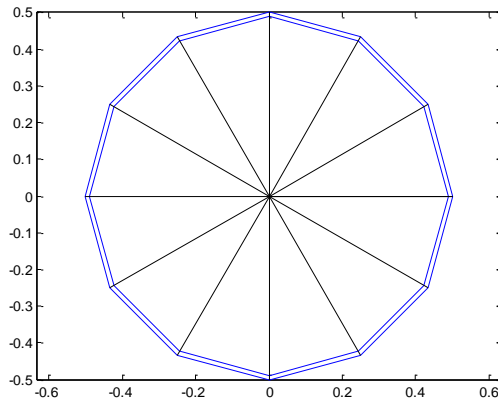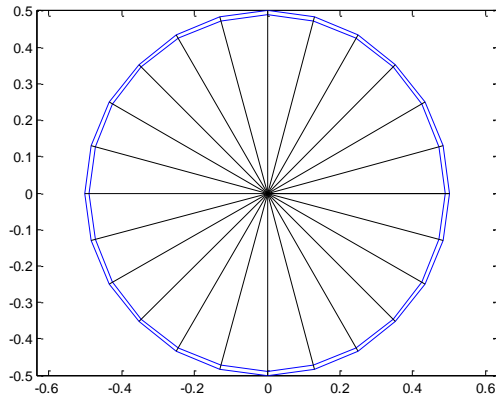
Figure 2-4 n=24 (15^0)
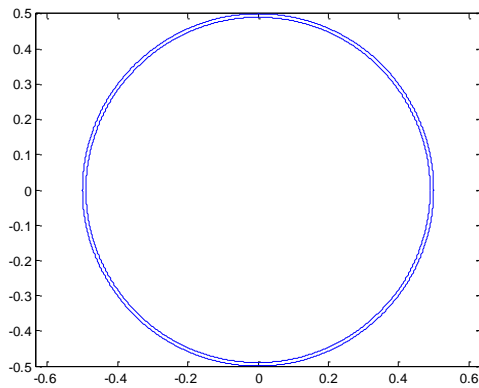
Figure 2-5 Ring

The regular polygonal sections are inscribed in a circle of diameter 1m and are modelled using the sketch feature of the part module in ABAQUS. Note that as the number of sides *n,* of the polygon increases, its shape starts to resemble a circle. Thus an *n*-sided polygon starts to approximate a circle, when $\alpha \to 0$ and $n \to \infty$. Table 2-1 gives a comparison of the outer perimeter of the polygons. The difference in the perimeter decreases as *n* increases. This further helps to quantify the convergence geometrically.

13

Table 2-1 Comparison of outer perimeter of the polygons with the circumscribing circle

Polygon	Outer Perimeter of the Polygons (m)	Outer Perimeter of the Circle (m)	% Difference
45^0 ($n = 8$)	3.061467459	3.141592654	2.5504642
30^0 ($n = 12$)	3.105828541	3.141592654	1.1384071
15^0 ($n = 24$)	3.132628613	3.141592654	0.2853343

2.1.2   Wall thickness Calculation

In case of the elastic body scattering, the total mass of the elastic scatterer (the polygonal pipes) and the circular cylinder is kept constant, with stiffness being varied. The total mass of the geometries are equal, but the mass distribution in the geometries are not. The characteristics are controlled by stiffness primarily but the change in the distribution of mass also plays a role. The total mass is kept constant by varying the thickness of the polygonal sections and keeping the diameter of the circumscribing circle and the depth constant.

The required condition is

$$M_{cir} = M_{poly}, \quad \Rightarrow \rho A_{cir} d = \rho A_{poly} d \tag{2.1}$$

Where M_{cir} is the mass of the circular cylinder and M_{poly} is the mass of the polygonal cylinder. The densities of the material for both of them is ρ and the depth of the cylinder d is 1m. A_{cir} and A_{poly} are the cross sectional areas of the circular and polygonal cylinders respectively.

Since ρ and d are the same for both the geometries, from (2.2), we have

$$A_{cir} = A_{poly} \tag{2.2}$$

14

Where, $A_{cir} = L_{cir} t_{cir}$, and (2.3)

$L_{cir} = 2\pi r$ is the circumference of the neutral fibre of the circular beam section an

t_{cir} is the thickness of the section.
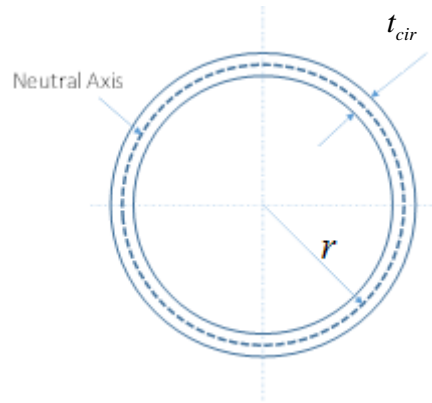
Figure 2-6 Circular Section of the cylinder

Thus (2.3) can be written as

$$A_{cir} = (2\pi r)t_{cir}$$ (2.4)

For the polygonal section,

$$A_{poly} = L_{poly} t_{poly}$$ (2.5)

Where, $L_{poly} = nL$ is the perimeter of the neutral fibre of the polygon beam and t_{poly} is the

thickness. (Figure 2-7)
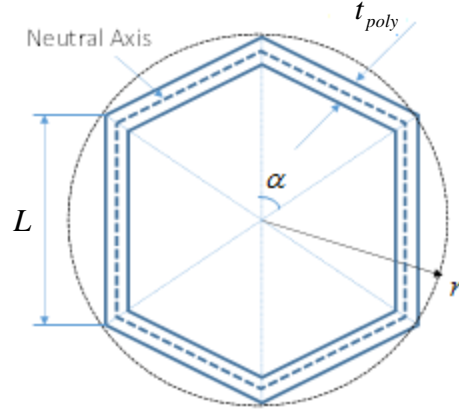
Figure 2-7 Polygonal Section of the cylinder

Hence the surface area of the polygon (equation (2.5)), can be written as

$$A_{poly} = nLt_{poly} \tag{2.6}$$

Where, $n = 360/\alpha$ gives the number of sides in the polygon, $L = r\sqrt{2-2\cos\alpha}$ is the

side length, and t_{poly} is the thickness of the section.

From equation (2.2), surface area of the circle is equal to the surface area of the

polygon. Surface area of the circle is given by (2.4) and surface area of the polygon is given

by (2.6). Hence using (2.4) and (2.6) and substituting in (2.2),

$$(2\pi r)\, t_{cir} = nLt_{poly},$$

$$\Rightarrow t_{poly} = \frac{(2\pi r)\, t_{cir}\alpha}{360L} \tag{2.7}$$

$$\Rightarrow \frac{t_{poly}}{t_{cir}} = \left(\frac{2\pi}{360}\right)\alpha\left(\frac{r}{L}\right) \Rightarrow \frac{\theta}{\sqrt{2-2\cos\theta}}$$

Where, θ is the angle subtended at the centre in radians. (2.7) shows a very

important relation between the wall thickness ratio of polygon to the circle. It can be seen

16

that this ratio is independent of the dimensions if the 2-D geometries and depends only on the angle subtended at the centre θ and the number of sides $n = 2\pi / \theta$.

In this work, a thin shell model is used with $t_{cir} = 10$mm for a circle of diameter $a = $ 1m. Thus $a / t_{cir} = 100$.

We can assume the side lengths of the polygon as a Euler-Bernoulli Beam, as the smallest side length corresponds to 15, which is 0.13 m and thickness of the cross section is 0.0100286m

Hence

$$\frac{L}{t_{poly}} = \frac{0.13}{0.0100286} = 12.96 > 10$$

Hence Euler-Bernoulli beam theory can be assumed. Table 2-2 gives the aspect ratio of all the geometries under investigation and the ratios justify the assumption that these geometries are Euler-Bernoulli beams.

Table 2-2 Aspect ratio of the 2-D polygons to justify the use of Euler-Bernoulli beam theory

α	L (m)	t_{poly} (m)	L / t_{poly}
45^0 ($n = 8$)	3.826834323650898e-01	1.026172152977031e-02	3.729232285780567e+01
30^0 ($n = 12$)	2.588190451025207e-01	1.011515159927463e-02	2.558726308373677e+01
15^0 ($n = 24$)	1.305261922200516e-01	1.002861507511791e-02	1.301537562688005e+01

2.1.3 Outer air domain

The outer air domain is modelled with a diameter of 1.5 meter, with the boundary truncated by acoustic infinite elements. (Figure 2-8)
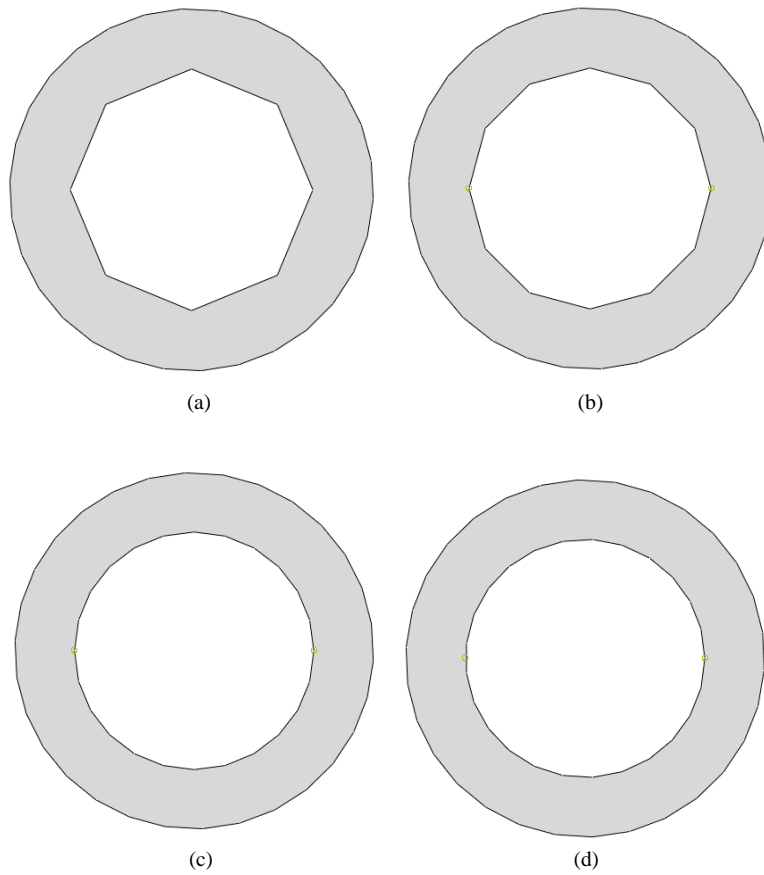
Figure 2-8 2-D outer air domain for (a) 45^0, (b) 30^0, (c) 15^0, (d) Ring

2.2   3D Finite Element Domain

To investigate the effect of facets at different orientations in space to a plane incident wave, a geodesic Sphere is modelled and is compared to the acoustic scattering of a sphere. The diameter of the sphere that encloses the geodesic Sphere is 1m.

The features of the geodesic are identified by the following,

1. Triangle face

    The face of an icosahedron (Figure 2-10). The icosahedron is a polyhedron made up of 20 equilateral triangular faces, has 12 vertices and 30 edges.

18

2. Sub-Triangle

The triangle face is divided in smaller triangles to construct the geodesic Sphere.

These triangles are referred to as sub-triangles. (Figure 2-9)
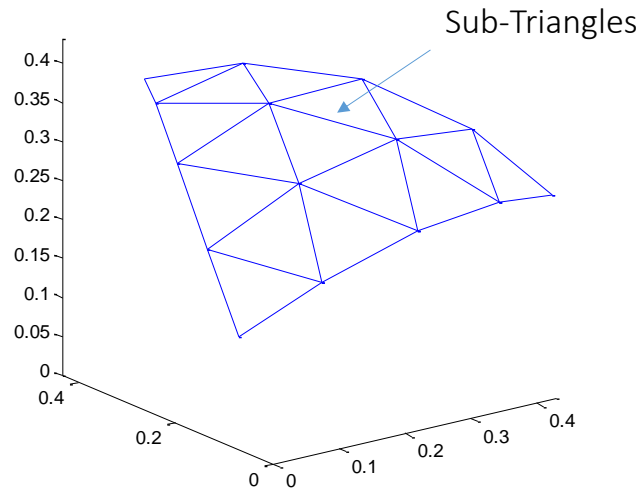
Figure 2-9 Triangular Surface generated by subdividing the triangle face of an icosahedron into sub-triangles and then projecting the vertices onto the surface of a sphere.

3. Triangular Surface

After the triangle face is divided into sub-triangles, the vertices are projected onto a sphere. This generates a triangular surface (Figure 2-9) which is then assembled, to model a geodesic sphere.

2.2.1   The geodesic sphere

The Sphere usually consists of equilateral triangular faces of an icosahedron (Figure 2-10), which then start to mimic the curvature of a sphere by coordinate transformation using vector geometry.

19
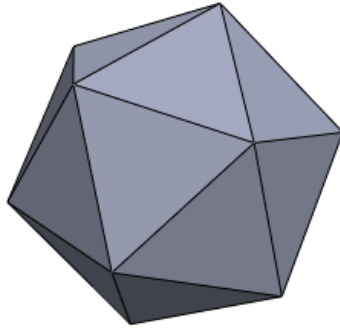
Figure 2-10 Icosahedron, having 20 equilateral triangle faces, 12 vertices and 20 edges

A sphere encloses maximum volume as compared to its surface area, hence giving the maximum volume at minimum material cost. To make spherical shapes directly by machining is an expensive option as most of the construction materials are straight or flat pieces. A triangle is a polygon which uses minimum number of struts, and even if the joints are not, structures made out of a triangle can be made relatively rigid.

Hence a geodesic Sphere is made out of triangles with nearly equal strut lengths, which makes uniform distribution of stresses along the struts.

The solids which consist of equilateral triangles inclined at equal angles to each other are the tetrahedron, the octahedron and the icosahedron. These are also known as platonic solids and are approximations to a sphere[22]. The icosahedron fits a sphere best and hence it is used to make a geodesic sphere.

When the Sphere is big in shape, single struts of an icosahedron will not be strong enough, hence the triangular facets are divided into a cluster of smaller triangles depending upon the degree of the geodesic Sphere. Degree is the number of subdivisions per edge of the triangle face. Figure 2-11 shows the division of the icosahedron triangular face into smaller triangles. The number of divisions determine the degree of the Sphere.

$$N = D^2$$

Where, N is the number of sub-divisions and D is the degree of the geodesic.

| Degree II (N = 4) | Degree III (N = 9) | Degree IV (N = 16) |
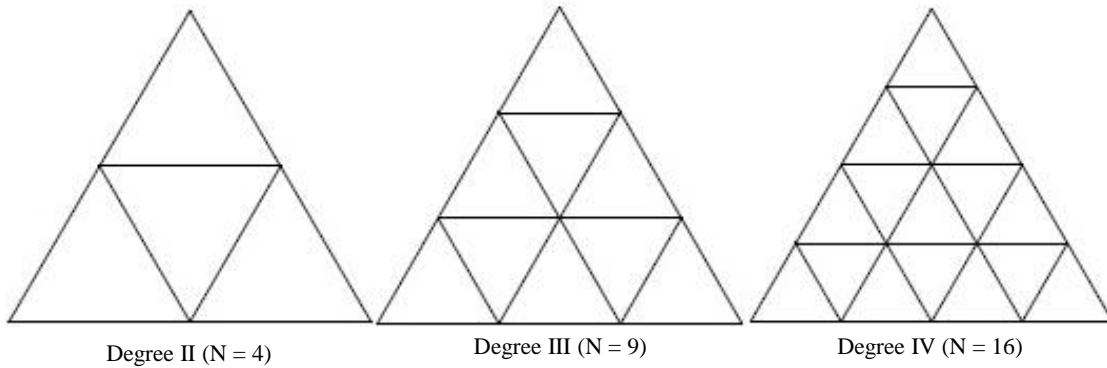
Figure 2-11 Division of the triangle face

The triangle face are divided into perfect square numbers as shown in the Figure 2-11. The vertex of the sub-divided triangles are then projected onto the surface of the enclosing sphere.

After projection, the resulting triangular surfaces of the reference icosahedron are assembled to form the geodesic sphere. The cases investigated are Degree II, Degree III, and Degree IV and a Spherical Shell. (Figure 2-12)

(a)

(b)

(c)

22

(d)
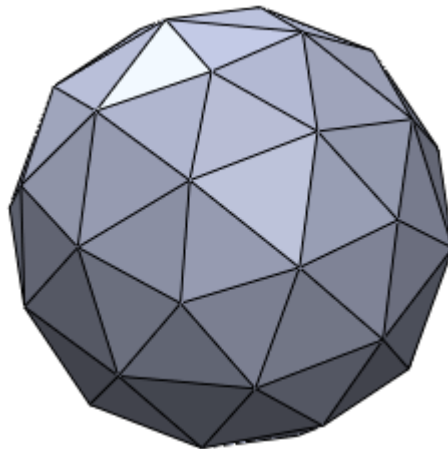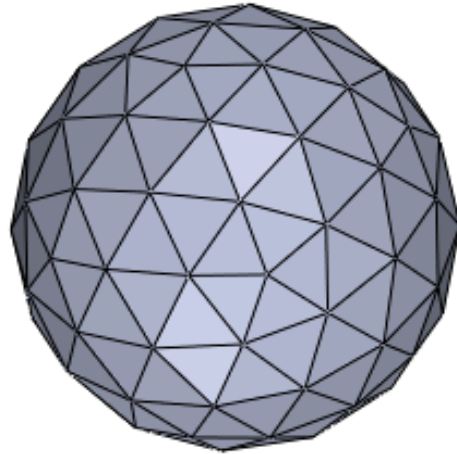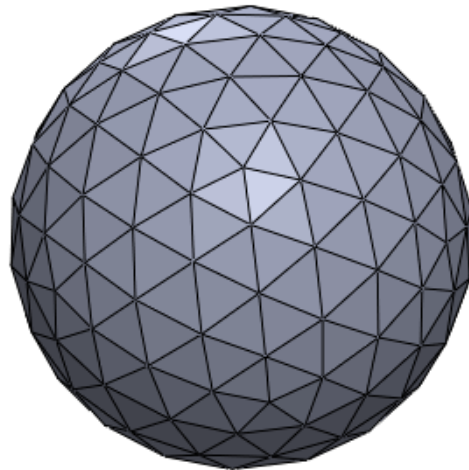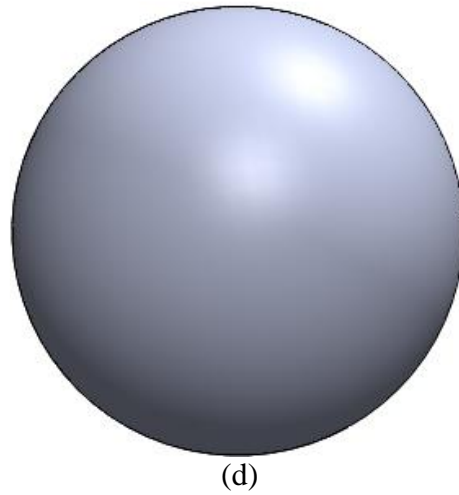
Figure 2-12 3-D Models in SOLIDWORKS (a) Degree II, (b) Degree III, (c) Degree IV, (d) Spherical Shell

Note that the Degree IV geodesic best approximates a sphere amongst the three geodesic degrees considered. Table 2-3 shows the comparison of the surface area of the Geodesic spheres and the spherical shell under investigation. As the degree of the geodesic increases, the difference in the surface area decreases. Thus, the surface area of a geodesic sphere starts approaching the surface area of a sphere enclosing it, as the degree of the geodesic increases. This comparison of the geodesic spheres and the sphere enclosing it, further quantifies the convergence geometrically.

Table 2-3 Comparison of surface areas of the Geodesic Spheres with a Sphere

Geodesic Degree	Surface area (m^2)	Sphere Surface area (m^2)	% Difference
Degree II	2.916482848	3.1415926	7.165466078
Degree III	3.037660542	3.1415926	3.308260200
Degree IV	3.082265697	3.1415926	1.888434003

2.2.1.1   Coordinates of the vertices of the sub-triangles

The radius of a sphere centred at origin enclosing the icosahedron can be calculated by

$$r = \sqrt{x_i^2 + y_i^2 + z_i^2} \qquad (2.8)$$

Where x_i, y_i, z_i are the coordinates of the vertices of the icosahedron. Note that the vertices of the icosahedron lie on the surface of the sphere.

Three rectangles are mutually perpendicular to each other can be inscribed into an icosahedron (Figure 2-13). The rectangles are golden rectangles, whose sides are in the aspect ratio $1:\phi$. Where $\phi = 1 + \sqrt{5}/2$, is the golden ratio. Its approximate value thus being 1.618.
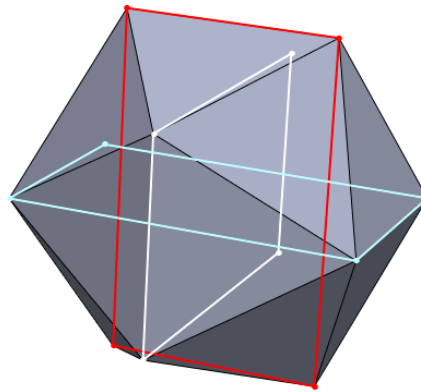
Figure 2-13 Golden Rectangles inscribed in an icosahedron

A set of coordinates given by Table 2-4 can be selected for an icosahedron centred at origin. As the vertices of the three mutually perpendicular golden rectangles lie on the vertices of the icosahedron (Figure 2-13), the coordinates of the vertices of the rectangle are

24

the coordinates of the vertices of the icosahedron. Thus for rectangles having the aspect ratio $1:\phi$, a convenient set of coordinates can be given by [16] Table 2-4.

Table 2-4 Coordinates of the vertices of an icosahedron

Vertices	X	Y	Z
A	0	1	ϕ
B	0	-1	ϕ
C	0	-1	$-\phi$
D	0	1	$-\phi$
E	ϕ	0	1
F	$-\phi$	0	1
G	$-\phi$	0	-1
H	ϕ	0	-1
I	1	ϕ	0
J	-1	ϕ	0
K	-1	$-\phi$	0
L	1	$-\phi$	0

With the set of coordinates, an icosahedron can be constructed with the radius of circumscribing sphere being (from(2.8)) $r = \sqrt{0^2 + 1^2 + \phi^2} = 1.902$. The coordinates are thus calculated with the normalized sphere having radius 1.902, and later scaled down to the required radius of the sphere.

Figure 2-14 shows the coordinates of the vertices of the sub-triangles for a typical triangle face of an icosahedron. Note that on edge AB, the coordinates of C is zero; on edge BC, coordinates of A is zero and on edge AC, the coordinates of B is zero.
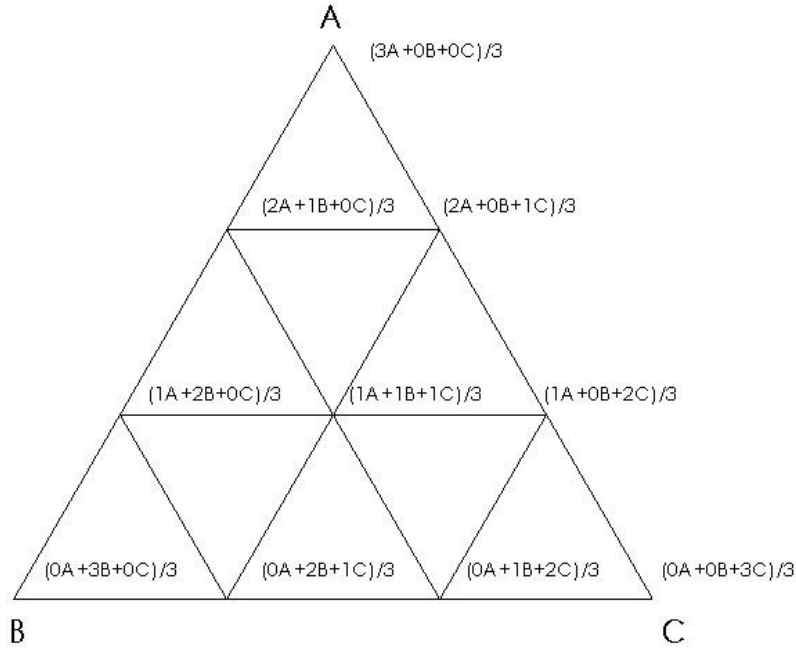
Figure 2-14 Vertices of the sub-triangles

For degree III geodesic, assume the coordinates,

$$A = (x_A, y_A, z_A), \ B = (x_B, y_B, z_B), \ C = (x_C, y_C, z_C)$$

Then, the coordinates from the centre point $(1A + 1B + 1C)/3$ can be calculated as

$$x = (1x_A + 1x_B + 1x_C)/3$$
$$y = (1y_A + 1y_B + 1y_C)/3$$
$$z = (1z_A + 1z_B + 1z_C)/3$$

Hence, once these coordinates are obtained, we now can project these points onto the surface of the sphere of a required radius *r*. In this case, the geodesic spheres are enclosed in a sphere of radius *r* = *a*/2 = 0.5m. Hence,

The position vector for the normalized coordinates of the geodesic sphere is given by

$$\vec{v}_i = x_i \hat{i} + y_i \hat{j} + z_i \hat{k}$$

26

The radial direction from the origin to the coordinates of the sub-triangles is given by the unit vector $\hat{n}$ as

$$\hat{n}_i = \frac{\vec{v}_i}{|\vec{v}_i|}$$

The coordinates of the geodesic sphere can be obtained by rescaling as $v_i = r\hat{n}_i$, for a sphere of radius $r = 0.5$m.

Table 2-5 shows the coordinates of the vertices of the sub-triangles in a degree IV Geodesic calculated. A precision in the coordinates was used to ensure that there is no imprecision in geometry.

Table 2-5 Coordinates of the vertices sub-triangles in space (Degree IV)

Sl.	X	Y	Z
1	0	2.62865556059566E-01	4.25325404176019E-01
2	7.38104522110815E-02	3.40859177035774E-01	3.58283461207589E-01
3	1.54508497187473E-01	4.04508497187473E-01	2.50000000000000E-01
4	2.21431356633244E-01	4.32093913418670E-01	1.19427820402529E-01
5	2.62865556059566E-01	4.25325404176019E-01	0
6	1.19427820402529E-01	2.21431356633244E-01	4.32093913418671E-01
7	2.12662702088010E-01	2.93892626146236E-01	3.44095480117793E-01
8	2.93892626146236E-01	3.44095480117793E-01	2.12662702088010E-01
9	3.40859177035774E-01	3.58283461207589E-01	7.38104522110815E-02
10	2.50000000000000E-01	1.54508497187473E-01	4.04508497187473E-01
11	3.44095480117793E-01	2.12662702088010E-01	2.93892626146236E-01
12	4.04508497187473E-01	2.50000000000000E-01	1.54508497187473E-01
13	3.58283461207589E-01	7.38104522110815E-02	3.40859177035774E-01
14	4.32093913418670E-01	1.19427820402529E-01	2.21431356633244E-01
15	4.25325404176019E-01	0	2.62865556059566E-01

Note that in degree IV, N = 16 and the number of vertices is 15.
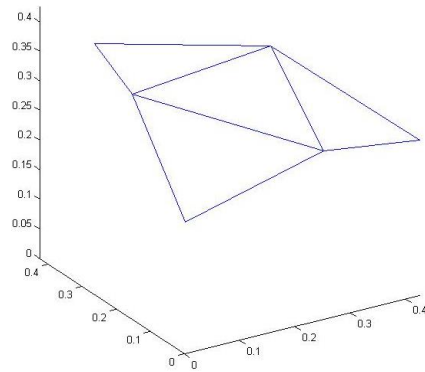
(a)
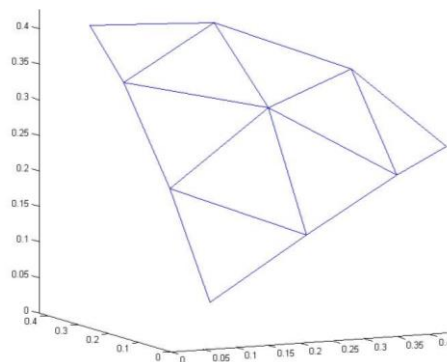
(b)
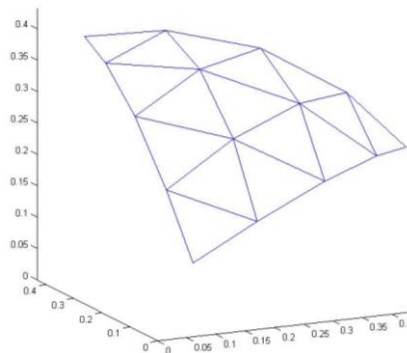
(c)

Figure 2-15 Triangular Surface plots generated in MATLAB (a) Degree II (4 Sub-Triangles), (b) Degree III (9 Sub-Triangles), (c) Degree IV (16 Sub-Triangles)

Figure 2-15 shows the triangular surface generated in MATLAB. It is noteworthy to see that as the degree of geodesic increases, the resolution becomes better as sub triangles increase. Thus a higher degree geodesic fits better on a spherical surface circumscribing it.

Just to make this point more clear, Figure 2-16 shows $D = 50$ geodesic which has $50^2=$ 2500 sub triangles.
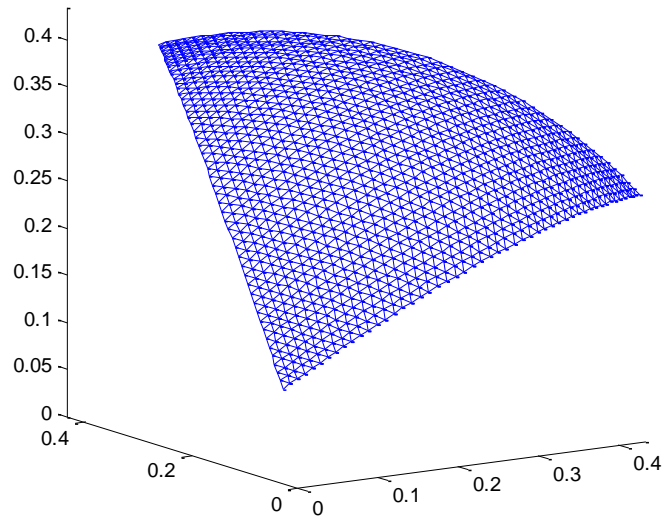
Figure 2-16 Triangular Surface of a Degree 50 Geodesic Sphere.

2.2.1.2   CAD model of the Geodesic Sphere in SOLIDWORKS

Once the coordinates of a triangular curved surface of a geodesic Sphere is obtained, it is used to generate a CAD model of the surface Figure 2-17
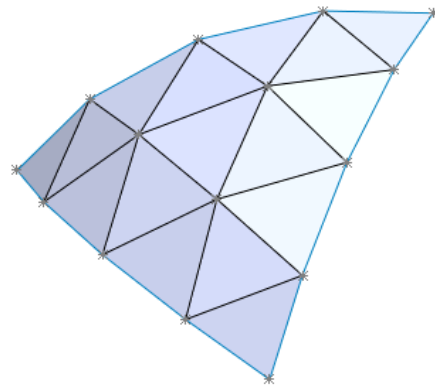
Figure 2-17 Triangular Surface of the Sphere modelled in SOLIDWORKS

This surface represents one triangular face of an icosahedron subdivided into different facets and the vertices of the sub triangles projected onto the sphere enclosing the icosahedron. These surfaces are then assembled in SOLIDWORKS assembly module to create a Geodesic Sphere of a given degree. Care has to be taken to make sure the origin and centre of the sphere circumscribing the Sphere coincide for ease in calculating coordinates later.
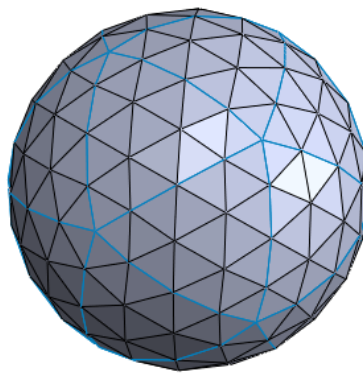
Figure 2-18 Geodesic Sphere (Degree IV) assembled in SOLIDWORKS

Figure 2-19(a) shows the imprecision in the geometry due to lesser accuracy in coordinate calculation. Table 2-5 shows the precision in coordinates considered. The double lines at the interface in (a) show the overlap in the edges of the triangular surfaces while assembly. This imprecision can later effect the meshing of the part in ABAQUS. Note that (b) has high precision of coordinates and the triangular surfaces can be "knit" at the edges in SOLIDWORKS as they lie within the knitting tolerance. Note that the un-knit model is imported as a part in ABAQUS. Here knitting is done just to emphasize on the accuracy of the model.
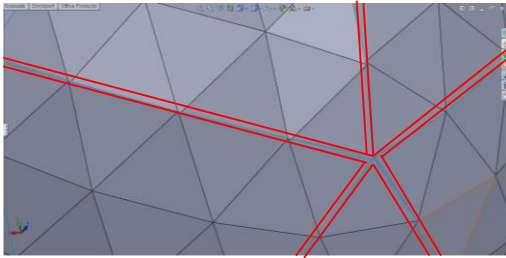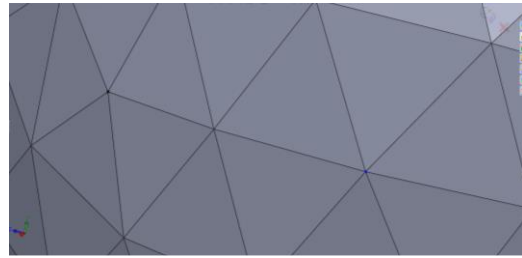
Figure 2-19 Mating in SOLIDWORKS done with Coordinates of the order (a) 3-4 significant digits (b)13-14 significant digits.

To import the model in ABAQUS, the precise assembled CAD model is then saved in .acis format. .acis format knits the geometry and keeps it as an enclosed shell. The blue lines at the edges of all the triangular surface (Figure 2-18) shows that they are not "knit" at the interface. If the surfaces in the geodesic is "knit" in SOLIDWORKS, then importing it to ABAQUS in .acis format makes it a solid geometry. Hence, after assembly, the model is saved in .acis format and is stitched automatically while importing it to ABAQUS. The unit is changed to meters in options for .acis format and the options "Combine into single part", "Merge Solid Regions" and "Retain intersecting boundaries are checked."

Figure 2-20 shows the imported model Geodesic Degree II in ABAQUS from SOLIDWORKS. Note that the structure is treated as an enclosed shell only when it is imported in un-knit .acis format
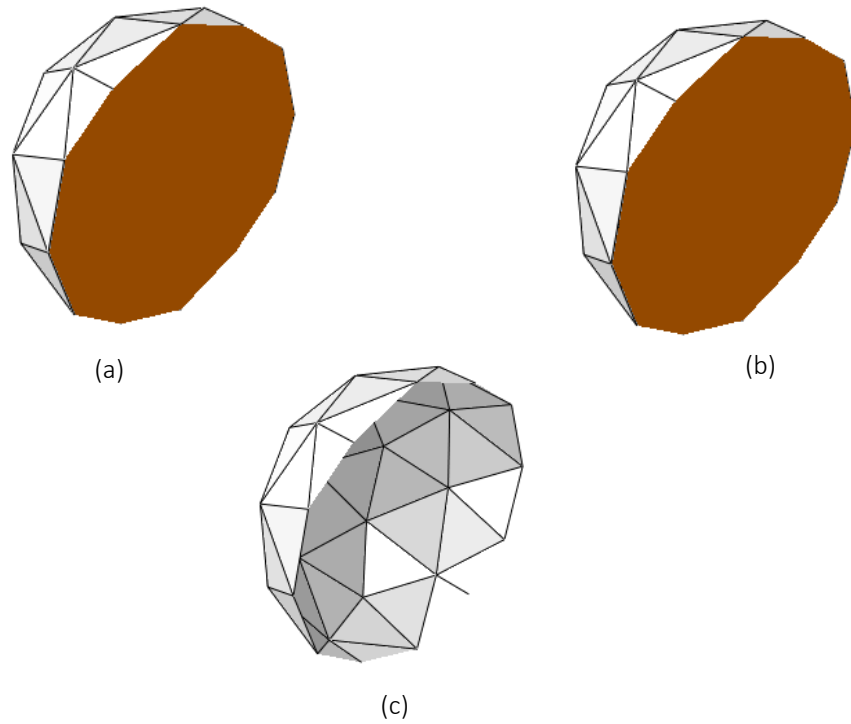
Figure 2-20 Imported parts in ABAQUS CAE from SOLIDWORKS (a) .acis format, knitted geometry, (b) .iges format (c) .acis format, un-knitted geometry

2.2.1.3   Shell thickness calculation

Just as in the case of 2-D, the total mass of the geometries is desired to be constant. The thickness of the geodesic Spheres is varied so that its mass is equal to that of the spherical shell

The spherical shell is of a outer diameter 1m with thickness 10mm. The total mass of the shell can be calculated by

$$M_{shell} = \rho V_{shell} \tag{2.9}$$

Where, ρ is the mass density of the material and $V_{shell} = A_{shell} t_{shell}$ is the volume of the shell, $A_{shell} = 4\pi r_{out}^2$ is the outer surface area, $r_{out} = 0.5\text{m}$ is the outer radius of the shell   and $t_{shell} = 10\text{mm}$ is the thickness of the shell.

Similarly, the mass of the geodesic sphere enclosed in a shell of diameter 1 m is given by

$$M_{geo} = \rho V_{geo} \qquad (2.10)$$

Where $V_{geo} = A_{geo} t_{geo}$ is the volume of the geodesic sphere. A_{geo} is the surface area of the geodesic and t_{geo} is the shell thickness of the geodesic.

Equating (2.9) and (2.10), substituting the equations for the volume, The thickness of the geodesic Spheres can be calculated as

$$\frac{t_{geo}}{t_{shell}} = \frac{A_{shell}}{A_{geo}} \qquad (2.11)$$

Where, t_{geo} is the thickness of the geodesic Sphere and A_{geo} is the surface area of the geodesic.

The surface area of the geodesic Sphere is calculated by finding out the area of the sub-triangles on one of the triangular surfaces of the geodesic Sphere (Figure 2-17). The area of each such sub-triangle is then added up to get the entire surface area of the triangular surface. Since a geodesic Sphere is made up of 20 such triangular surfaces the total surface area is given by multiplying the area of one triangular surface with 20.

2.2.1.4   Surface area calculation of the triangular surface

In previous sections, we have already calculated the coordinates for the sub triangles. With these coordinates, the side length of the subdivided triangles can be calculated. Then, the area of a triangle with sides lengths a, b and c can be given by heron's formula as

$$\Delta = \sqrt{s(s-a)(s-b)(s-c)} \tag{2.12}$$

Where, s is the semi-perimeter of the triangle $s = \dfrac{1}{2}(a+b+c)$

A MATLAB code is written (Appendix 6.3) to calculate the surface area. An index of node connectivity table is created to identify the coordinates connected to particular subdivided triangle (Figure 2-21).
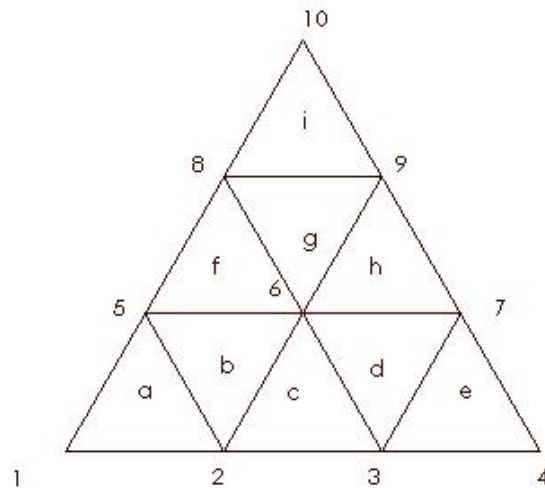
Figure 2-21 Numbering Scheme for IEN (DEGREE III)

Referring Figure 2-1 the following table can be constructed

Table 2-6 IEN for degree III

Triangle number	Vertex numbers			Area (m²)
a	1	2	5	1.434051608279486e-02
b	2	6	5	1.814357981154381e-02
c	2	3	6	1.814357981154381e-02
d	3	7	6	1.814357981154381e-02
e	3	4	7	1.434051608279485e-02
f	5	6	8	1.814357981154380e-02
g	6	9	8	1.814357981154380e-02
h	6	7	9	1.814357981154381e-02
i	8	9	10	1.434051608279486e-02

Table 2-6 shows the IEN for degree III geodesic Sphere. This helps in identifying the coordinates connected to a given subdivided triangle. With this information, the area is then calculated. The table also shows the values of calculated area of each sub-triangles. Note that the area of the sub-triangles near the vertices of the triangle face is equal.

2.2.2   The Outer Acoustic Domain

For the acoustic domain, an enclosing shell is constructed having diameter 1.5m, which represents the boundary of the acoustic domain.
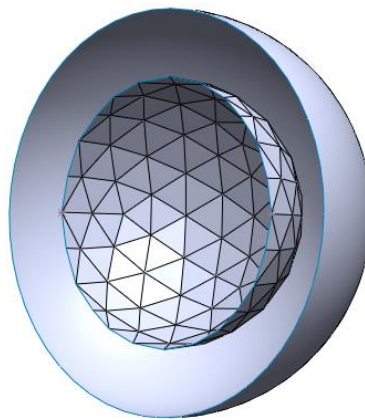
Figure 2-22 Sectional View of the outer air domain modelled in SOLIDWORKS

Figure 2-22 shows the sectional view of the acoustic domain. When saved in .iges format, and imported to ABAQUS, the empty space between the surfaces of Sphere and the shell is transformed into solid.
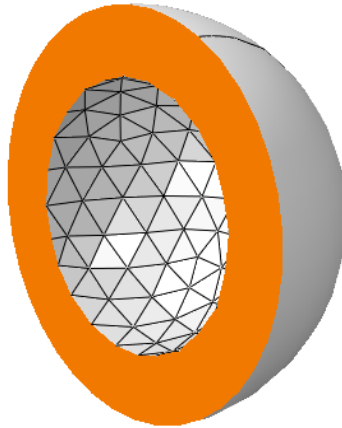
Figure 2-23 Sectional view of the acoustic domain in ABAQUS. Note that .iges format converts the section in solid

Figure 2-23 shows the imported acoustic domain in ABAQUS. The orange coloured section is thus the solid section generated during the model import.

2.2.3   Acoustic Infinite region

The infinite elements represent the region outside the bounded computational domain Ω by assuming a radial approximation with outgoing wave behaviour [23].
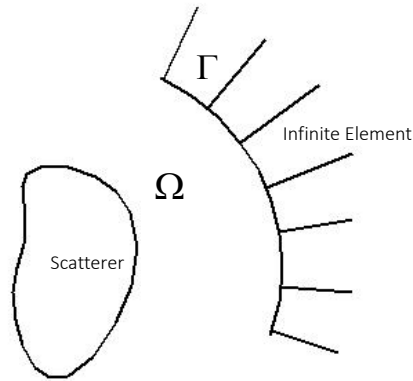
Figure 2-24 Infinite Elements

Infinite elements replace the non-reflecting boundary condition on Γ, with a single layer of elements with infinite extent. These elements are constructed with radial wave functions which satisfy the Somerfield Condition at infinity [17].

$$\lim_{r \to \infty} r \left(\frac{\partial u}{\partial r} - iku \right) = 0 \qquad (2.13)$$

Where, u(x) is the spatial part of acoustic pressure or velocity potential, k is the wavenumber. r is the radius centred near the origin of the sound source. The Sommerfield radiation condition allows only outgoing wave proportional to exp (ikr) at infinity. [17]

In this thesis, Acoustic infinite elements are used to truncate the acoustic boundary. There is no interaction in ABAQUS for Infinite boundary unlike Impedance Boundary Condition. A separate part thus is created to simulate the behaviour of infinite elements. This part is a 2-D wireframe circle for 2-D polygon and is a hollow 3-D revolved shell for the 3-D geometries. That part is referred to as acoustic domain. The part is later tied to the acoustic domain.

For 2-D, the infinite element needs to be defined as a SOLID SECTION. The ABAQUS GUI doesn't allow a SOLID SECTION assignment to a wire part. Hence the assignment is done later in the input file as explained in the Appendix.6.2

For 3-D geometries, acoustic infinite elements can be assigned in the interface, but the reference node for the infinite elements is later defined in the input file.   (Appendix 6.4)
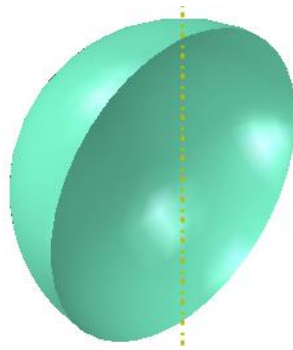
Figure 2-25 Acoustic Infinite

CHAPTER THREE

3 NATURAL FREQUENCY EXTRACTION

In this chapter, the Natural Frequency of the structures is calculated in ABAQUS. These frequencies are later used in the acoustic scattering problem. When the structure is coupled to air domain, the added mass on the structure is negligible, hence damping is negligible and the Natural Frequency of the system remains almost the same. Hence it is imperative to calculate the natural frequency of the structure, to obtain resonance peaks later in the scattering analysis.

3.1 Theory

The equation of motion to describe a vibrating structure with n- degrees of freedom can be written as

$$M\ddot{x} + C\dot{x} + Kx = 0 \tag{3.1}$$

Where M is the mass matrix, C is the damping matrix and K is the stiffness matrix and x is the harmonic displacement vector.

Substituting

$$\begin{aligned} x &= e^{-i\omega t}, \\ \dot{x} &= \mu e^{-i\omega t} \\ \ddot{x} &= \mu^2 e^{-i\omega t} \end{aligned} \tag{3.2}$$

Where $\mu = (-i\omega)$

Substituting (3.2) in (3.1), we get

$$\mu^2 M + \mu C + K = 0 \tag{3.3}$$

The natural frequency extraction problem is basically an eigenvalue extraction problem. The natural modes are the harmonic solutions of (3.3)with frequency ω in the absence of a driving term [24]

The eigenvalue problem can then be set-up as

$$(\mu^2 M + \mu C + K)\{\phi\} = 0 \tag{3.4}$$

Where $\{\phi\}$ is the eigenvector, which represents the mode of vibration.

As, μ is complex, (3.4) will yield complex eigenvalues and eigenvectors. When no damping is present, $C = 0$. Which makes the solution real. Hence (3.4) can be rewritten as

$$(\mu^2 M + K)\{\phi\} = 0 \tag{3.5}$$

Spectral analysis theory shows that [18]

$$\begin{aligned}\phi_m^T M \phi_n &= 0 \\ \phi_m^T K \phi_n &= 0, \quad for \ n \neq m\end{aligned} \tag{3.6}$$

Hence using the orthogonality properties of the eigenvector it is possible to decouple the multi-dof system into single dof systems as the modes are mechanically independent. (The uncoupling is done in analytical solutions solve each equation separately. For complex geometries numerical approximation like FEA are used)

The equation can be uncoupled by substituting $x = \Phi u$ in (3.1) and keeping $C = 0$. Then we have

$$M\Phi\ddot{u} + K\Phi u = 0 \tag{3.7}$$

Where Φ is known as the modal matrix , $\Phi = [\phi_1 \ \phi_2 \ \phi_3 ....\phi_n]$

40

Where ϕ_n is the nth mode corresponding to the nth natural frequency. Using the knowledge from (3.6), and multiplying (3.7) with $\mathbf{\Phi}^T$ we can reduce (3.7) into diagonal matrices

$$(\mathbf{\Phi}^T M \mathbf{\Phi})\ddot{u} + (\mathbf{\Phi}^T K \mathbf{\Phi})u = 0 \tag{3.8}$$

Where,

$$\mathbf{\Phi}^T M \mathbf{\Phi} = \begin{bmatrix} m_1 & 0 & 0 & 0 & 0 \\ 0 & m_2 & 0 & 0 & 0 \\ 0 & 0 & . & 0 & 0 \\ 0 & 0 & 0 & . & 0 \\ 0 & 0 & 0 & 0 & m_n \end{bmatrix} \text{ and } \mathbf{\Phi}^T K \mathbf{\Phi} = \begin{bmatrix} k_1 & 0 & 0 & 0 & 0 \\ 0 & k_2 & 0 & 0 & 0 \\ 0 & 0 & . & 0 & 0 \\ 0 & 0 & 0 & . & 0 \\ 0 & 0 & 0 & 0 & k_n \end{bmatrix}$$

The decoupled single dof equations can then be written as

$$m_i \ddot{u}_i + k_i u_i = 0, \quad \text{where i} = 1,2,3....n$$

n is the number of modes and the natural frequency for a single dof system without damping having a modal stiffness k_i and a modal mass m_i are related as

$$\omega_i = \sqrt{\frac{k_i}{m_i}} \tag{3.9}$$

3.2   Beam Element Size

To study the wave behaviour with accuracy, it is imperative to have an element size that can approximate a sinusoidal wave of a given wavelength with appreciable accuracy. Thompson *et. al.*, [25] suggested at least 10 elements should be considered per smallest wavelength in order to capture the nature of wave with reasonable accuracy.

Amongst the structural waves (Longitudinal, Shear, and Bending), the bending wave speed is a function of ω. The bending is the slowest propagating wave amongst the structural waves. The relation between wave speed, frequency and wavelength is given as

$$\lambda = \frac{c_{medium}}{f} = \frac{2\pi c_{medium}}{\omega} \qquad (3.10)$$

where c_{medium} is the speed of wave in the medium, ω is the frequency in rad/s and $f = \omega / 2\pi$ is the frequency in Hz.

When a longitudinal wave or a transverse wave is obliquely incident upon a stress-free surface it generates both reflected longitudinal and transverse waves. This transformation process in beam and plate structures produces a hybrid form of wave called bending or flexural wave [26]. The effect of bending wave causes the structure to deform transversely as well as the cross sections to rotate about their neutral axis. The bending wave speed is given as

$$c = \sqrt[4]{\frac{EI\omega^2}{\rho A}} \qquad (3.11)$$

where E is the young's modulus, I is the moment of inertia of the cross section, ρ is the mass density, A is the cross sectional area.

Note that the bending wave speed is proportional to the square-root of frequency, $c_{bending} \propto \sqrt{\omega}$.

Thus, as c_{medium} is least in case of bending waves, the smallest wavelengths are associated with it.

For the rectangular cross sectional area of the geometries, we have $A = Dt_e$, which is the area of the cross-section of the beam element, where D is the depth (1m) and t_e is the thickness of the beam element. The area moment of inertia of a rectangular cross section about its centroid is given by $I = Dt_e^3 / 12$.

From (3.10) and (3.11), and substituting numerical values for E, ρ gives

$$\lambda_{bending} = 150.94 \sqrt{\frac{t_e}{f}}$$

For the maximum frequency considered, 3000 Hz, the smallest wavelength of interest is then,

$$\lambda_{bending} = 3.37512 \sqrt{t_e}$$

For 10 elements per wavelength, the minimum element size should be

$$l_e = 0.337512 \sqrt{t_e}$$

and depends on the beam element thickness.

3.3   Natural Frequency 2-D

After calculating the proper mesh density, the Natural frequency is extracted by ABAQUS for all the geometries under investigation. The Model Set-up for the natural frequency of the geometries is given by Table 3-1

Table 3-1 Model Set-up for Structural Domain

Domain	2-D Planar – Deformable	
Material	Aluminium	Density = 2700 kg/m^3
		Young's modulus = 7.1e10 Pa
		Poisson's ratio = 0.33
		Structural Damping = 0.01
Section	Beam Section	
Beam Profile	Rectangle	
	D = depth in z-direction = 1m	
	t_e = thickness of beam element,	
	varying according to geometry to keep mass constant	
Mesh	Beam elements: B22 – A 3 node quad beam element in a plane.	
Step	1) 'Initial Step' – default	
	2) 'Linear Perturbation – Frequency' Step	
	– maximum frequency of interest: 3000 Hz	

The natural frequency obtained from ABAQUS for the shell geometry is further validated with an analytical solution [Thompson: Matlab Program (Appendix 6.5)]:

$$\omega = 2\pi \sqrt{\frac{EI}{\rho A R^4} \frac{n^2(n^2-1)^2}{(n^2+1)}}$$

Where, E is the young's modulus, $I = Dt_e^3/12$ is the moment of inertia, where D is the depth (1m) and t_e is the thickness of the element, ρ is the mass density, A is the cross sectional area, R is the radius of the ring, n is the mode number of vibration.

Figure 3.1 shows a comparison of the analytical and numerical results obtained. The mesh seed size for the natural frequency extraction in ABAQUS is 0.01m.
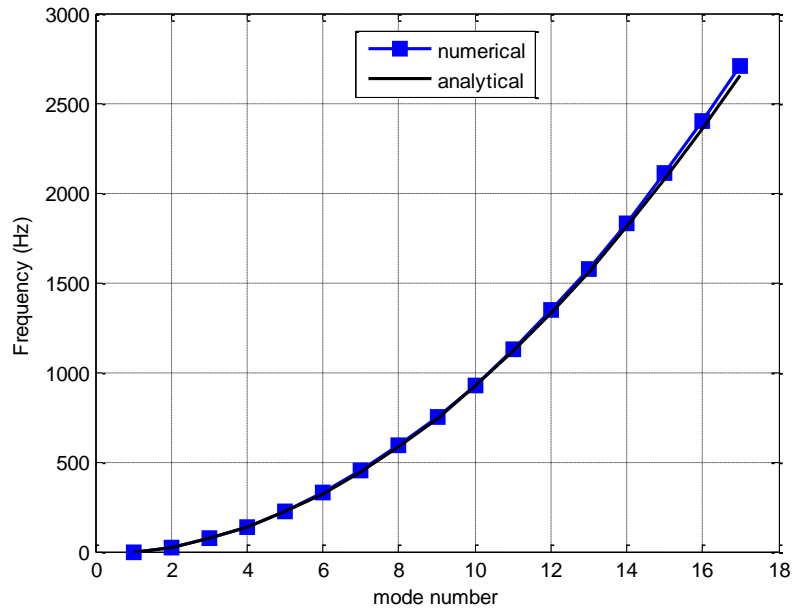
Figure 3-1 Comparison of numerical and analytical values of natural frequency of a ring

Figure 3-1 shows the comparison between the numerical and analytical values. The agreement of the numerical with the analytical values confirm the mesh density to be accurate enough.

Table 3-2 Natural Frequency of the 2-D geometries calculated by ABAQUS

Mode number	15	30	45	Ring
1	0	0	0	0
2	25.57	26.457	27.656	25.28
3	72.297	74.775	77.87	71.478
4	138.55	143.19	138.71	136.99
5	223.92	231.02	160.82	221.4
6	328.22	327.46	239.81	324.55
7	451.31	350.18	337.99	446.3
8	593.07	464.94	357.98	586.55
9	753.35	606.55	398.02	745.17
10	931.97	731.18	651.74	922.03
11	1128.7	758.5	694.69	1117
12	1332.4	889.18	879.73	1329.9

Mode number	15	30	45	Ring
13	1355.2	895.33	1102	1329.9
14	1481.4	1400	1271.9	1560.6
15	1576.6	1428	1432.7	1632.3
16	1826.3	1671.1	1603.3	1808.9
17	2077.6	1997.4	1763.6	2074.6
18	2092.9	2322.3	1805.2	2308.4
19	2375.6	2645	1854	2357.5
20	2673.2	2736.2	2558.8	2657.5
21	2982.8	2898.5	2836.1	2974.2
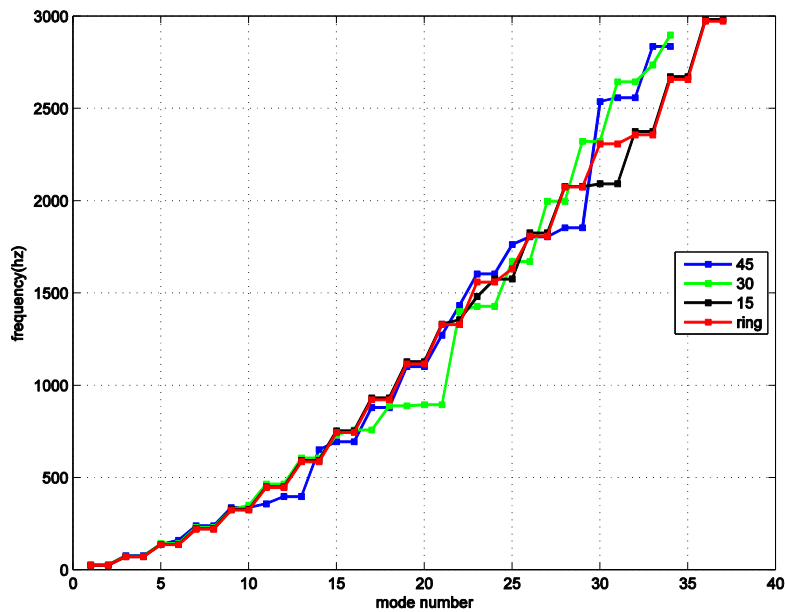
Figure 3-2 Comparison of Natural Frequencies of the 2D Structures

Figure 3-2 shows a comparison of the Natural Frequencies of the structure up to 3000 Hz frequency range. The Natural Frequency of 2D-polygon 15 is following the Natural Frequency curve of the ring closely. This is quite intuitive, as 15 approximates a ring the best amongst the 2D polygons considered in the thesis.

46

These natural frequencies thus obtained are later used in the scattering analysis. (Chapter 4)

3.4 Natural Frequency 3-D

The natural frequency extraction of 3-D geometries presented in section 2.2.1 is discussed in this section.

3.5 Shell Element Size

In case of 3-D, the size of the domain increases and the degrees of freedom too. Hence computational cost is an important variable to be pondered upon. A trade-off between the computational cost and the desired accuracy has to be done.

A convergence study is done for the homogeneous shell, for seed sizes 0.01m, 0.015m and 0.02m.
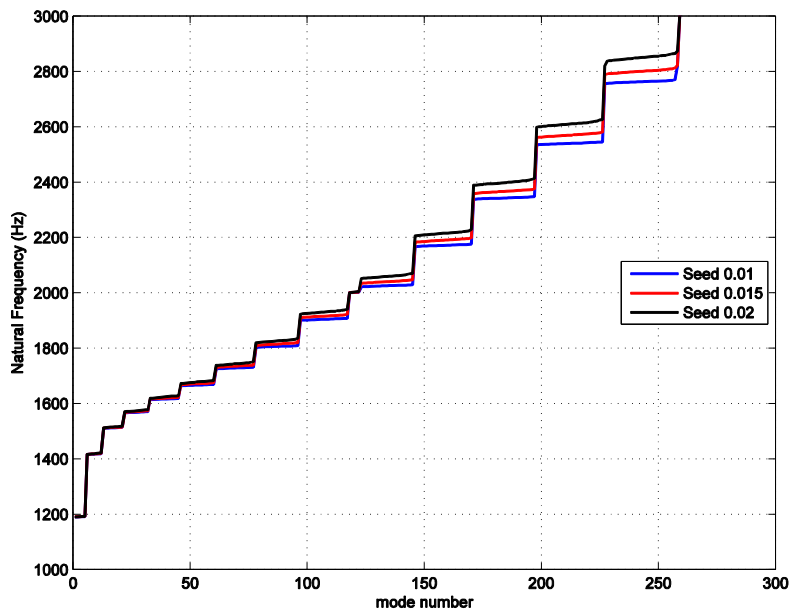
Figure 3-3 Comparison of the natural frequency of the spherical shell with different mesh size.

At higher frequencies, the natural frequency for the model starts to differ for different element sizes which is as expected (Figure 3-3). Table 3-3 shows the natural frequencies of the last 20 modes for comparison.

Table 3-3 Comparison of the Natural Frequencies of the last 20 modes extracted in ABAQUS with different mesh size.

Seed 0.01	Seed 0.015	Seed 0.02
2762.5	2799.2	2848.1
2762.7	2799.6	2849.1
2763.0	2800.1	2849.7
2763.2	2800.4	2850.5
2763.5	2800.9	2851.2
2764.0	2802.0	2851.7
2764.3	2802.8	2852.3
2764.4	2803.3	2853.5
2764.9	2803.5	2853.9
2765.1	2804.0	2854.8
2765.3	2804.3	2855.5
2765.7	2805.2	2855.8
2766.1	2806.0	2857.3
2766.6	2806.5	2858.8
2766.7	2807.4	2858.8
2767.5	2808.6	2860.7
2767.7	2809.6	2862.7
2768.6	2810.0	2863.9
2770.4	2812.2	2865.0
2820.5	2822.1	2873.8

At the last mode for the highest frequency, the difference between seed 0.01 and seed 0.02 is less than 2%. In case of natural frequency extraction the domain is smaller and hence the computational time is not a big concern, but in case of acoustic scattering (section 4.12) the size of the domain increases. Thus to be consistent with the mesh size chosen for the

structure in acoustic scattering analysis (section 4.12) and in the natural frequency

extraction, a seed size of 0.02 is considered to be reasonably accurate. (Figure 3-4)

(a)   (b)   (c)
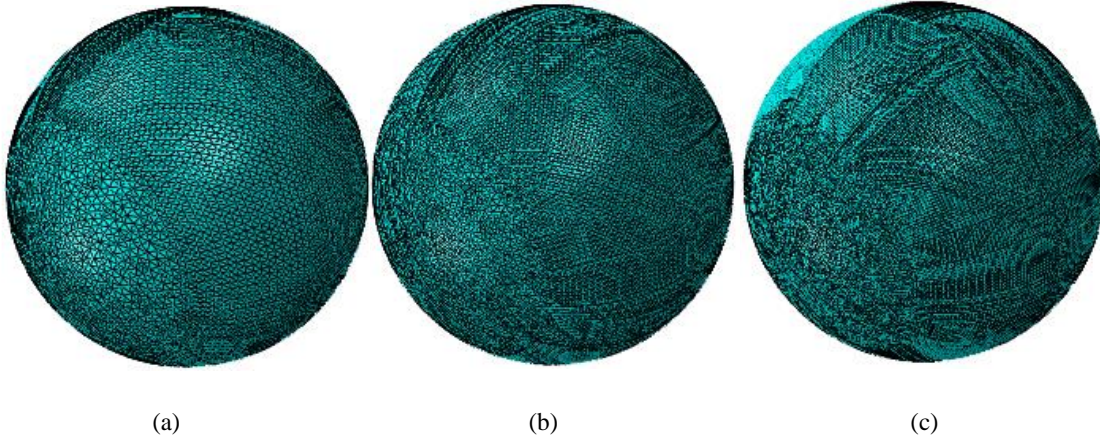
Figure 3-4 Mesh Density (a) Seed 0.02, (b) Seed 0.015 (c) Seed 0.01

Figure 3-5 shows the mesh density with seed size 0.02 m of the geodesic spheres (Degree

II, Degree III, Degree IV) under investigation.

(a)   (b)   (c)
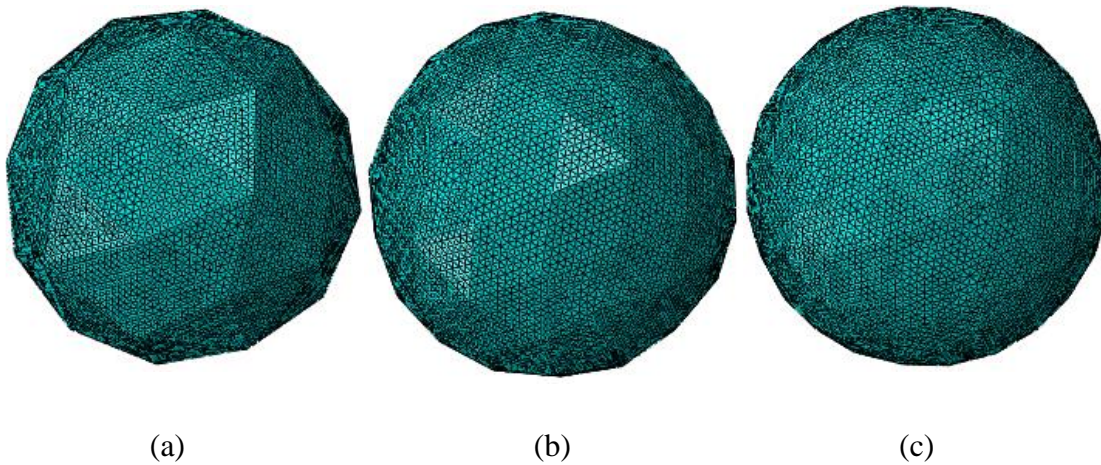
*Figure 3-5 Mesh Density (seed size 0.02*m) of the Geodesic Spheres *selected for the analysis (a)
Degree II (b) Degree III (c) Degree IV*

3.5.1   Natural Frequency extraction 3D

The cad model is first imported as a part into ABAQUS from SOLIDWORKS by

saving it as an ".acis" file. The model setup is given by Table 3-4

Table 3-4 Model Set-up in ABAQUS for 3D Geometry

Domain	3-D Planar – Deformable	
Material	Aluminium	Density = 2700 kg/m^3
		Young's modulus = 7.1e10 Pa
		Poisson's ratio = 0.33
		Structural Damping = 0.01
Section	Homogeneous Shell	
Thickness Value	Varying according to geometry to keep mass constant. Simpson integration rule with 5 integration points.	
Mesh	Shell Elements: S3 – A 3-node triangular general purpose shell, finite member strains	
Step	1) 'Initial Step' – default 2) 'Linear Perturbation – Frequency' Step – maximum frequency of interest: 3000 Hz	

Table 3-5 lists the natural frequencies of the 3D geometries under investigation. The

frequencies start to get closer to that of a spherical shell as the degree of the geodesic

increases. In case of the shell, the frequencies occur in clusters of 3-4 equal values. One

value is picked from that cluster, and used later in the calculation of scattering response.

These clusters represent the orientation of the same mode shapes along different axis in the

space. In case of geodesics, for frequencies higher than around 1500Hz, no such identical

clusters of frequencies is obtained. Table 3-4 gives the natural frequencies for the

geometries used for the calculation of the scattering response. All the calculated natural

frequencies are tabulated in the Appendix.6.7

Table 3-5 Natural Frequencies of the 3D geometries.

Mode No.	Degree II	Degree III	Degree IV	Shell
1	914.71	1113.30	1166.40	1191.20
2	933.31	1300.10	1377.00	1416.30
3	973.44	1370.90	1380.10	1511.60
4	1002.40	1398.20	1455.10	1568.60
5	1047.80	1404.20	1472.70	1616.20
6	1052.30	1420.00	1503.60	1667.60
7	1076.70	1442.80	1515.80	1729.90
8	1107.10	1461.00	1541.00	1810.00
9	1159.30	1475.80	1549.70	1909.40
10	1167.50	1499.90	1569.50	2001.50
11	1183.80	1516.20	1586.40	2034.50
12	1237.80	1521.20	1600.40	2183.50
13	1250.70	1527.20	1628.90	2358.90
14	1346.00	1598.50	1651.10	2561.20
15	1392.30	1603.00	1678.30	2580.50
16	1438.50	1648.20	1684.60	2789.30
17	1463.60	1652.90	1709.40	2822.10
18	1477.20	1659.80	1718.20	3000.00
19	1527.60	1665.60	1758.70	
20	1552.90	1676.70	1781.90	
21	1587.30	1713.70	1797.40	
22	1610.00	1762.10	1827.40	
23	1766.40	1827.20	1844.90	
24	1824.20	1858.60	1887.70	
25	1842.20	1900.20	1894.10	
26	1851.80	1931.70	1938.30	
27	1882.80	1998.60	1971.70	
28	1930.10	2021.20	2000.30	
29	1983.40	2049.60	2027.00	
30	2049.70	2116.00	2033.80	
31	2083.60	2150.30	2069.50	
32	2135.30	2168.90	2103.60	
33	2210.30	2212.20	2158.10	
34	2232.70	2244.40	2163.30	
35	2267.80	2278.20	2194.70	
36	2331.50	2306.00	2204.80	

37	2379.50	2380.90	2241.10
38	2415.80	2388.20	2261.20
39	2475.20	2398.90	2283.60
40	2531.20	2423.70	2293.30
41	2615.50	2491.80	2368.00
42	2706.60	2527.20	2373.50
43	2723.80	2553.00	2431.80
44	2743.10	2585.40	2452.60
45	2772.40	2635.30	2466.90
46	2825.60	2691.80	2481.80
47	2861.60	2720.30	2562.60
48	2870.50	2752.70	2597.70
49	2908.40	2788.10	2633.00
50	2922.50	2847.20	2664.70
51	2957.40	2874.90	2672.60
52	2979.50	2907.60	2718.70
53	2981.60	2911.90	2809.90
54			2823.70
55			2835.50
56			2870.50
57			2879.00
58			2994.10

Figure 3-6 the mode number v/s natural frequency plot for the structures under investigation. The plot shows as the degree of the geodesic increases, it starts to behave more and more like a sphere, which is quite intuitive. The plot also shows the degree II geodesic is less stiff than the higher degree geodesics at low frequencies, which is understood as it has longer struts. But at higher frequency, between 2000-3000 Hz, it shows more stiffness than the other models in study, which is interesting to observe.
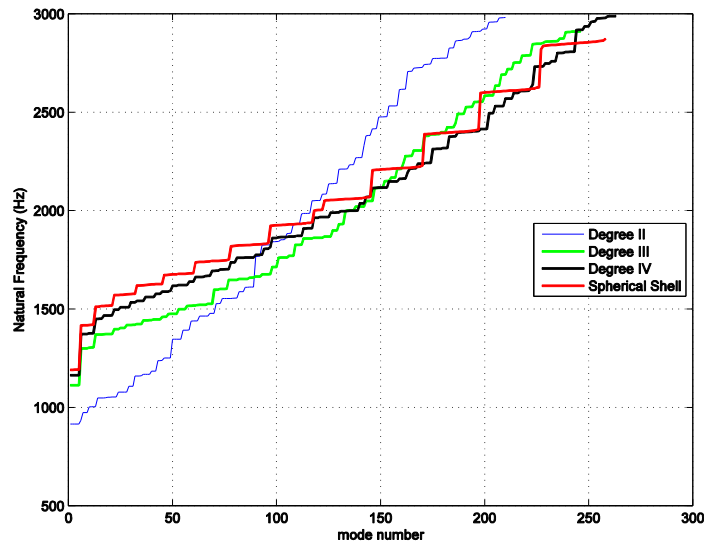
Figure 3-6 Comparison of Natural Frequencies extracted from ABAQUS of the different 3-D Geometries
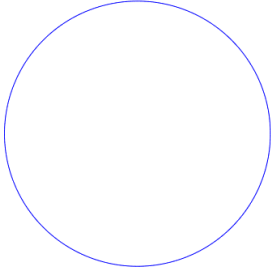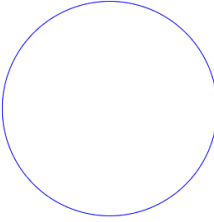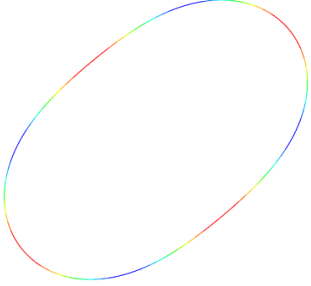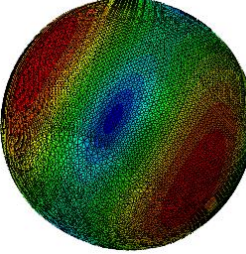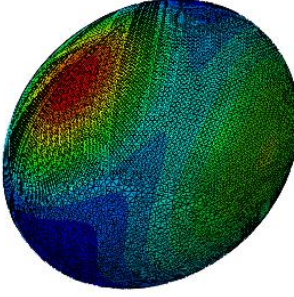
3.6   Mode Shapes

Mode shapes are the characteristic spatial distribution of vibrations associated with corresponding natural frequencies natural frequencies. The mode shapes should be captured accurately, as they play a significant role in capturing the acoustic scattering response. The displacements at the structure boundary is thus directly related to the mode shapes. The structural-acoustic coupling couples this displacement at the structure – fluid interface such that the structure and the fluid move together. Thus the study of the modes shapes is important in analysing and understanding the scattered wave characteristics.

We observe two kind of mode shapes in modal analysis, 1) Flexural mode and 2) Dilatational Mode. During the flexural mode of vibration, the surface deforms in the same direction at any point inside or outside the structure. In Dilatational Mode, the entire surface expands or contracts compared to its base state (breathing mode).

Shows the dilatational and flexural mode of the ring and shell models under investigation in this thesis. The flexural mode occurs at the lower natural frequencies and the first dilatational mode is observed at higher frequencies. At frequencies beyond the dilatational mode, the mode shapes are observed to have more local deformations.

Table 3-6 Flexural and Dilatational Mode of the Ring and Sphere

Geometry	Base State	Dilatational Mode	Flexural Mode
Ring		@ 1632.3 Hz	@ 25.280 Hz
Shell		@2001.5 Hz	@ 1191.2 Hz

The figures below present the first five mode shapes and natural frequencies of the geometries in 2-D and 3-D. The natural frequencies become closer to the ring/shell, when

54

the number of sides n of the polygon (for 2-D) and the degree of the geodesic increases. For 2-D, in case of Figure 3-9 and Figure 3-10, the mode shapes and the natural frequency start to converge to that of the ring. For 3-D, in case of Figure 3-13 and Figure 3-14, the mode shapes and the natural frequency start to converge to that of the shell.

27.656 Hz   77.870 Hz   138.71 Hz   160.82 Hz   293.81 Hz
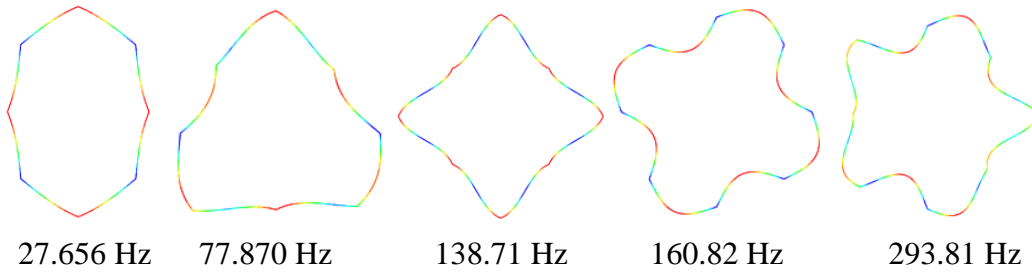
Figure 3-7 First five mode shapes and natural frequencies of 45^0 (n = 8).

26.457 Hz   74.775 Hz   143.19 Hz   231.02 Hz   327.46 Hz
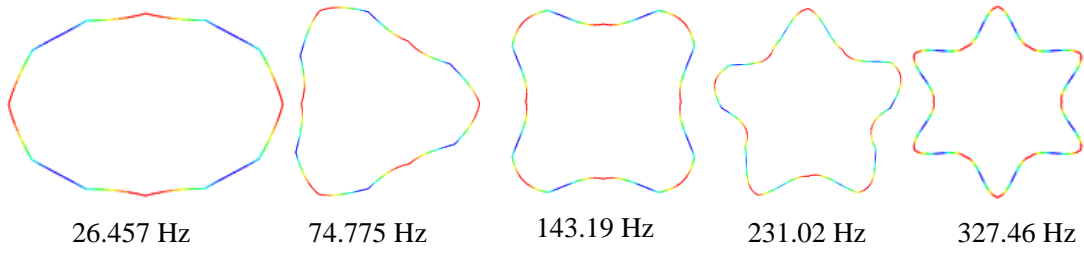
Figure 3-8 First five mode shapes and natural frequencies of 30^0 (n = 12).

25.570 Hz   72.297 Hz   138.55 Hz   223.92 Hz   328.22 Hz
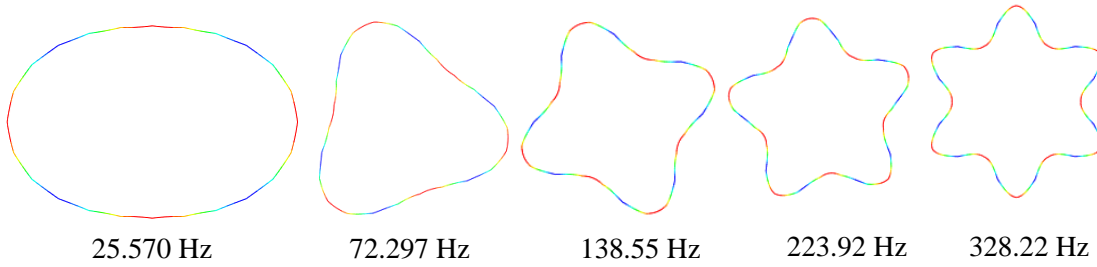
Figure 3-9 First five mode shapes and natural frequencies of 15^0 (n = 24).

25.570 Hz   71.478 Hz   136.99 Hz   221.40 Hz   324.55 Hz
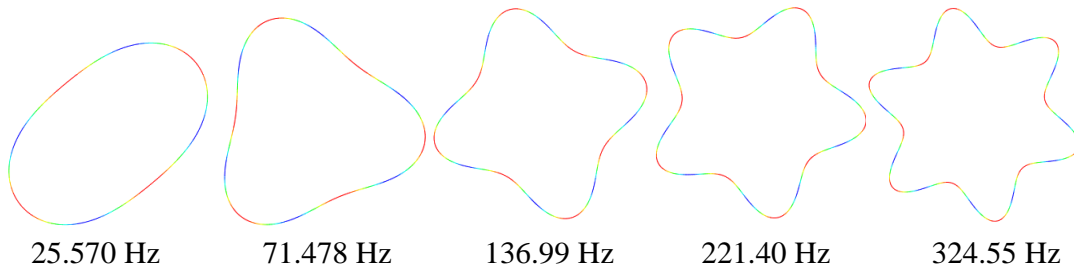
Figure 3-10 First five mode shapes and natural frequencies of ring.

914.71 Hz   933.31 Hz   973.44 Hz   1002.4 Hz   1047.8 Hz
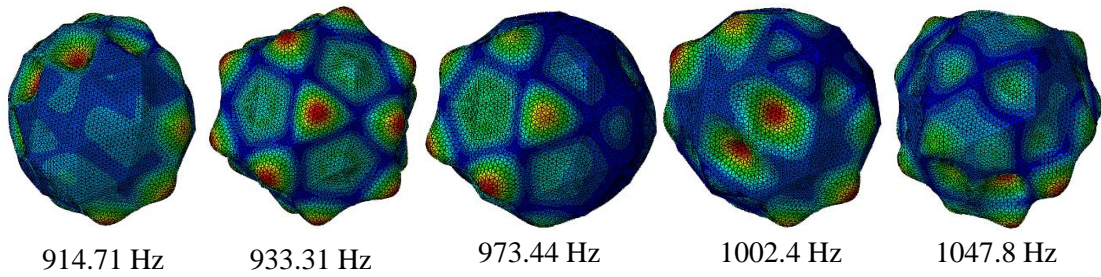
Figure 3-11 First five mode shapes and natural frequencies of Degree II Geodesic.

1113.3 Hz   1300.1 Hz   1370.9 Hz   1398.2 Hz   1404.2 Hz
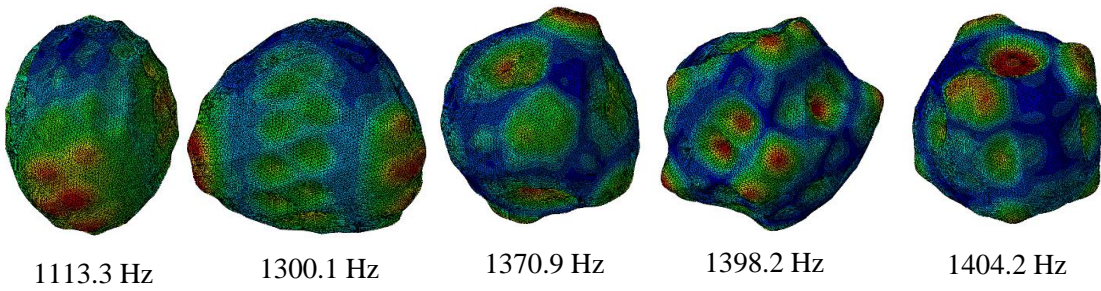
Figure 3-12 First five mode shapes and natural frequencies of Degree III Geodesic.

1164.1 Hz   1373.5 Hz   1451.0 Hz   1467.9 Hz   1497.7 Hz
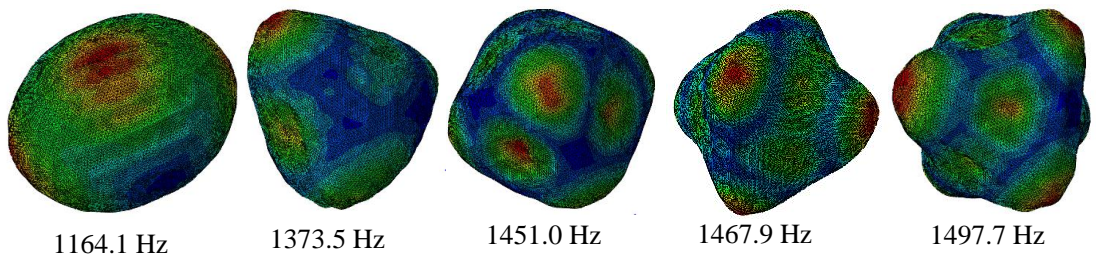
Figure 3-13 First five mode shapes and natural frequencies of Degree IV Geodesic.

1191.2 Hz   1416.3 Hz   1511.6 Hz   1568.6 Hz   1616.2 Hz
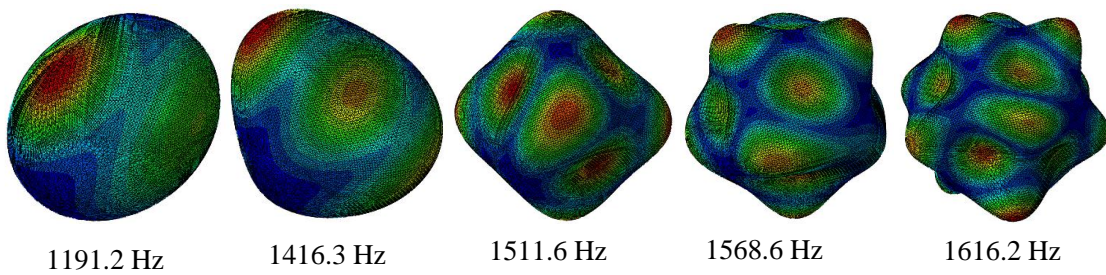
Figure 3-14 First five mode shapes and natural frequency of the sphere.

CHAPTER FOUR

4   ACOUSTIC SCATTERING RESPONSE

Scattering describes waves that are induced due to an abrupt impedance change in space, especially when waves are spread out in space [27]. Due to the impedance mismatch, the incident waves get disrupted. Hence when a wave is incident onto a surface of a medium which has a different characteristic impedance than that of a medium it was travelling in, there can exist a scattered wave (along with reflected and diffracted, depending upon the impedance mismatch) in all the directions from the surface along with the undisturbed incident wave. Scattering depends upon the wavelength and the geometry of the scatterer.

In this chapter, the scattering response of the different structures (2-D and 3-D) are studied and are compared to a reference structure. Later, a value of the ratio of wavelength to the characteristic dimension of the facet is proposed which relates their behaviour to the reference structure. The Target Strength (TS), which just a scaled form of the acoustic pressure is calculated at the near end and far end for all the geometries.

To get a better understanding of the scattering by an elastic body, first a rigid body scattering analysis is performed, in which there is pressure is considered to be zero at the structure-fluid interface (rigid boundary condition). The next section shows how the wave equation, which is the governing equation for all the waves propagating in space is derived. Which is the basis to understand theory behind the scattering from a rigid body and the structure-acoustic coupling.

4.1   Structural-Acoustic Theory

The section presents the theory and equations behind the Structural-Acoustic Coupling. First, the theory behind the acoustic equations is discussed, later the structural-acoustic formulation in FEA is discussed.

4.1.1   The Wave Equation

Sound results from a time-varying perturbation of dynamic and thermodynamic variables. The independent variables that basically govern the wave equation are pressure (p), fluid velocity (v) and density (ρ).

We have

$$
\begin{aligned}
p &= p_0 + p^{'} \\
\rho &= \rho_0 + \rho^{'} \\
v &= v_0 + v^{'}
\end{aligned}
\tag{4.1}
$$

Where, the subscript "0" denotes the quantities appropriate to the ambient medium and prime represents the perturbation in the quantity.

The conservation of mass is described by the partial differential equation as

$$
\frac{\partial \rho}{\partial t} + \nabla.(\rho v) = 0
\tag{4.2}
$$

The governing equation for a fluid is given by the Navier Stokes equation. But, if the viscosity, thermal conductivity and gravity are neglected, Navier Stokes equation reduces to Euler equation which can be given after linearization as

$$
\rho \frac{\partial v}{\partial t} = -\nabla p
\tag{4.3}
$$

The differential relation between the thermodynamic coefficients can be given as

$$\frac{\partial p}{\partial t} = c^2 \frac{\partial \rho}{\partial t} \tag{4.4}$$

Using (4.4) in (4.2) we get

$$\frac{\partial p}{\partial t} + \rho c^2 \nabla \mathbf{v} = 0 \tag{4.5}$$

Where $\rho c^2 = K$ is the bulk modulus.

Taking time derivative of (4.5), we have

$$\frac{\partial^2 p}{\partial t^2} + \rho c^2 \nabla \frac{\partial \mathbf{v}}{\partial t} = 0 \tag{4.6}$$

Substituting (4.3) in (4.6), with constant density, gives the wave equation for linear acoustics as

$$\nabla^2 p - \frac{1}{c^2} \frac{\partial^2 p}{\partial t^2} = 0 \tag{4.7}$$

Where p is the time harmonic acoustic pressure and c is the speed of light in the fluid medium.

4.1.2   Rigid Body Scattering

Scattering describes waves that are induced due to an abrupt impedance change in space, especially when waves are spread out in space [20]. Scattering depends upon the wavelength and frequency of the wave. It also depends upon the geometry of the scatterer. We aim to find the relation between these three parameters to obtain scattering characteristics.
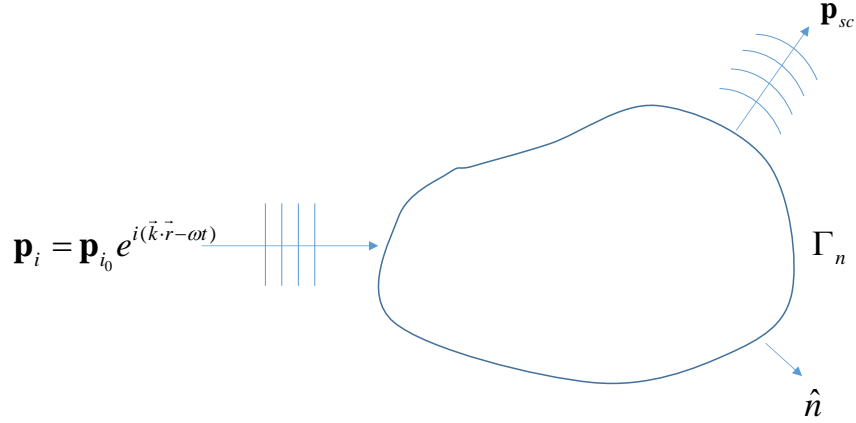
Figure 4-1 Scattering from a rigid body.

The total time harmonic sound pressure is given by the sum of the complex amplitude of

the incident wave ($\mathbf{p}_i$) and the complex amplitude of the scattering wave ($\mathbf{p}_{sc}$).

$$\mathbf{p}_t = \mathbf{p}_i + \mathbf{p}_{sc} \tag{4.8}$$

Since the boundary is acoustically rigid, $v_n = 0$, thus the boundary condition is given as

$$\nabla \mathbf{p}_t \cdot \hat{n} = 0 \tag{4.9}$$

p_i is the incident pressure propagates in the direction of wave number vector $\vec{k}$, incident

wave at position $\vec{r}$ can be written as

$$\mathbf{p}_i = \mathbf{p}_{i_0} e^{i(\vec{k}\cdot\vec{r}-\omega t)} \tag{4.10}$$

Where p_{i_0} is the complex amplitude of incident wave.

Taking gradient of (4.8) and multiplying by $\hat{n}$ and then using (4.9) in (4.8) we have

$$\nabla \mathbf{p}_{sc} \cdot \hat{n} = -i\mathbf{p}_{i_0} \vec{k} \cdot \hat{n} e^{i(\vec{k}\cdot\vec{r}-\omega t)} \tag{4.11}$$

The linearized Euler equation (4.3)gives

61

$$\nabla \mathbf{p}_{sc} = i\omega\rho \vec{v}_{sc_0} e^{-i\omega t} \tag{4.12}$$

Where scattering velocity ($\vec{v}_{sc}$) is assumed to be harmonic in time and is given by

$$\vec{v}_{sc} = \vec{v}_{sc_0} e^{-i\omega t} \tag{4.13}$$

Consider the scatterer to be a sphere in a 2-D plane of radius a (Figure 4-2), with a plane wave incident on it in the direction of the wavenumber vector ($\vec{k}$) then (4.11) can be rewritten as

$$\nabla p_{sc} \cdot \hat{n} = -i p_{i_0} k_x \cos\theta e^{i(k_x a \cos\theta - \omega t)} \tag{4.14}$$

Where $\vec{k} \cdot \hat{n} = k_x \hat{i} \cdot (\cos\theta \hat{i} + \sin\theta \hat{j}) = k_x \cos\theta$ and $\vec{k} \cdot \vec{r} = k_x \hat{i} \cdot |\vec{r}| \hat{n} = k_x a \cos\theta$

Where θ is the angle between the wavenumber vector $\vec{k}$ and the normal vector $\hat{n}$.
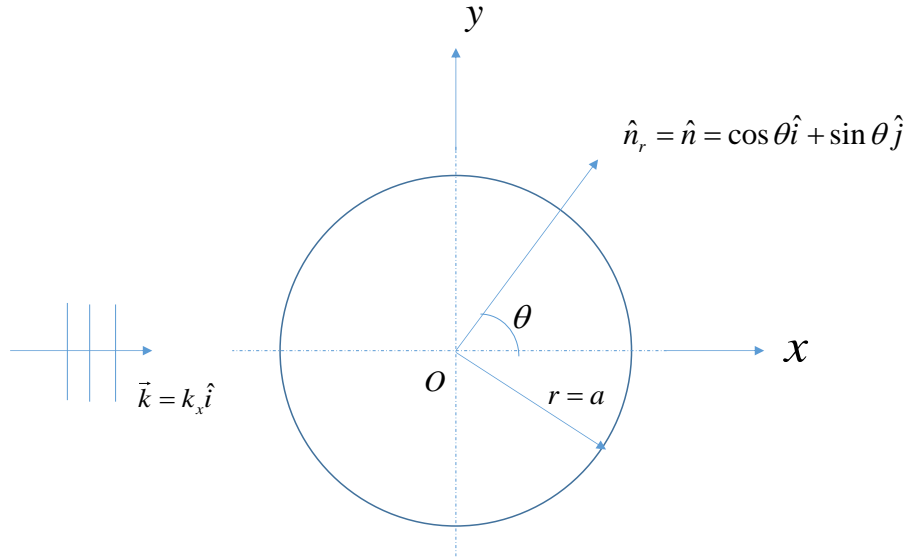
Figure 4-2 Scattering from a rigid sphere in 2-D plane

From (4.12) and (4.14),

$$\vec{v}_{sc_0} \cdot \hat{n} = \frac{-ip_{i_0} k_x \cos\theta e^{i(k_x a \cos\theta - \omega t)}}{i\omega\rho e^{-i\omega t}}$$

$$= \frac{-ip_{i_0} k_x \cos\theta e^{i(k_x a \cos\theta - \omega t)}}{i\frac{\omega}{c}\rho c e^{-i\omega t}} \qquad (4.15)$$

$$= \frac{-p_{i_0} \cos\theta e^{ika\cos\theta}}{\rho c}$$

Thus the normal velocity on the rigid sphere is a function of θ. In special case, if size of the scatterer is smaller than the wavelength of interest i.e. $ka \ll 1$, (4.15) can be expanded using Taylor series as (neglecting the higher order terms) and writing $k_x = k$,

$$v_{sc_0} \cdot \hat{n} \cong \frac{-p_{i_0}}{\rho c} \cos\theta (1 + ika\cos\theta) \qquad (4.16)$$

(a)   (b)
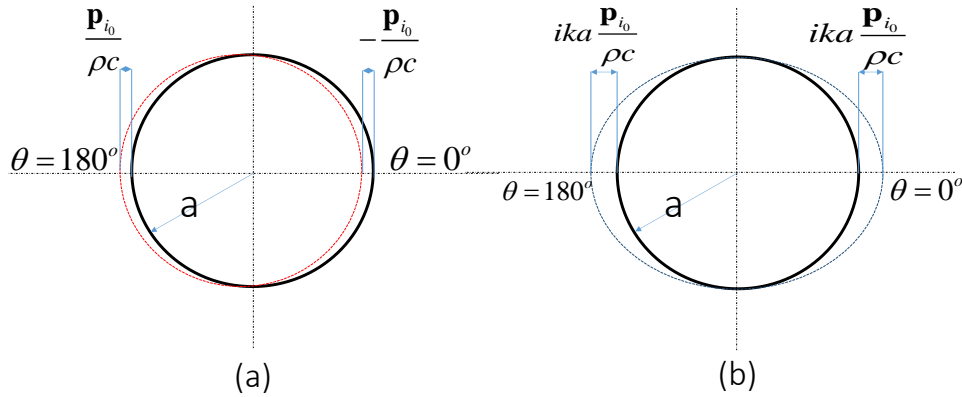
Figure 4-3 A velocity profile showing (a) the trembling effect due to first term in the normal velocity (b) the breathing effect due to the second term in the normal velocity.

From (4.16), the normal velocity has two components, one depends on $\cos\theta$ and the other

on $\cos^2\theta$. At $\theta = 0^o$ and $\theta = 180^0$ the first term is $\dfrac{-p_{i_0}}{\rho c}$ and $\dfrac{p_{i_0}}{\rho c}$ respectively, which shows

the magnitude of the velocity is the same but the negative sign shows that it is opposite to

the normal. Thus the first term demonstrates the trembling effect of the sphere (Figure

4-3(a))

The second component on the other hand is $ika\mathbf{p}_{i_0} / \rho c$ which has the same

magnitude and direction as the normal. Thus the second term demonstrates the breathing

effect of the sphere. (Figure 4-3 (b))

If the sphere is smaller than the wavelength of interest, the contribution form the

second term is much lesser. Hence a small sphere (when compared to the wavelength of

interest) will display more of a trembling effect.[20]

4.1.3   Structural Acoustic coupling
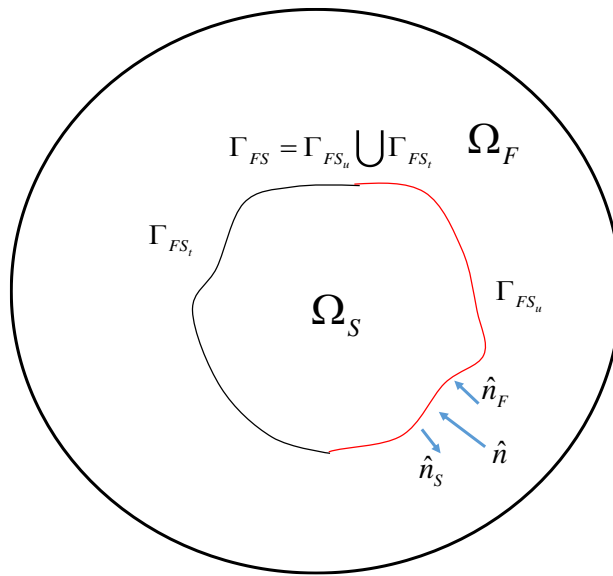
Figure 4-4 The Structural-Acoustic Domain

The governing differential equations for the structure-acoustic systems is presented.[28] The equation of motion for a continuum body assuming small deformations is given by (4.17). On the structure domain. Here σ is the stress acting at a point in the domain, b is the body force, ρ is the density and u is the displacement. The governing differential equation for the structural domain is mainly balancing out forces based on Newton's second law of motion.

$$\nabla\sigma + b = \rho\frac{\partial^2 u}{\partial t^2} \tag{4.17}$$

With boundary conditions

$$\begin{aligned}
u &= u_S &&\text{on } \Gamma_{FS_u} \text{ (Dirichlet B.C.)} \\
\sigma n_S &= t &&\text{on } \Gamma_{FS_t} \text{ (Neumann B.C.)}
\end{aligned} \tag{4.18}$$

4.2 Finite Element formulation for the coupled problem

Using weight functions and subsequently the green's theorem to obtain the weak form of the boundary value problem, (4.17), which can be defined as

Find u such that traction at $\Gamma_{FS_t} = t$ and for all arbitrary w satisfying the constraint $w = 0$ at Γ_{FS_u}

$$\int_{\Omega_S} w_s^{\mathrm{T}}\rho\frac{\partial^2 u}{\partial t^2}d\Omega_S + \int_{\Omega_S}(\nabla w_s)^{\mathrm{T}}\sigma d\Omega_S - \int_{\Gamma_{FS}} w_s^{\mathrm{T}}td\Gamma_{FS} - \int_{\Omega_S} w_s^{\mathrm{T}}bd\Gamma_{FS} = 0 \tag{4.19}$$

Discretizing using FEA elements and interpolation Shape functions we get discretized form as

$$w_s^{eT}\int_{\Omega_S} N_s^{eT}\rho N_s^e d\Omega_S \ddot{d}_s^e + w_s^{eT}\int_{\Omega_S}(\nabla N_s^e)^{\mathrm{T}}D\nabla N_s^e d\Omega_S d_s^e = w_s^{eT}\int_{\Gamma_{FS}} N_s^{eT}td\Gamma_{FS} + w_s^{eT}\int_{\Omega_S} N_s^{eT}bd\Omega_S$$

Where $\boldsymbol{D}$ is the constitutive matrix for an isotropic material.

Assembling the finite elements in the structural domain Ω_s, we get the set of equations in

matrix form as

$$\boldsymbol{M}_s \boldsymbol{d}_s + \boldsymbol{K}_s \boldsymbol{d}_s = \boldsymbol{F}_s \qquad (4.20)$$

where,

$$\boldsymbol{M}_s = \int_{\Omega_s} \boldsymbol{N}_s^{eT} \rho \boldsymbol{N}_s^e d\Omega_s$$

$$\boldsymbol{K}_s = \int_{\Omega_s} (\nabla \boldsymbol{N}_s^e)^{\mathbf{T}} \boldsymbol{D} \nabla \boldsymbol{N}_s^e d\Omega_s$$

$$\boldsymbol{F}_s = \boldsymbol{f}_t + \boldsymbol{f}_b \qquad (4.21)$$

$$\boldsymbol{f}_t = \int_{\Gamma_{FS}} \boldsymbol{N}_s^{eT} t d\Gamma_{FS}$$

$$\boldsymbol{f}_b = \int_{\Omega_s} \boldsymbol{N}_s^{eT} b d\Omega_s$$

The governing equation for a fluid is based on the linearized wave equation (4.7)..

Subject to boundary conditions

$$\boldsymbol{p} = \boldsymbol{p_s} \qquad \text{on } \Gamma_{FS_u} \text{ (Dirichlet B.C.)}$$

$$\boldsymbol{v}_n = \nabla \boldsymbol{p} \cdot \hat{n} \qquad \text{on } \Gamma_{FS_t} \text{ (Neumann B.C.)}$$

Using weight functions and subsequently the green's theorem to obtain the weak form of

the boundary value problem, which can be given as

$$\int_{\Omega_F} \boldsymbol{w}_F^{\mathbf{T}} \frac{\partial^2 \boldsymbol{p}}{\partial t^2} d\Omega_s + c^2 \int_{\Omega_S} (\nabla \boldsymbol{w}_F)^{\mathbf{T}} \nabla \boldsymbol{p} d\Omega_s - c^2 \int_{\Gamma_{FS}} \boldsymbol{w}_F^{\mathbf{T}} \nabla \boldsymbol{p} \boldsymbol{n}_F d\Gamma_{FS} = 0$$

Discretizing using FEA elements and interpolation Shape functions we get discretized

form as

$$w_F^{e\,\mathbf{T}} \int\limits_{\Omega_F} N_F^{e\,T} N_F^e d\Omega_S \ddot{\boldsymbol{p}} + c^2 w_F^{e\,\mathbf{T}} \int\limits_{\Omega_S} (\nabla N_F^e)^{\mathbf{T}} \nabla N_F^e d\Omega_S \boldsymbol{p} = c^2 w_F^{e\,\mathbf{T}} \int\limits_{\Gamma_{FS}} N_F^{e\,T} n_F{}^T \nabla p d\Gamma_{FS}$$

Assembling the finite elements in the fluid domain Ω_F, we get the set of equations in matrix form as

$$M_F \ddot{\boldsymbol{p}} + K_F \boldsymbol{p} = F_F \tag{4.22}$$

where,

$$M_f = \int\limits_{\Omega_F} N_F^{e\,T} N_F^e d\Omega_S$$

$$K_f = c^2 \int\limits_{\Omega_S} (\nabla N_F^e)^{\mathbf{T}} \nabla N_F^e d\Omega_S$$

$$F_F = f_f = c^2 \int\limits_{\Gamma_{FS}} N_F^{e\,T} n_F{}^T \nabla p d\Gamma_{FS}$$

Structure - acoustic coupling takes place at the interface of fluid and structural boundary Γ_{FS}. The displacement at the boundary is the same for both fluid and structural domain, as they move together. Also, the acoustic pressure can be related to the surface traction on the structure. (4.23) show the coupling boundary conditions (on Γ_{FS})

$$\begin{aligned} -u_S n_S &= u_F n_F \\ -\sigma n_S &= p n_F \end{aligned} \tag{4.23}$$

let $\boldsymbol{n} = -\boldsymbol{n}_S = \boldsymbol{n}_F$, then

$$\begin{aligned} -u_S n &= u_F n \\ \sigma n &= p n \end{aligned}$$

from (4.18)

$$\boldsymbol{t} = \boldsymbol{pn} \tag{4.24}$$

Thus from (4.21) and (4.24) we get

$$\boldsymbol{f}_t = \int_{\Gamma_{FS}} \boldsymbol{N}_S^{eT} \boldsymbol{pn} d\Gamma_{FS}$$

$$= \int_{\Gamma_{FS}} \boldsymbol{N}_S^{eT} \boldsymbol{n}^T p d\Gamma_{FS}$$

$$= \int_{\Gamma_{FS}} \boldsymbol{N}_S^{eT} \boldsymbol{n}^T \boldsymbol{N}_F^e d\Gamma_{FS} \boldsymbol{p}$$

Using Euler's equation, we have

$$\nabla p = -\rho \frac{\partial \boldsymbol{v}}{\partial t} = -\rho \frac{\partial^2 \boldsymbol{u}_f}{\partial t^2}$$

$$\boldsymbol{n}^T \nabla p = -\boldsymbol{n}^T \rho \frac{\partial^2 \boldsymbol{u}_f}{\partial t^2}$$

$$= -\boldsymbol{n}^T \rho \frac{\partial^2 \boldsymbol{u}_S}{\partial t^2}$$

Now,

$$\boldsymbol{f}_f = c^2 \int_{\Gamma_{FS}} \boldsymbol{N}_F^{eT} \boldsymbol{n}_F^T \nabla p d\Gamma_{FS}$$

$$= -c^2 \int_{\Gamma_{FS}} \boldsymbol{N}_F^{eT} \boldsymbol{n}^T \rho \frac{\partial^2 \boldsymbol{u}_S}{\partial t^2} d\Gamma_{FS}$$

$$= -c^2 \rho \int_{\Gamma_{FS}} \boldsymbol{N}_F^{eT} \boldsymbol{n}^T \boldsymbol{N}_S^e d\Gamma_{FS} \ddot{\boldsymbol{d}}_S$$

Thus,

$$\boldsymbol{f}_t = \int_{\Gamma_{FS}} \boldsymbol{N}_S^{eT} \boldsymbol{n}^T \boldsymbol{N}_F^e d\Gamma_{FS} \boldsymbol{p}$$

$$\boldsymbol{f}_f = -c^2 \rho \int_{\Gamma_{FS}} \boldsymbol{N}_F^{eT} \boldsymbol{n}^T \boldsymbol{N}_S^e d\Gamma_{FS} \ddot{\boldsymbol{d}}_S$$

(4.25)

(4.25) Shows the coupling of acoustic pressure and structural displacement in the force terms. Note that the shape functions are also coupled and the integral terms are basically transpose of each other.

Hence, we can write

$$\int_{\Gamma_{FS}} N_S^{eT} \boldsymbol{n}^T N_F^e d\Gamma_{FS} = \boldsymbol{H}_{SF} \quad \text{and}$$

$$\int_{\Gamma_{FS}} N_F^{eT} \boldsymbol{n}^T N_S^e d\Gamma_{FS} = \boldsymbol{H}_{SF}^T$$

(4.26)

Using (4.25) and (4.26) in (4.20) and (4.22), we can write the following structural-

acoustic coupled equations

$$\boldsymbol{M}_S \boldsymbol{d}_S + \boldsymbol{K}_S \boldsymbol{d}_S - \boldsymbol{H}_{SF} \boldsymbol{p} = \boldsymbol{f}_b$$

$$\boldsymbol{M}_F \ddot{\boldsymbol{p}} + \boldsymbol{K}_F \boldsymbol{p} + \rho c^2 \boldsymbol{H}_{SF}^T \ddot{\boldsymbol{d}}_S = 0$$

In matrix form,

$$\begin{bmatrix} \boldsymbol{M}_S & 0 \\ \rho c^2 \boldsymbol{H}_{SF}^T & \boldsymbol{M}_F \end{bmatrix} \begin{bmatrix} \ddot{\boldsymbol{d}}_S \\ \ddot{\boldsymbol{p}} \end{bmatrix} + \begin{bmatrix} \boldsymbol{K}_S & -\boldsymbol{H}_{SF} \\ 0 & \boldsymbol{K}_F \end{bmatrix} \begin{bmatrix} \boldsymbol{d}_S \\ \boldsymbol{p} \end{bmatrix} = \begin{bmatrix} \boldsymbol{f}_b \\ 0 \end{bmatrix}$$

4.3 Scattering from an Elastic Body 2-D

Before considering 3-D geometries, the scattering behaviour of 2-D geometries is

first studied. Infinite elements have been used on a surrounding circular boundary to

truncate the infinite acoustic domain for all analysis present in this thesis.

4.3.1　Model set-up in ABAQUS
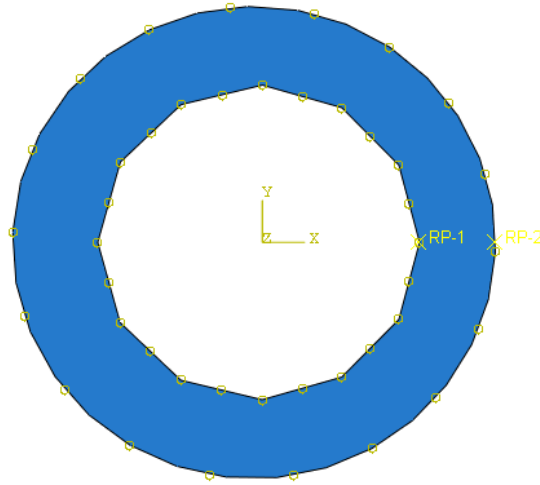
Figure 4-5 2-D faced polygon surrounded by infinite acoustic domain truncated at outer circle.

The acoustic wave speed and wavelength is used as a guide in selecting the element size in the acoustic region. The incident wave for entire frequency range of 1-3000 Hz has constant unit amplitude and scatters back into the acoustic domain. Considering air in the outer acoustic domain, speed of sound in air is given by $c = \sqrt{K/\rho}$, where is $K = 1.42e5\ Pa$ is the bulk modulus of air, ρ = 1.2 kg/m³, is the density of air. Thus, speed of sound in air is c = 343.996 m/s. Using relation $\lambda = c/f$, where λ is the acoustic wavelength and is the f frequency of the sound in Hz. For our analysis, the maximum frequency considered is f =3000 Hz, which corresponds to the shortest wavelength. Thus the smallest wavelength considered is λ_{min} = 0.11467 m. For 10 elements per smallest wavelength, the maximum element length should be 0.011467m. For a ring of diameter 1 m, frequency at 3000 Hz, corresponds more than eight wavelengths per diameter, a/λ = 8.72. Since the medium is the same in 2-D and 3-D, the maximum element size is the same.

4.3.1.1   Domain

The finite element domain is made up of 3 parts for 2-D scattering response analysis.

Air domain is a 2D Planar-Deformable-Shell. Discretized by AC2D8: An 8-node quad 2-D acoustic quadrilateral FEA element. This air domain has a diameter of 1.5m and a depth of 1m. The domain has the properties of air as given by

Table 4-1 and a Solid, Homogeneous section, with a plane stress/strain thickness of 1. The section is created and assigned in the property module of ABAQUS.

The Part for the infinite boundary is a 2D Planar-Deformable-Wire. Discretized by ACIN2D3: A 3-node acoustic infinite element with quadratic surface interpolation. This domain has the properties of air as given by Table 4-2 and a Solid, Homogeneous section. For 2D geometries, wire geometries cannot be assigned a solid section, the section assignment is done by editing the input file generated by abaqus. Explained in Appendix 6.2. The boundary is cylindrical having a diameter of 1.5m and a depth of 1m. The diameter of the boundary is set by doing a convergence study.

The elastic structure is a 2D Planar-Deformable-Wire. Discretized by B22: A 3 node quad beam in a plane. The part is modelled with varying thickness and has the properties as explained in Natural Frequency extraction. (Section 3.3)

Table shows the summary of the properties of the parts created.

1.   Elastic Domain can be referred from Table 3-1

2.   Acoustic Domain

Table 4-1 Model Set-up for Acoustic Domain

Domain	2-D Planar – Deformable	
Material	Air	Density = 1.2 kg/m^3
		Bulk Modulus = 1.42e5 Pa
Section	Solid Homogeneous, with plane stress/strain thickness 1	
Mesh	Acoustic elements: AC2D8 – An 8 node 2D acoustic quad element	

3. Acoustic Infinite Domain

Table 4-2 Model Set-up for Infinite Boundary Domain

Domain	2-D Planar – Deformable	
Material	Air	Density = 1.2 kg/m^3
		Bulk Modulus = 1.42e5 Pa
Section	Solid Homogeneous, with plane stress/strain thickness 1 (Defined in the input file)	
Mesh	Acoustic infinite elements: ACIN2D3 – A 3 node acoustic infinite element with quadratic surface interpolation	

4.3.1.2   Step

'Steady State Dynamics – Direct' analysis is carried out for a frequency range of 1-3000 Hz. The natural frequencies extracted earlier are then used as frequency sweep input with sufficient number of points in between each frequency range and a bias of 2. The bias intends to put more points near the natural frequency of the structure for better refinement of acoustic response near the structure natural frequency than at a frequency point in-between two consecutive natural frequencies

Step 1: Initial – ABAQUS default step

Step 2: Steady State Dynamics – Direct – Loading step, with linear scale from 1-3000 Hz.

4.3.1.3   Interaction Properties

An interaction property defines the properties of the propagating wave through the given medium. Hence, the fluid density, the speed of the wave in that medium is defined.

4.3.1.3.1   Amplitude

Amplitude of the incoming plane wave is defined by interpolating between frequency values. Amplitude is defined as given by the following Table. A unit amplitude is specified since results will be scaled with the incoming wave pressure amplitude.

Table 4-3 Amplitude Definition

Span	Frequency	Amplitude
Minimum	0	1
Maximum	3000	1

4.3.1.3.2   Interactions

The interaction properties are discussed in this section.

Incident Wave

As there are two surfaces at the structure-fluid interface, two interaction properties need to be specified. To define the incident wave, a source and a stand-off point needs to be specified. The reference points created and their coordinates are specified below Figure 4-6

RP-1 – Source point – (0.75, 0)

RP-2 – Stand-off point – (0.5, 0)

Then, surface upon which the wave is incident has to be specified. The surfaces at which the wave is incident for the two interactions, are the inner surface of the acoustic domain and the outer surface of the elastic body.
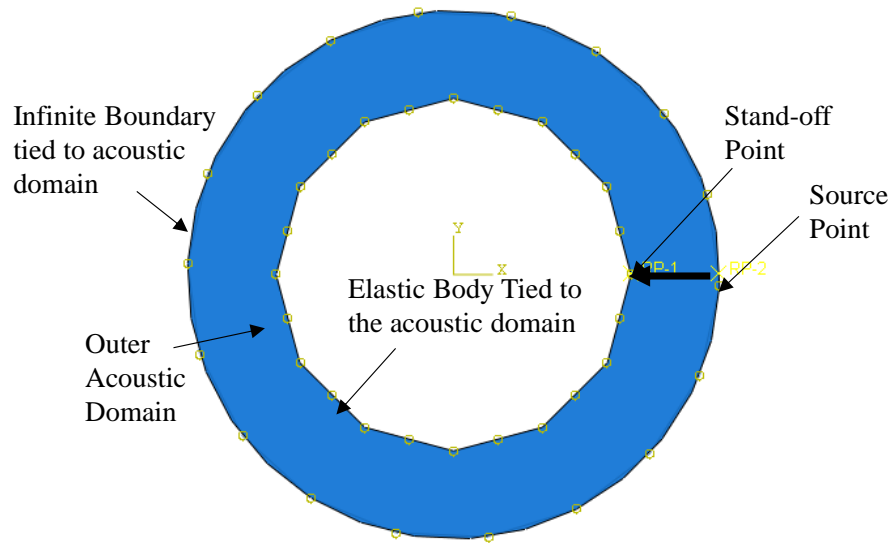
Figure 4-6 Interaction definition for 2-D geometry.

The incident wave is defined as a "Pressure" wave, with a Reference magnitude of 1 with an amplitude defined earlier.

The wave properties are defined in the interaction properties, which is given by

Table 4-4 Wave propagation properties

Medium	Wave Definition	Speed of sound in fluid (m/s)	Density (Kg/m^3)	Bulk Modulus (Pa)
Air	Planar	343.996	1.2	1.42e5

4.3.1.4 Constraints

The model has two constraints. One ties the structure to the acoustic domain and the other constraint ties the infinite boundary to the outer surface of the acoustic domain.

ABAQUS manual says the coarser mesh to be the master surface and the finer mesh to be the slave surface. For all the models present in the thesis, especially in 3-D, care has been taken to have the same type of Mesh Controls (i.e. tri for shell and tetrahedron for solids) and have the same element size, so that more accuracy can be obtained from the tie constraint.

For coupling structure and acoustic, the structure is made the master and the acoustic medium is the slave. The infinite boundary is tied to the outer surface of the acoustic domain using tie constraint. As, the inner surface of an infinite element doesn't exist, outer surface of the infinite boundary has to be selected and subsequently tied to the outer surface of the acoustic domain.

4.3.1.5   Field Output Requests

Acoustic Pressure (POR) is requested as a field output for the node sets mentioned in Table 4-5 . This acoustic pressure is later used to calculate the target strength and plotted against the frequency.

Table 4-5Field Output Request on Nodes

Position	X-coordinate	Y-coordinate
Front near node	0.5	0
Back near node	-0.5	0

4.3.1.6   Job

After setting up the entire model, a job is created in a desired folder by setting up the work directory. As calculations for the numerical problem require more computational resources, the input files are created first and then submitted onto the Palmetto cluster.

4.4　Target Strength

Target Strength is a frequency dependent parameter defined by the ratio of magnitude of pressure of scattered wave with respect to the magnitude of the pressure of incident wave [29]. Mathematically, the target strength is given by

$$TS = 20\log_{10}\left(\frac{|P_o(r,\theta,\omega)|}{|P_i(r,\theta,\omega)|}\right) \tag{4.27}$$

Target strength is a function of position in space and the frequency, as shown by (4.27). Here, P_0 is the pressure of the scattered wave and P_i is the pressure of the incident wave. To enable us to compare the degree of loudness of sound, the P_i is replaced by $P_{ref} = 2\times10^{-5}$ Pa , which is the threshold pressure of human hearing.

Thus from (4.27)

$$TS = 20\log_{10}\left(\frac{|P_o(r,\theta,\omega)|}{|P_{ref}|}\right)$$

The target strength is a function of position in space and the frequency. The target strength has been calculated at the front and the back end of the geometries as shown in Figure 4-7. The target strength is calculated at front and the back near end of the geometry. For each geometry, same points have been selected for consistency.
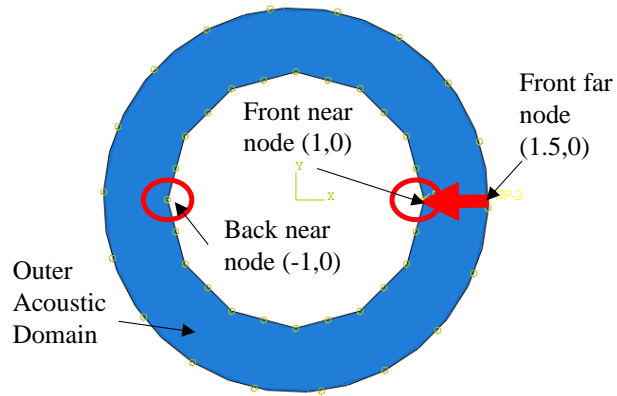
Figure 4-7 The target strength is calculated at the front and back near node of 2-D

4.5   Mesh Convergence

Figure 4-8 and Figure 4-9 show the plots for mesh convergence at the front near

and back near node.
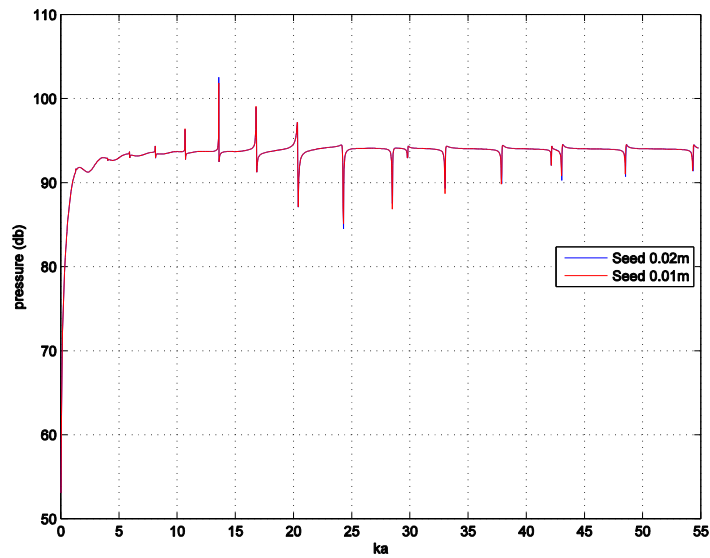
Figure 4-8 Mesh convergence for Elastic Scattering response of 2-D geometries at front near node.
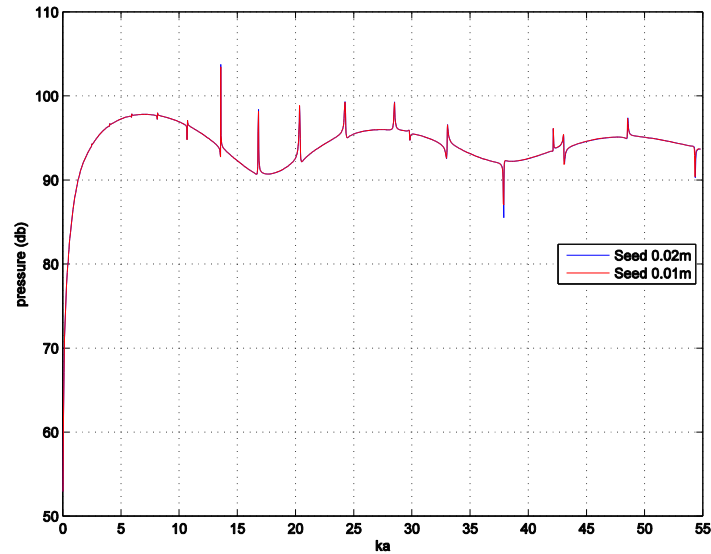
Figure 4-9 Mesh convergence for Elastic Scattering response of 2-D geometries at back near node.

Mesh density is convergent for a seed size of 0.01m and 0.02m, but at higher frequencies, for better accuracy, the finer mesh with seed size 0.01m is selected.

4.6 Location of the infinite boundary

A convergence study is done to truncate the acoustic domain by the infinite boundary condition. Two factors have been taken into consideration 1) Convergence (especially towards the lower frequency range; 1-2000 Hz (ka = 36.5). 2) Computational cost. The acoustic scattering is requested at the same points at the front and the back end of the surface of the 1 m circular elastic ring scatterer. Three different circular outer boundaries are investigated 1) Diameter 1.5m 2) Diameter 1.75m 3) Diameter 2m
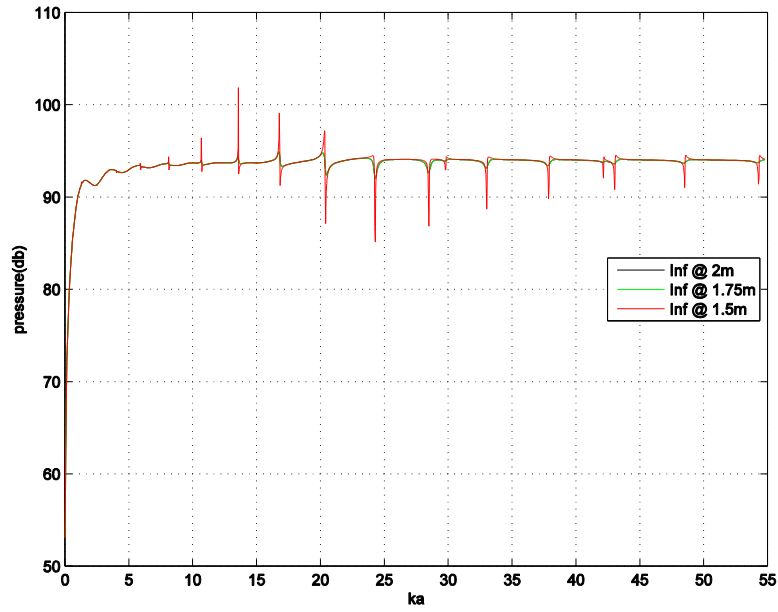
Figure 4-10 Elastic Scattering response at different diameters of the circular infinite boundary at the front near node.
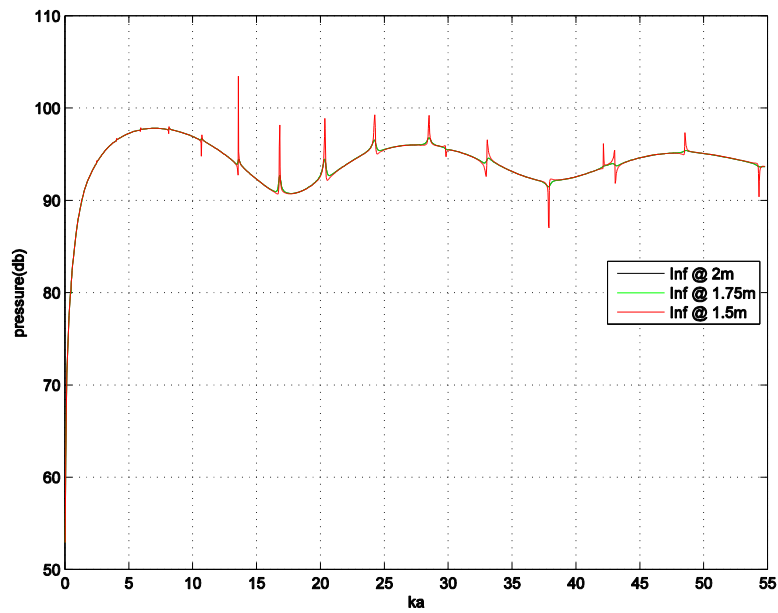
Figure 4-11 Elastic Scattering response at different diameters of the circular infinite boundary at the back near node.

Figure 4-10 and Figure 4-11 show the convergence study to find the ideal location of the infinite boundary considering accuracy and computational cost. The curves for all the three diameters of the circular infinite boundary are in good agreement to each other.

Figure 4-12, the bar graphs show the memory required in Gigabytes and the wall time in hours. The number of CPUs is 8 for all the cases. It can be seen clearly, that for the same number of processors, memory required and the wall time is the least for infinite boundary @ 1.5m. Hence the location of the infinite boundary is circle with a diameter of 1.5 m.
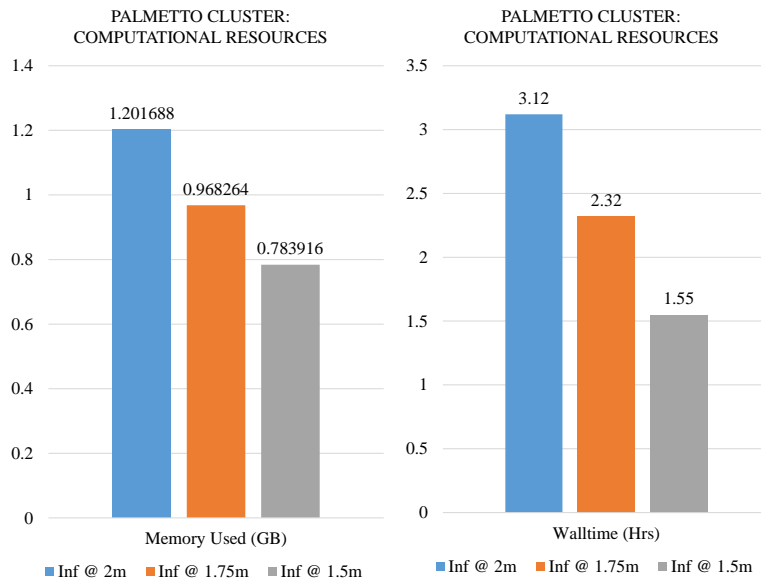
Figure 4-12 Bar Graphs comparing the computational resources utilized for the numerical calculations. For all the cases, mesh density is the same with seed size 0.02m and number of cpus is 8.

4.7   Elastic Scattering response of the geometry 2-D

Figure 4-13 and Figure 4-14 show the target strength plots of scattering from the 2-D elastic bodies at the front and back near node.
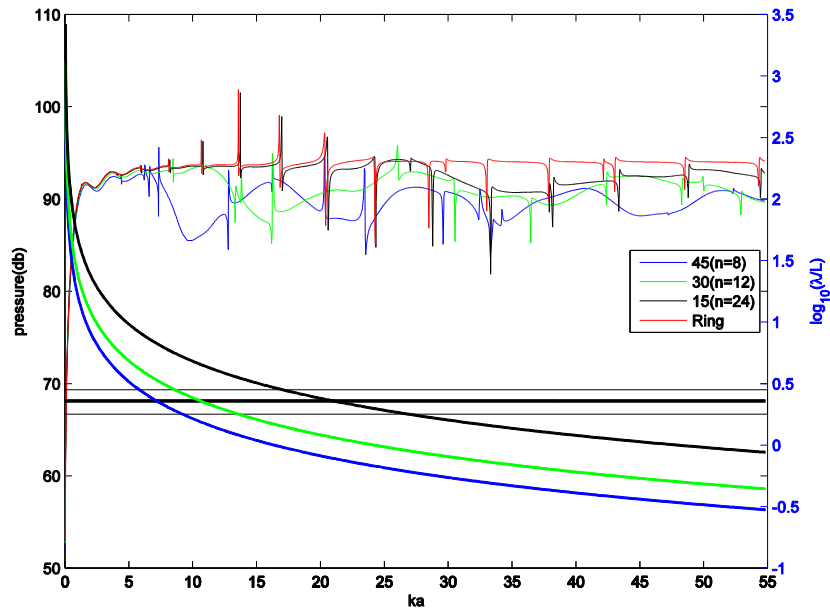
Figure 4-13 Elastic Scattering response @ Front near node
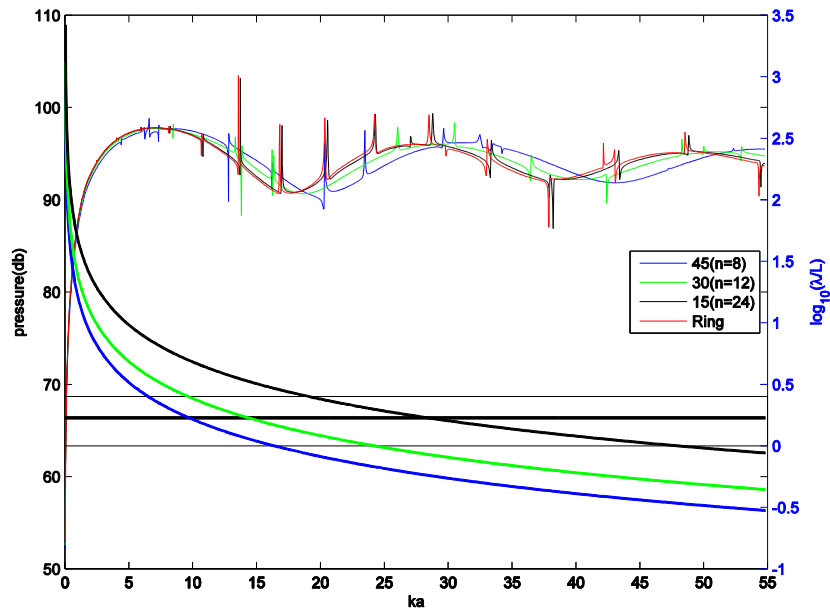
Figure 4-14 Elastic Scattering response @ back near node

81

Plots in Figure 4-13 and Figure 4-14 have two y-axes. The left y-axis is a measure of the Target strength (black axis) and the y-axis on the right (red) represents the log scale of the ratio of wavelength to chord length for different geometries. The x-axis represent the frequency range of interest normalized into ka. This non-dimensional frequency is calculated as $ka = a(\omega/c) = a(2\pi f/c) = a(2\pi/\lambda)$, where a = 1m, is the diameter of the circular ring. k is the wavenumber, ω is the angular frequency in rad/s, f is the frequency in Hz, c is the speed of sound in the medium and λ is the wavelength of interest.

As ka is inversely proportional to the wavelength λ, the largest value of ka corresponds to smallest λ. In this case maximum $ka = 55$. This gives a/$\lambda = 55/2\pi$. Which results in a/$\lambda = 8.75$. Thus, the shortest wavelength of interest is around 9 times smaller than the diameter of the spherical shell.

The three curves on the bottom half of the plot are interpreted by the red y axis and scattering response curves at the top half by the black y axis.

As the angle subtended by the polygon at the centre decreases, the chord length decreases and it takes up more surface area of the circle it was inscribed in. In other words, the polygon starts to approximate a circle geometry. This trend is also evident in the scattering behaviour. The results show that the polygon with the smallest angle considered, 15 degrees (24 sides), more closely matches the scattering behaviour of the circular ring, as compared to the other polygon scatterers with larger angles (less number of sides).

The horizontal band in the plot gives a range of the ratio of wavelength to the chord length upto which the scattering characteristics of a polygon can be approximated as a ring. It is interesting to note that the width of the band is smaller for the target strength calculated

82

at front near node than that of the back near node, showing more variation in the scattering characteristics of the model at the back near node. The ratio of wavelength to the chord length is expected to be near to the upper band value for larger chord lengths, i.e., the polygons which are lesser approximations of a circle, and at the lower band value for polygons with shorter side lengths.

The thick black horizontal line in the plot gives a mean value of the band. This value is subjective and can be considered as a rule of thumb for predicting the threshold frequency at which the scattering from a polygon matches closely with the circular ring. The frequencies at which the line intersects corresponding these curves are considered to be points at which the respective geometry deviates from behaving like a circular scatterer.

From the scattering response of the front node (Figure 4-13), the dotted black line intersects the red y axis at around 0.35. Hence for a faceted geometry, when a low frequency wave is incident on one of its corners, its response matches closely with a circular scatterer if,

$$\log_{10}\left(\frac{\lambda}{L}\right) \approx 0.35, \quad \Rightarrow \quad \left(\frac{\lambda}{L}\right) \approx 2.24$$
(4.28)

Hence, the threshold ratio of wavelength to the chord length (facet) is approximately 2.5. The bandwidth considering the polygons under consideration, lies between $0.25 < \log_{10}(\lambda / L) < 0.45$, which gives

$$1.78 < (\lambda / L) < 2.82$$

For the polygons, which have $n > 12$, the ratio is expected to be near the lower 1.78 value (the lower value of the band), whereas for $n<12$, the ratio value is expected to be near the

higher value 2.82. This is expected to happen, as the polygons which are coarser i.e. they are not a good approximation to the geometry of a circle, will have scattering characteristics which will deviate from the scattering characteristics of a circular scatterer at lower frequencies. This will give them a larger ratio as the threshold wavelength will be longer as compared to finer polygons. Note that the ratio of wavelength to chord/side length is inversely proportional to the length of the side. Hence for coarser geometries, both the wavelength and the chord length will be large. From the trend of the plots, it can be inferred that the increase in wavelength has more effect on the ratio than that of the increase in chord length. Thus, for lower *n*-sided polygons, the ratio is expected to be towards the higher value of the band.

It is important to note that this numerical factor is subjective and depends upon the tolerance value used.

Similarly at the back near node (Figure 4-14), the ratio is given by

$$\log_{10}\left(\frac{\lambda}{L}\right) \approx 0.2, \quad \Rightarrow \quad \left(\frac{\lambda}{L}\right) \approx 1.6$$

The range of the band in terms of the ratio of the wavelength to the chord length for the back near node is given as $0 < \log_{10}(\lambda/L) < 0.4$ which can be written as

$$1 < (\lambda/L) < 2.5$$

For the back near node, it is interesting to note that the bandwidth is more as compared to the front near node. In this case also, the coarser polygon will have a ratio towards the higher value of the band and the finer will have the ratio towards the lower value.

84

Scattering response at the inner acoustic nodes have also been calculated for 15^0 and the ring. Figure 4-15, Figure 4-16 and Figure 4-17 show the polar plots comparing 15^0 and ring at different frequencies of interest. 4.15 shows the polar plot at the threshold frequency where the scattering behaviour of 15 deviates from that of the ring. 4.16 shows the scattering response at first natural frequency after the threshold frequency. The pressure disturbances are more prominent along the inner acoustic surface, due to resonance at natural frequency. At around 1800Hz (ka = 33) the resonant peaks differ for 15^0 and the ring at the front near node. The difference in the target strength can be seen at the front near node in 4.16 ($\theta = 0^0$).
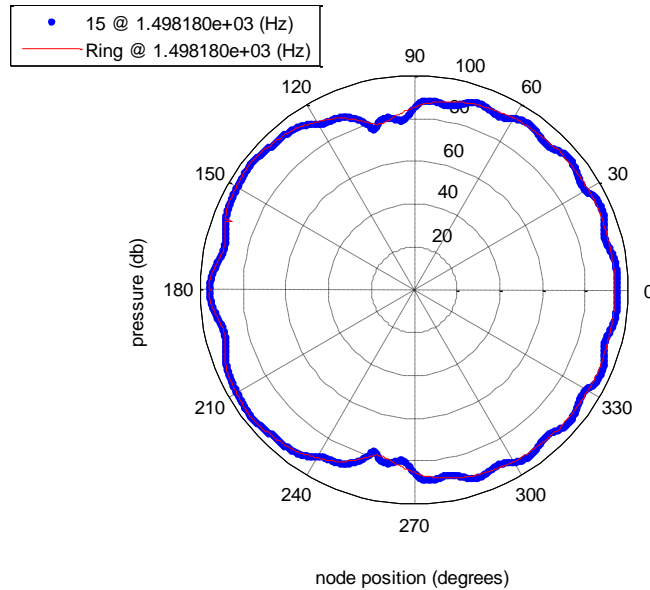
Figure 4-15 Polar plot comparing ring and the 15^0 at the threshold frequency (~ 1500 Hz).
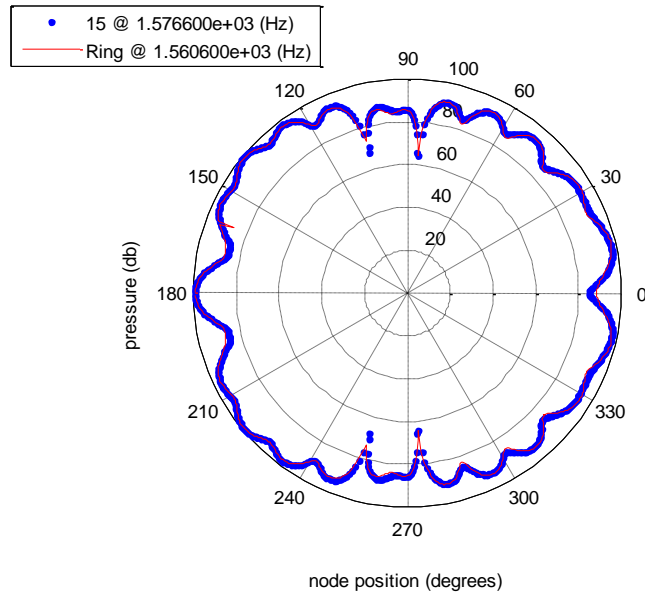
Figure 4-16 Polar plot comparing the ring and 15⁰ at the first natural frequency after the threshold frequency.
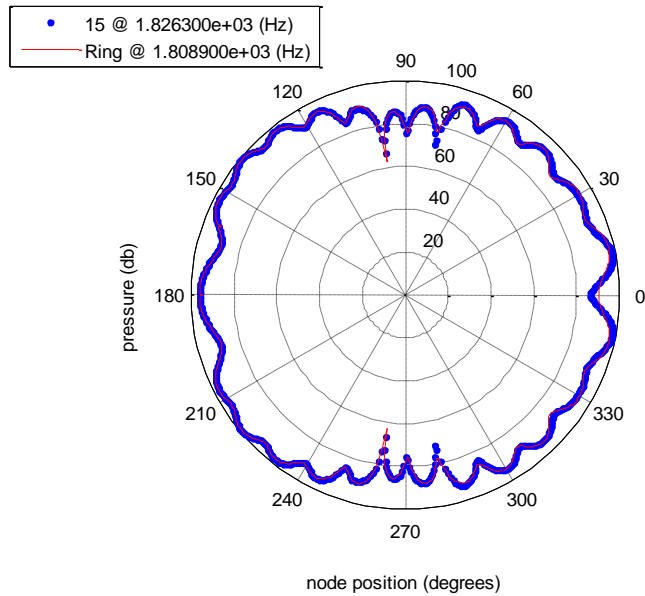
Figure 4-17 Polar plot comparing the 15⁰ and ring at ~ 1800Hz, where the resonance peaks differ at the front near node.

The ratio can be used in a converse manner too. If a known scattering response of a 2-D regular polygonal structure is compared to a circumscribing 2-D circular cylinder, length of the facet of the polygon can be determined by this ratio.

An example is presented below.
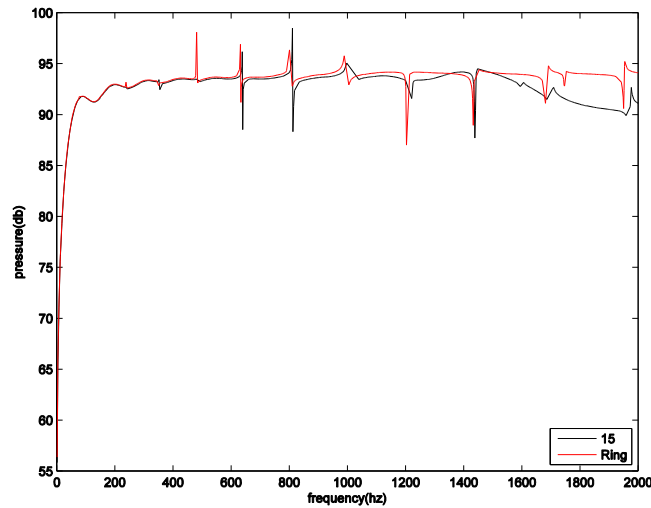
Figure 4-18 Elastic Scattering response of 15^0 compared to a ring at the front near node

Figure 4-18 shows an elastic scattering response of a polygon with angle 15 degrees (24 sides) compared to a ring of the same mass which has a diameter equal to the circle circumscribing the polygon. It is desired to calculate the facet length of the 2-D polygon. Suppose the angle subtended by the polygon is unknown and the scattering response plot is only available. From, (4.28), the threshold ratio is

$$\frac{\lambda}{L} \approx 2.24$$

From the plot, we can approximate the similarity in the scattering response characteristics of the 2-D regular polygon up to a frequency of 1500Hz, which corresponds to a wavelength of

$$\lambda = \frac{c}{f} = \frac{343.996}{1500} = 0.22933\,\text{m}$$

Thus, from the ratio, $L = 0.10238$ m.

Once the facet length is obtained, the overall polygon geometry can be approximated if it is assumed to be regular, by calculating the value of α from law of cosines. Figure 4-19
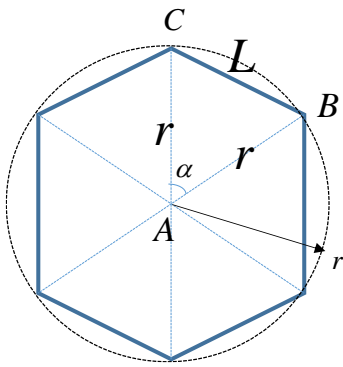
In $\triangle ABC$,

$$L^2 = r^2 + r^2 - 2r \times r \cos\alpha, \quad \Rightarrow L = r\sqrt{2 - 2\cos\alpha}$$

Figure 4-19 Law of cosines in trigonometry

From Figure 4-19, $\alpha = \cos^{-1}\left(\dfrac{2r^2 - L^2}{2r^2}\right)$, $\Rightarrow \alpha = \cos^{-1}\left(\dfrac{2 \times 0.5^2 - 0.10238^2}{2 \times 0.5^2}\right) = 11.75°$

Thus, number of sides of the polygon can be given as

$$n = 360/\alpha = 360/11.75 = 30.6 \approx 31$$

Now, to validate the results from the approximation, as it is known in this case, the angle subtended by the polygon at the centre $\alpha = 15°$, from law of cosines in trigonometry,

(Figure 4-19) $L = 0.5\sqrt{2 - 2\cos 15} = 0.13053$ m, which is quite good approximation when compared to 0.1433 m as obtained from the ratio of λ / L calculated above.

For $\alpha = 15°$, $n = 24$, which is also a good approximation, considering nothing was known about the geometry, apart from the initial assumption of the polygon being regular.

Table 4-6 Polygon variables: Comparison of the exact values with values obtained from the ratio.

Polygon Variables	Exact values	Approximate Calculation by ratio $\lambda / L \approx 2$
Length	0.13503 m	0.10238 m
Number of sides of the polygon	24	31

4.8   Acoustic Scattering by an Elastic Body - 3D

A faceted geometry (Geodesic Sphere) has been compared to a spherical shell in this section. A ratio of wavelength to the diameter of the circle circumscribing the facet (Figure 4-20) is selected to compare the acoustic scattering characteristics of the geometry. The geometric parameter in the ratio is the diameter of the circumcircle, which helps to get a sense of the overall size of the facet.
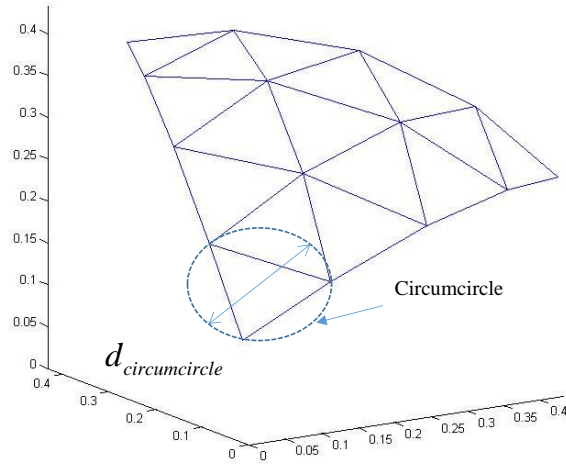
Figure 4-20 The circumcircle of a Sub-Triangle in the triangular surface.

Figure 4-20 shows a circumcircle of the Sub-Triangle. The diameter of a circumcircle is given by $d_{circumcircle} = abc/2A$, where a , b , c are the length of the sides, and A is the area of the triangle.

Since the sub-triangles are not equal, an averaged diameter of the semi-circle is calculated. Which is given as

$$d_{avg} = \frac{\sum_{i=1}^{N} d_{circumcircle,i}}{N} \tag{4.29}$$

Where N is the number of subdivisions in the geodesic.

4.8.1 Model Set-up in ABAQUS

As the acoustic medium in this case is air too, the speed of acoustic waves remain the same (342.996 m/s), which gives the wavelength 0.11467 m corresponding to highest frequency of interest (3000 Hz). Thus, the desired element length to achieve sufficient accuracy is the same discussed in Section 4.3.1 for the acoustic domain.

90

4.8.2   Domain

The domain in 3-D also has three parts similar to the case of 2-DAir domain is modelled in SOLIDWORKS and is imported into ABAQUS in .iges format. This makes the cross section solid. The 3D Shell Discretized by AC3D4: A 4-node linear acoustic tetrahedron. This air domain has an outer diameter of 1.5m and the inner diameter of 1m. The air domain is of two types which depends on the geometry. 1) The Geodesic Sphere: - The inner surface of the acoustic domain is the outer surface of the geodesic Sphere. Thus the inner surface can be enclosed in a shell of dia 1m (Figure 4-21). 2) The Spherical Shell: The inner surface of the acoustic domain is the outer surface of the shell. Thus the inner surface is a shell of dia 1m (Figure 4-22).
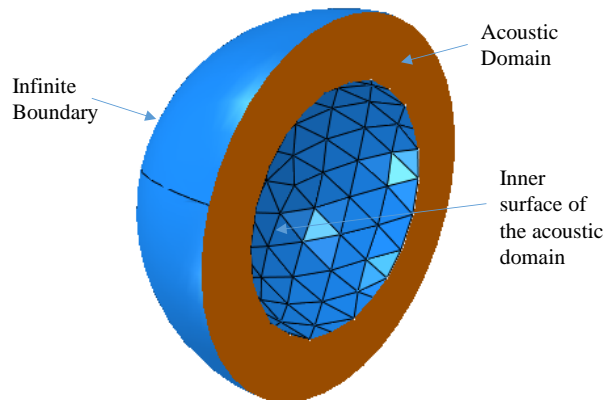
Figure 4-21 The 3-D-acoustic domain for geodesic Sphere.
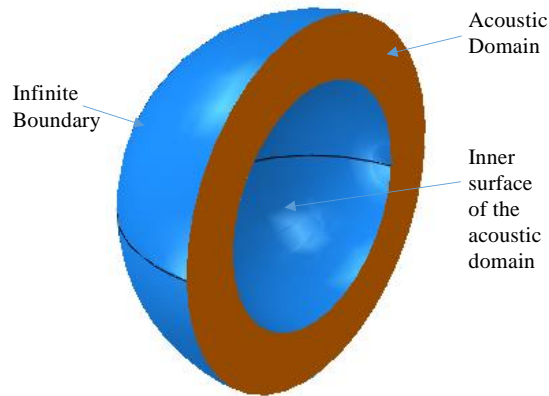
Figure 4-22 The acoustic domain for a spherical shell

The domain has the properties of air as given by

Table 4-7 and a Solid, Homogeneous section. The section is created and assigned in the property module of ABAQUS.

The Part for the infinite boundary is a 3D Deformable-Shell. , type revolution, modelled in ABAQUS sketch module. The part has an acoustic infinite section of an order 10, discretized by ACIN3D3: A 3-node acoustic infinite element with linear surface interpolation. This domain has the properties of air as given by

Table 4-8 and an Acoustic infinite section. The reference node for the infinite elements is given by editing the input file generated by abaqus. Explained in Appendix.6.4 The boundary is spherical having a diameter of 1.5m. The diameter of the boundary is set by doing a convergence study.

The elastic structure is a 3D Shell modelled in SOLIDWORKS and is imported into ABAQUS in .acis format. This format keeps the model as an enclosed shell. The part is discretized by S3: A 3 node triangular general-purpose shell, finite membrane strains.

The part is modelled with varying thickness and has the properties as explained in Natural Frequency extraction. (Chapter 3)

Table shows the summary of the properties of the parts created.

1. Elastic Domain can be referred from Table 3-4

2. Acoustic Domain

Table 4-7 Properties of the acoustic domain

Domain	3-D Solid – Deformable (Modelled in SOLIDWORKS)	
Material	Air	Density = 1.2 kg/m^3
		Bulk Modulus = 1.42e5 Pa
Section	Solid Homogeneous	
Mesh	Acoustic elements: AC3D4 – A 4 - node linear acoustic tetrahedron.	

3. Acoustic Infinite Domain

Table 4-8 Properties of the Infinite Domain

Domain	3-D Deformable – Shell	
Material	Air	Density = 1.2 kg/m^3
		Bulk Modulus = 1.42e5 Pa
Section	Acoustic Infinite, order 10.	
Mesh	Acoustic infinite elements: ACIN3D3 – A 3 node acoustic infinite element with linear surface interpolation	

4.8.3 Step

The step definition is the same as in the case of 2-D with the frequency sweep from 1-3000Hz.

4.8.3.1   Interaction properties

The properties of the incident wave remain the same as in 2-D, with the amplitude defined in Table 4-3. The interaction is defined twice as the structure fluid interface has two surfaces.

For all the geometries, the same source and stand-off point is to be chosen to have a fair comparison of the results. The stand-off point is taken as one of the vertex of the triangle of the icosahedron. The incident wave is in the radial direction, and the corresponding point in the acoustic domain is calculated. The position vector ($\vec{r}_{in}$) of one of the vertices of triangle face is $\vec{r}_{in} = x\hat{i} + y\hat{j} + z\hat{k}$, where x, y and z are same for all the geodesics. The magnitude is calculated as $|\vec{r}_{in}| = \sqrt{(x)^2 + y^2 + (z)^2} = 0.5m$, the unit vector in that direction is $\hat{n} = \vec{r}_{in}/|\vec{r}_{in}|$. The source point is in the same direction (radial) and has a magnitude equal to the radius of outer boundary of the acoustic domain, which is 0.75m. Thus the source point is calculated as $\vec{r}_{out} = 0.75\hat{n}$. The calculation done in this thesis is presented below. The stand-off point is vertex of the icosahedron triangle face. (Vertex 15 in Table 2-5)

$$\vec{r}_{in} = 0.4253254041760199\hat{i} + 0\hat{j} + 0.2628655560595668\hat{k}$$

$$|\vec{r}_{in}| = \sqrt{(0.4253254041760199)^2 + 0^2 + (0.2628655560595668)^2}$$

$$= 0.4999999999999999 \text{ m} \approx 0.5\text{m}$$

$$\hat{n} = \vec{r}_{in} / |\vec{r}_{in}|$$

$$|\vec{r}_{out}| = 0.75\text{m}$$

$$\vec{r}_{out} = 0.75\hat{n}$$

Which gives RP-2 = $0.6379881062640299\hat{i} + 0\hat{j} + 0.3942983340893503\hat{k}$

Thus, the source and stand-off point selected is exactly the same for all the geometries.
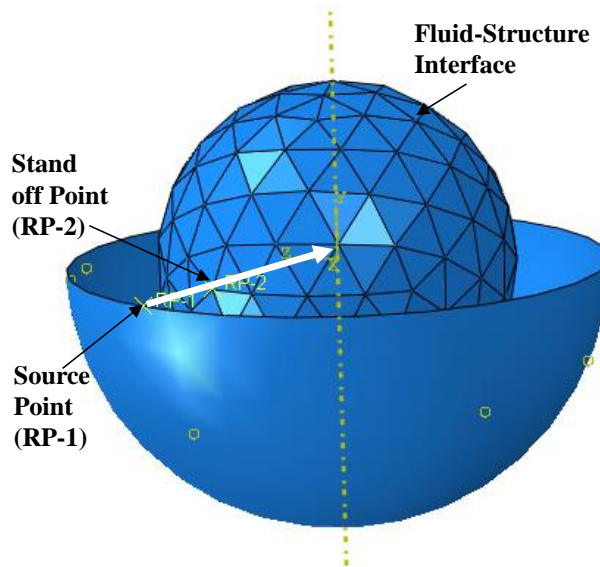
Figure 4-23 Interaction definition of the 3-D Model

4.8.4   Constraints

In this case too, the structure-acoustic coupling is done by using the TIE constraint. The structure is the master surface and the acoustic domain is the slave. The infinite

boundary is also tied to the outer surface of the acoustic domain by TIE constraint. In this case the acoustic domain is the master surface and the infinite domain is the slave.

4.8.5 Field Output Requests

Acoustic Pressure (POR) is requested as a field output for the node sets mentioned Table 4-9. This acoustic pressure is later used to calculate the target strength and plotted against the frequency.

Table 4-9 Field Output Requests at Nodes

Position	X-coordinate	Y-coordinate	Z-coordinate
Front near node	0.425325394	0	0.262865543
Back near node	-0.425325394	0	-0.262865543

4.8.6 Job

After setting up the entire model, a job is created in a desired folder by setting up the work directory. As calculations for the numerical problem require more computational resources, the input files are created first and then submitted onto the Palmetto cluster.

4.9 Target Strength

The target strength is calculated at the front and back near node. The front far node is in the same direction as the front near node is from the origin. The source point and the nodes at which the target strength is calculated is kept the same for all models for consistency in scattering characteristics.

Front near node
(0.4253254041760199, 0,
0.2628655560595668)

Front far node (Source Point)
(0.6379881062640299, 0,
0.3942983340893503)

Back near node
(-0.4253254041760199,
0, -0.2628655560595668)
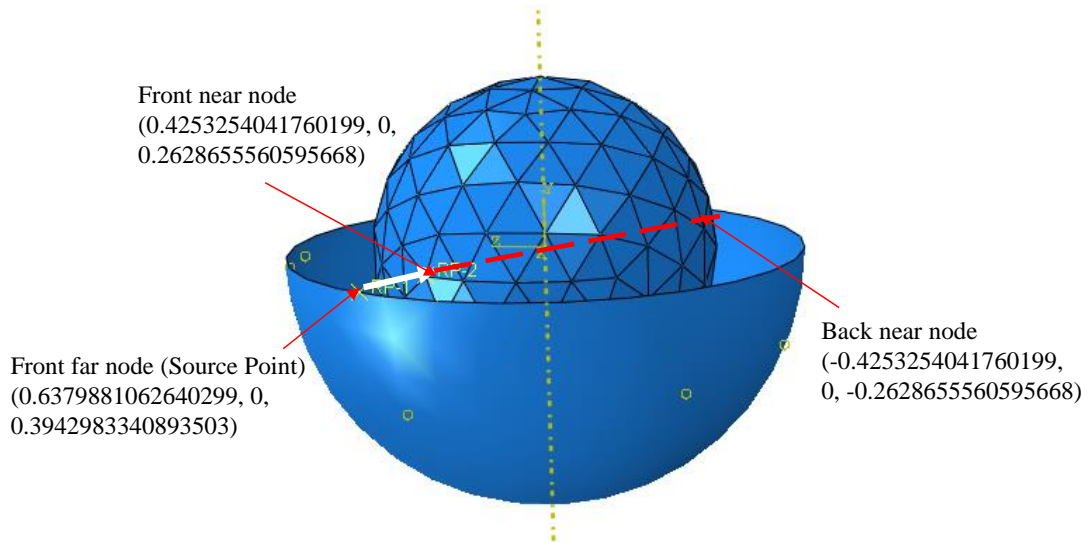
Figure 4-24 Front and back near nodes at which the Target Strength is calculated.

4.10 Mesh Convergence

Figure 4-25 and Figure 4-26, show the mesh convergence study for the front near and the back near node respectively. The scattering response of a spherical shell is compared for a seed size of 0.02m and 0.015m.
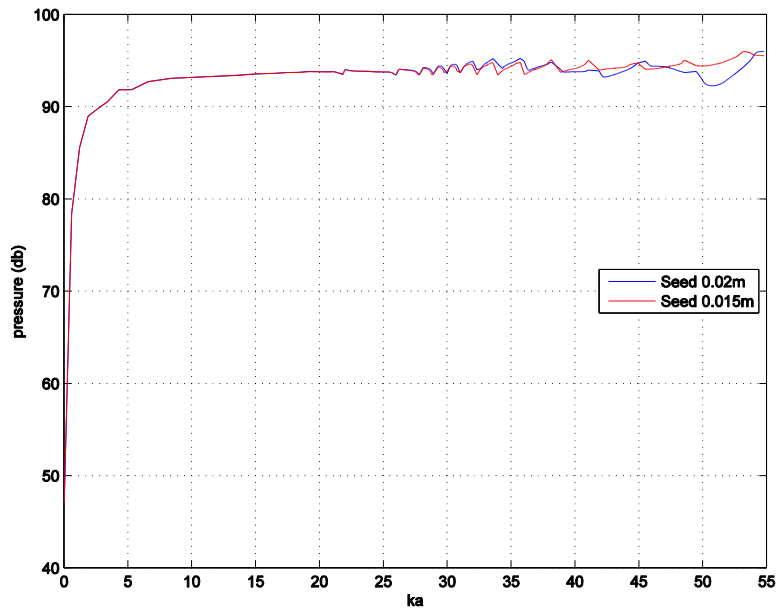
Figure 4-25 Mesh Convergence study for the front near node
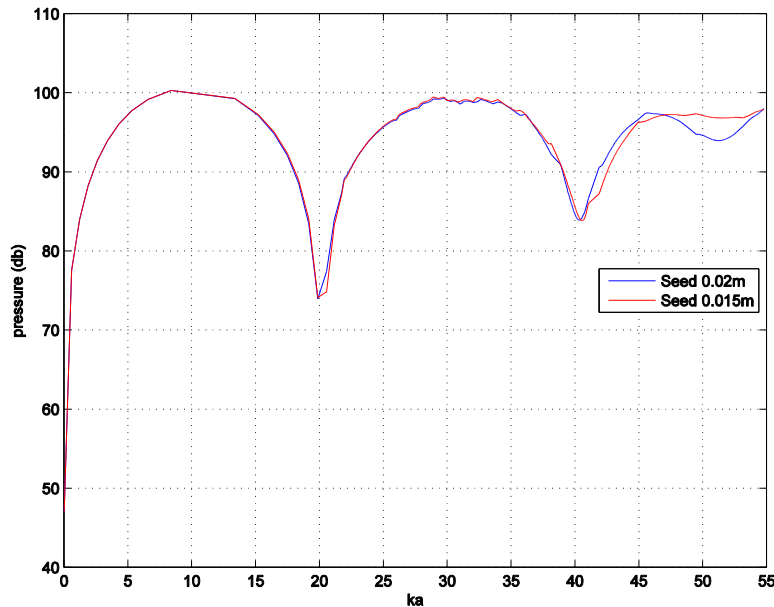
Figure 4-26 Mesh convergence study at the back near node

The seed size is not an accurate measure of the element size, but it gives a guide, which can be considered as an approximation for the size of the element. The seed size of 0.02m, corresponds to approximately 6 elements per smallest wavelength in the Acoustic Domain, whereas 0.015m corresponds to approximately 9 elements per smallest wavelength (i.e. f = 3000 Hz) (Figure 4-27) . As, the elements with seed size 0.015m have more number of elements per wavelength, they can better approximate a sinusoidal wave and give more accurate results at higher frequencies. It should be noted that increasing the number of elements, increases the number of nodes, which inturn increases the degrees of freedom. This leads to an increase in computational cost. In case of 3D, as size of the finite element domain is considerably large than that of the 2D finite element domain, the computational cost becomes a big factor in the selection of the element size.
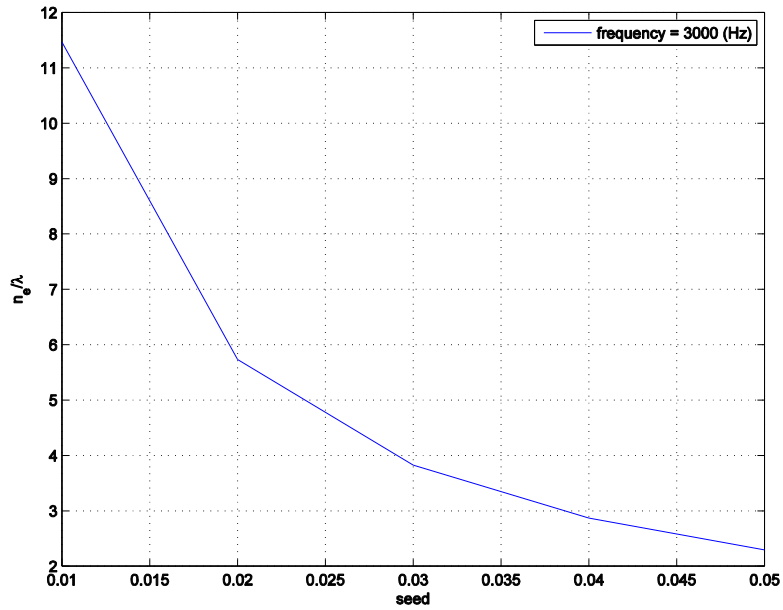
Figure 4-27 seed size v/s number of elements for a frequency of 3000 Hz.

Figure 4-28 shows a bar graph comparison of the computational resources utilized. The memory required for seed 0.02 m is almost half of the memory required for seed 0.015 m. And comparing the wall time, calculation with the mesh density with seed 0.02 m takes around 15 hours and seed 0.015 takes around 43 hours. The considerable computational cost for the seed size 0.015m and acceptable error in the scattering response at higher frequency makes the seed size 0.02 m as the selected mesh size.

PALMETTO CLUSTER:
COMPUTATIONAL RESOURCES

PALMETTO CLUSTER:
COMPUTATIONAL RESOURCES
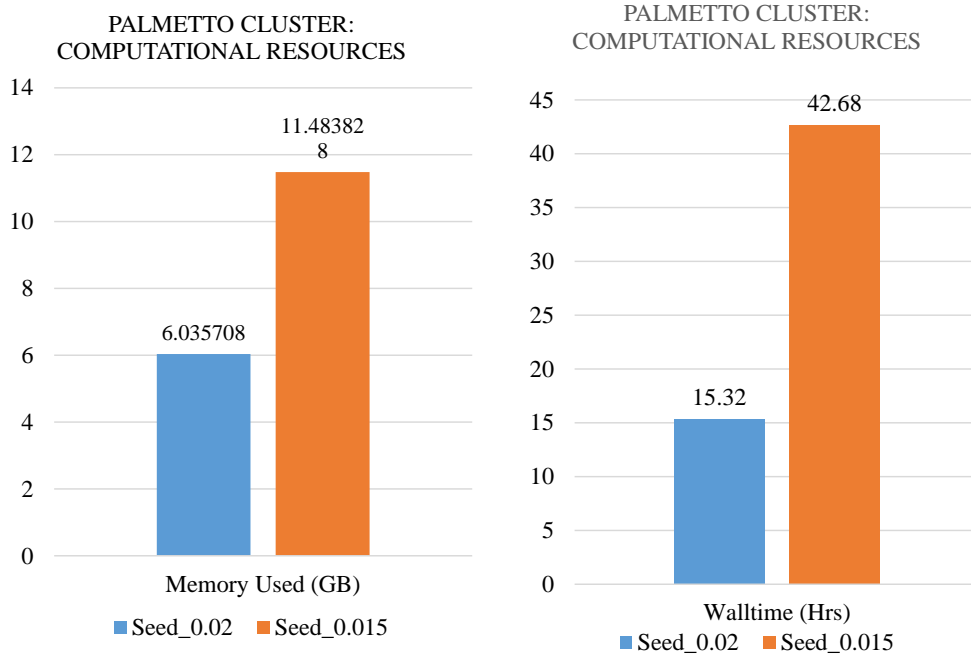
Figure 4-28 Bar Graphs comparing the computational resources utilized for the numerical calculations. For all the cases number of cpus is 64.

4.11 Location of the infinite boundary

A convergence study is done to truncate the acoustic domain by the infinite boundary condition. Two factors have been taken into consideration 1) Convergence (especially towards the lower frequency range; 1-2000 Hz). 2) Computational cost. The acoustic scattering is requested at the same points at the front and the back end for the same spherical shell geometry under investigation. Three different boundaries are investigated 1) Diameter 1.5m 2) Diameter 1.75m 3) Diameter 2m
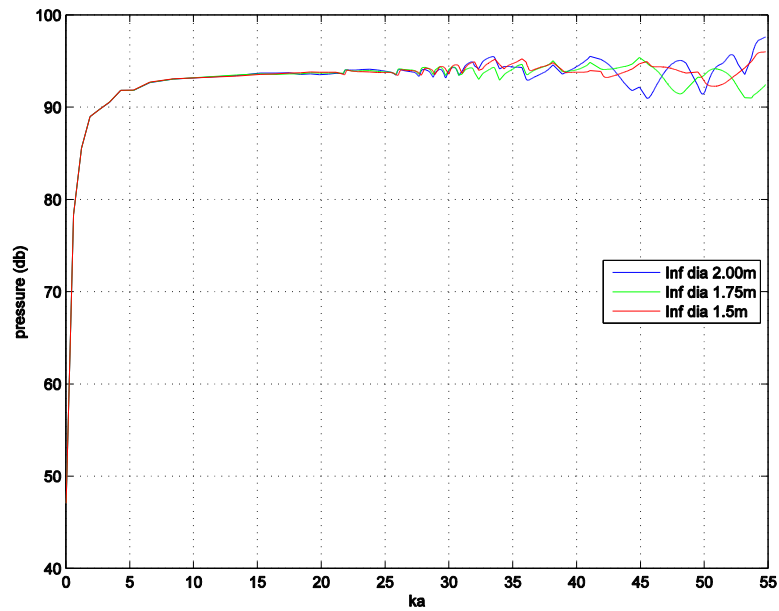
Figure 4-29 Convergence study for the location of the infinite boundary at the front end.
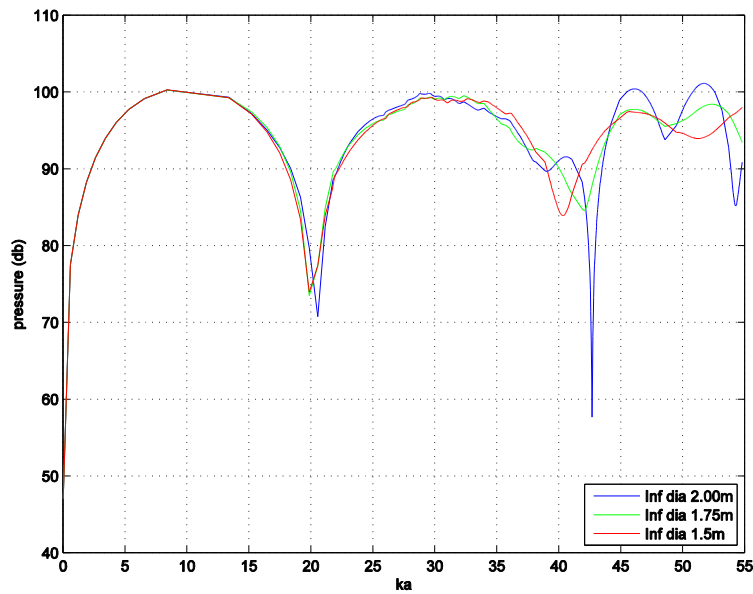
Figure 4-30 Convergence study for the location of the infinite boundary at the back end.

Figure 4-29 and Figure 4-30 show the convergence study for the location of the infinite

boundary. The curves show good agreement, especially for the front end. Beyond ka = 35

(f ~ 2000 Hz), however, the curves show a good trend but desirable convergence is not achieved, especially at the back end, where the scattering response requires more accuracy.

Figure 4-31, the bar graphs show the memory required in Gigabytes and the wall time in hours. The number of cpus is 64 for all the cases. It can be seen clearly, that for the same number of processors, memory required and the wall time is the least for infinite boundary @ 1.5m. Upto ka = 35, both at the front and back end, good agreement is observed for all three locations of the infinite boundary, and considering the computational resources required, the spherical acoustic domain is truncated by the infinite boundary at 1.5m.
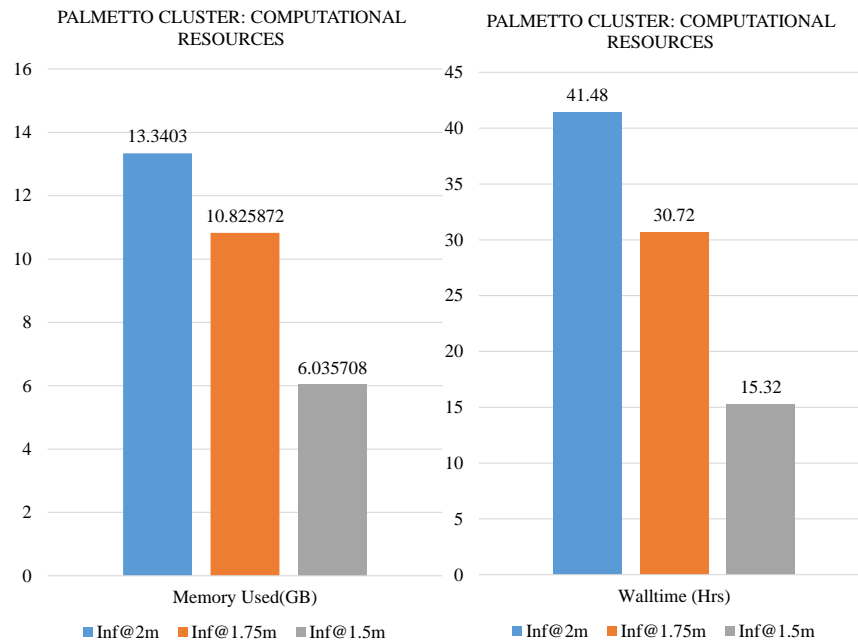
Figure 4-31 Bar Graphs comparing the computational resources utilized for the numerical calculations. For all the cases, mesh density is the same with seed size 0.02m and number of cpus is 64.

4.12 Scattering response of the geometry 3-D

Figure 4-32 and Figure 4-33 show the target strength plots of scattering from the 3-D elastic bodies at the front and back near node.
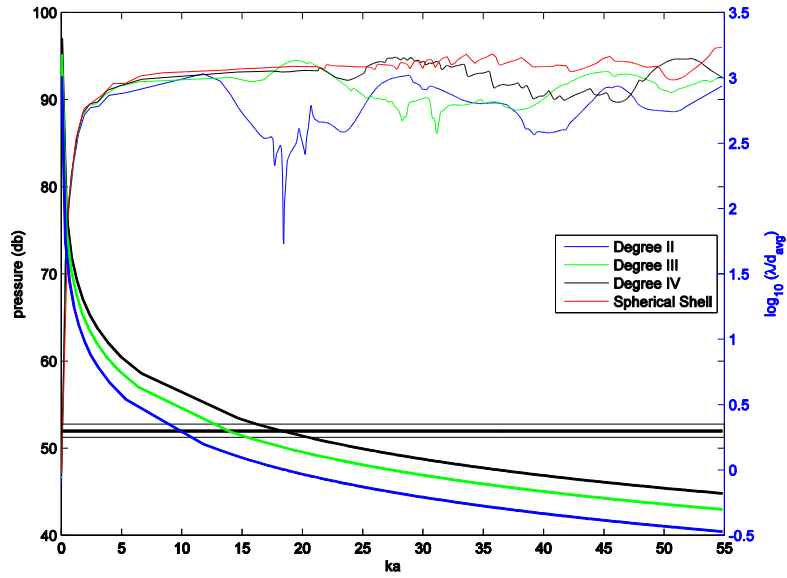
Figure 4-32 Elastic Scattering response at front end (3-D)
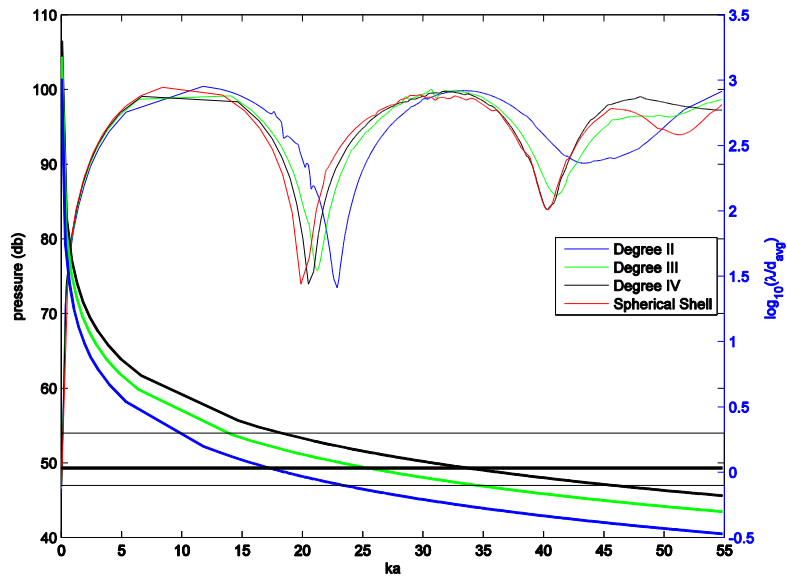
Figure 4-33 Elastic Scattering response at back end (3-D)

A similar study has been done like the 2-D case. The left y-axis is a measure of the Target strength (black axis) and the y-axis on the right (red) represents the log scale of the ratio of wavelength to average circumcircle diameter for different geometries. The x-axis represents the frequency range normalized into *ka*. This non-dimensional frequency is calculated in the same way as in the case of 2-D. The shortest wavelength of interest is around 9 times smaller than the diameter of the spherical shell.

The three curves on the bottom half of the plot are interpreted by the red y axis and scattering response curves at the top half by the black y axis.

As the degree of geodesic increases, the number of sub - triangles the triangular surface is divided into increases. Hence increasing the resolution and thereby approaching the surface area of the circumscribing sphere. The acoustic scattering response trend also starts to match closely up to higher frequency limits as the degree of the geodesic increases.

The horizontal band in the plot gives a range of the ratio of wavelength to the average circumcircle diameter upto which the scattering characteristics of a geodesic shell can be approximated as a spherical shell. It is interesting to note that the width of the band is smaller for the target strength calculated at front near node than that of the back near node, showing more variation in the scattering characteristics of the model at the back near node.

The thick black horizontal line in the plot gives a mean value of the band. Just as in the case of 2-D, this value is subjective and can be considered as a rule of thumb for predicting the threshold frequency at which the scattering from a geodesic sphere matches closely with the shell. The frequencies corresponding to the point at which the line

intersects these curves are considered to be the frequency when the respective geometry deviates from behaving like a spherical scatterer.

Hence analogous to 2-D, for a faceted 3-D geodesic sphere, when an acoustic wave is incident on one of its corners, its response matches closely with a spherical shell if,

$$\log_{10}\left(\frac{\lambda}{d_{avg}}\right) \approx 0.3, \quad \Rightarrow \left(\frac{\lambda}{d_{avg}}\right) \approx 2 \tag{4.30}$$

The threshold ratio of wavelength to the average circumcircle diameter is approximately 2, when the acoustic response from front near node is considered.

The range of the bandwidth is given as $0.25 < \log_{10}(\lambda / d_{avg}) < 0.35$, which gives

$$1.78 < (\lambda / d_{avg}) < 2.24$$

For a higher degree of geodesic sphere, the ratio is found to be closer to the lower level of the band. This is expected, as the threshold frequency is higher for the higher degree of the geodesic spheres. Thus, the corresponding wavelength is smaller for higher degree of the geodesic, thus giving a smaller ratio. It is important to note that as the degree of geodesic increases, the average diameter of the circumcircle decreases. As d_{avg} is inversely proportional to the threshold ratio, one could expect it to increase as d_{avg} decreases. From the trend of the plots, it can be inferred that the decrease in the average circumcircle diameter is less effective than the decrease in the wavelength, which reduces the ratio as we move to higher degree geodesics.

It is important to note that this numerical factor is subjective and depends upon the tolerance value used.

Similarly at the back node, the ratio is given by

$$\log_{10}\left(\frac{\lambda}{d_{avg}}\right) \approx 0.03, \quad \Rightarrow \left(\frac{\lambda}{d_{avg}}\right) \approx 1.07$$

The range of the band in terms of the log of the ratio of wavelength to the average circumcircle diameter for the back near node is given as $-0.1 < \log_{10}(\lambda / d_{avg}) < 0.3$ which can be written as

$$0.79 < \lambda / d_{avg} < 1.99$$

In this case also, the lower degree (<2) will have a ratio towards the higher value of the band and the higher degree will have the ratio towards the lower value.

Acoustic scattering response at the inner surface acoustic nodes have been calculated for comparing degree IV geodesic with the spherical shell. The contour plots on the surface are presented at some frequencies of interest. Figure 4-34 to Figure 4-37 show the contour plots of acoustic pressure at different frequencies. Figure 4-34 shows the contour plot at the first natural frequency of the shell (f = 1199 Hz) and geodesic degree IV (f = 1166 Hz). The acoustic pressure distribution on the inner front and back surfaces is similar for both the cases. The scattering response curves for shell and geodesic degree IV in Figure 4-32 and Figure 4-33also matches closely. Further, it was noted in Section 3.6, that the mode shapes of shell and geodesic degree IV were similar. Hence this was an expected result. Note that the legend in these contour plots show the acoustic pressure and not the Target strength.

Figure 4-35 Shows the contour plot at a frequency beyond the threshold frequency for the front near node. It can be clearly seen, that the pressure distribution varies for both the geometries especially at the front surface around the front near node. (Figure 4-35(a)). The target strength plot at the back near node for shell and geodesic degree IV matches closely, hence the back inner surface does not show much variation in the pressure distribution. This further validates the scattering response curves at the front near node and back near node.

Shell (f = 1199 Hz; *ka* = 21.9)   Degree IV Geodesic (f = 1166 Hz; *ka*=21.29)
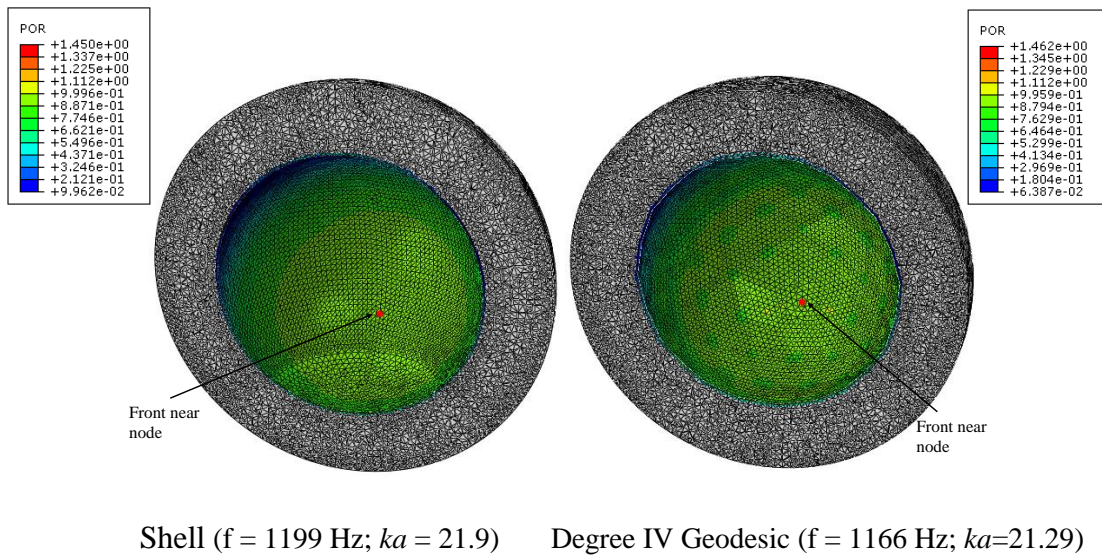
(a) Front Near Surface
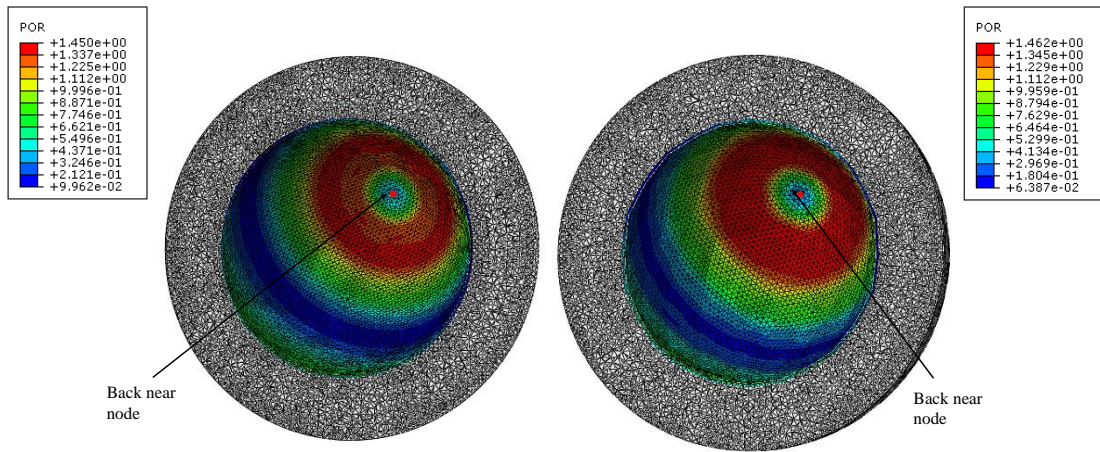
Shell (f = 1199 Hz; *ka* = 21.9)   Degree IV Geodesic (f = 1166 Hz; *ka* = 21.29)

(b) Back near Surface

Figure 4-34 Contour plots of Acoustic Pressure (POR) comparing shell and degree IV geodesic at the first natural frequency for the (a) front near surface (b) back near surface.
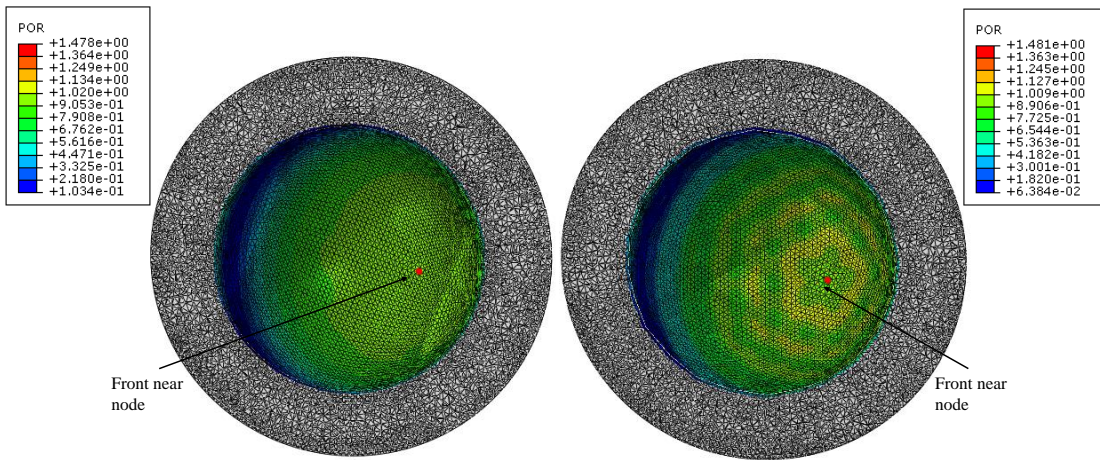
Shell (f = 1338 Hz; *ka* = 24.4)   Degree IV Geodesic (f = 1338 Hz; *ka* = 24.4)

(a) Front near Surface

POR
+1.478e+00
+1.364e+00
+1.249e+00
+1.134e+00
+1.020e+00
+9.053e-01
+7.908e-01
+6.762e-01
+5.616e-01
+4.471e-01
+3.325e-01
+2.180e-01
+1.034e-01

Back near node

POR
+1.481e+00
+1.363e+00
+1.245e+00
+1.127e+00
+1.009e+00
+8.906e-01
+7.725e-01
+6.544e-01
+5.363e-01
+4.182e-01
+3.001e-01
+1.820e-01
+6.384e-02
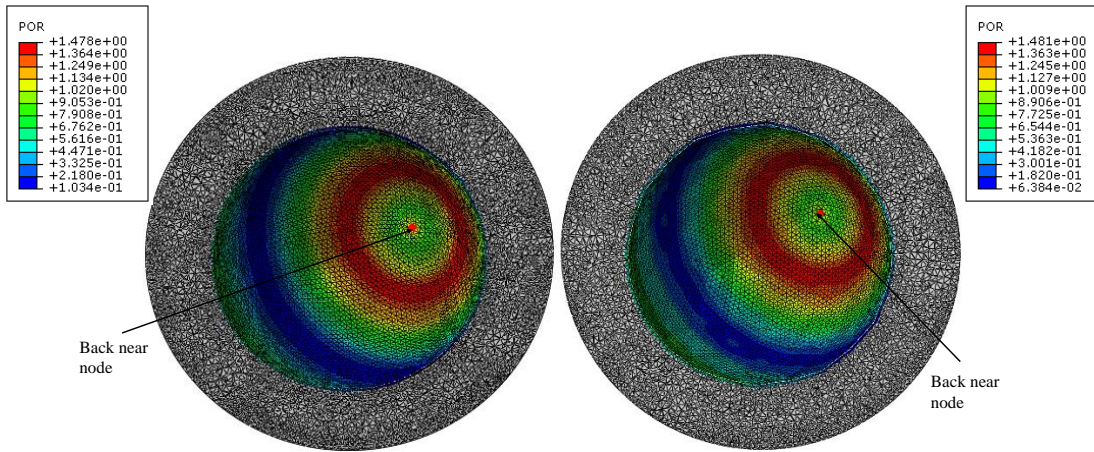
Back near node

Shell (f = 1338 Hz; *ka* = 24.4)   Degree IV Geodesic (f = 1338 Hz; *ka* = 24.4)

(b) Back near Surface

Figure 4-35 Contour plots of Acoustic Pressure (POR) comparing shell and degree IV geodesic at a frequency beyond the threshold frequency for the front near node ka ~ 24(~1300 Hz) at (a) front near surface (b) back near surface.

Figure 4-36 now shows the contour plot at a frequency (f = 2710 Hz) beyond the threshold frequency at the back near node. The acoustic pressure distribution can be seen to vary at both the front and the back inner surfaces. Figure 4-37 shows the acoustic pressure distribution for the highest frequency of interest i.e 3000 Hz.
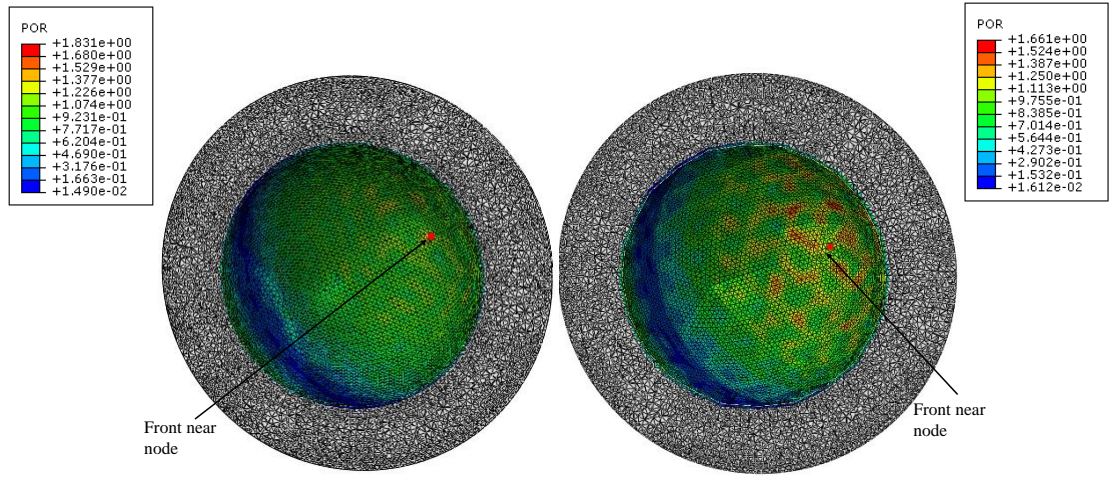
Shell (f = 2710 Hz; *ka* = 49.5)   Degree IV Geodesic (f = 2711 Hz; *ka* = 49.5)

(a) Front near Surface
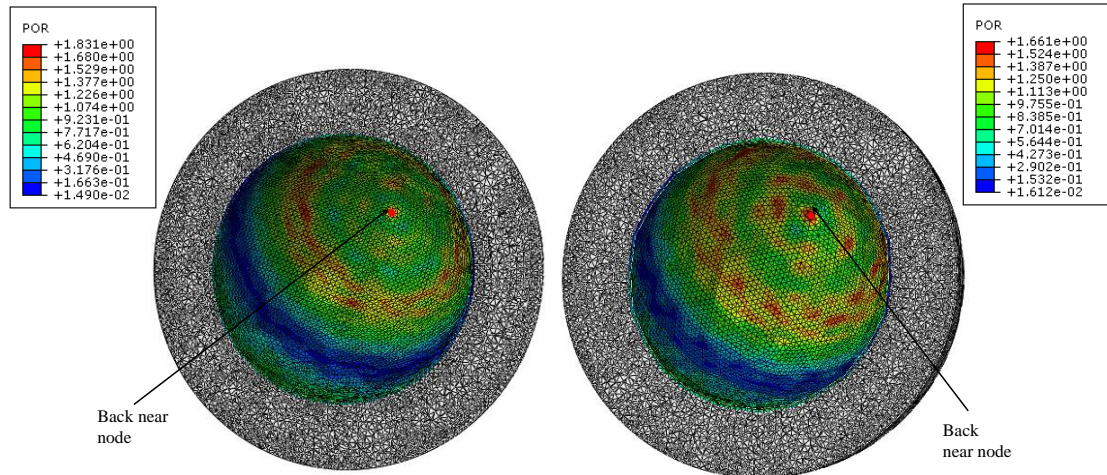
Shell (f = 2710 Hz; *ka* = 49.5)   Degree IV Geodesic (f = 2711 Hz; *ka* = 49.5)

(b) Back near Surface

Figure 4-36 Contour plots of Acoustic Pressure (POR) comparing shell and degree IV geodesic at the threshold frequency for the back near node (2710 Hz) at (a) front near surface (b) back near surface.
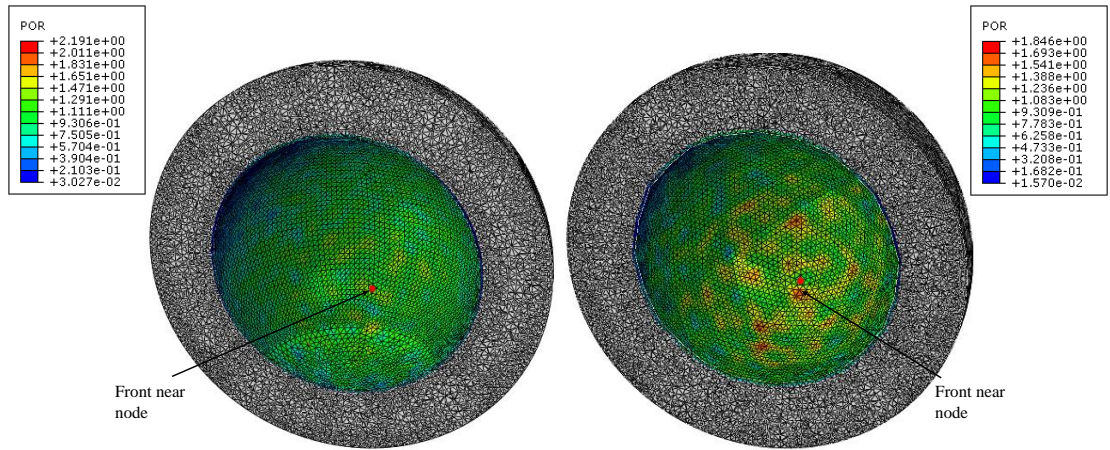
Shell (f = 3000 Hz; *ka* = 54.79)   Degree IV Geodesic (f = 3000 Hz; *ka*=54.79)

(a) Front Near Surface
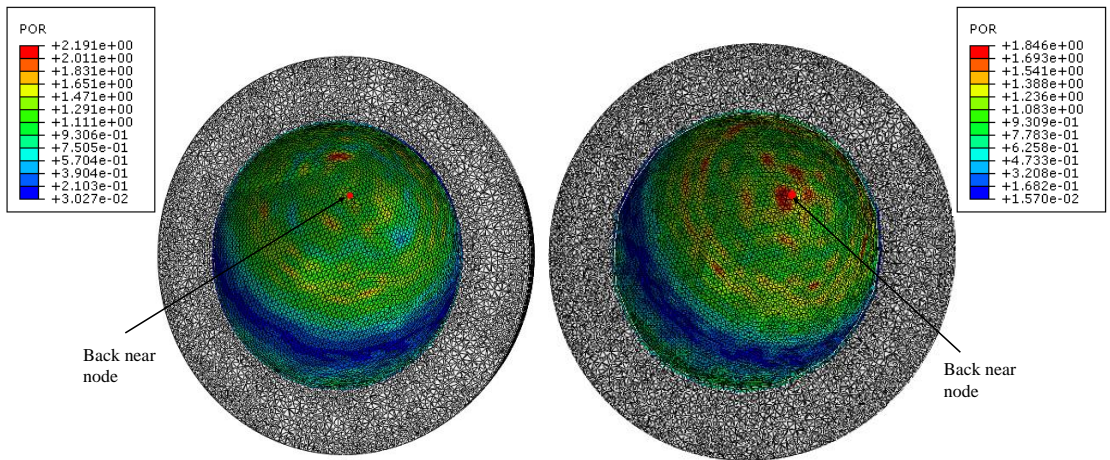
Shell (f = 3000 Hz; *ka* = 54.79)   Degree IV Geodesic (f = 3000 Hz; *ka*=54.79)

(a) Back Near Surface

Figure 4-37 Contour plots of Acoustic Pressure (POR) comparing shell and degree IV geodesic at the 3000 Hz for the (a) front near surface (b) back near surface.

With this ratio, conversely, knowing the scattering response of an unknown geometry at the target point, for low frequencies and comparing it with a shell can help approximately determine the facet size of the geometry.

An example is presented just like the case in 2-D.
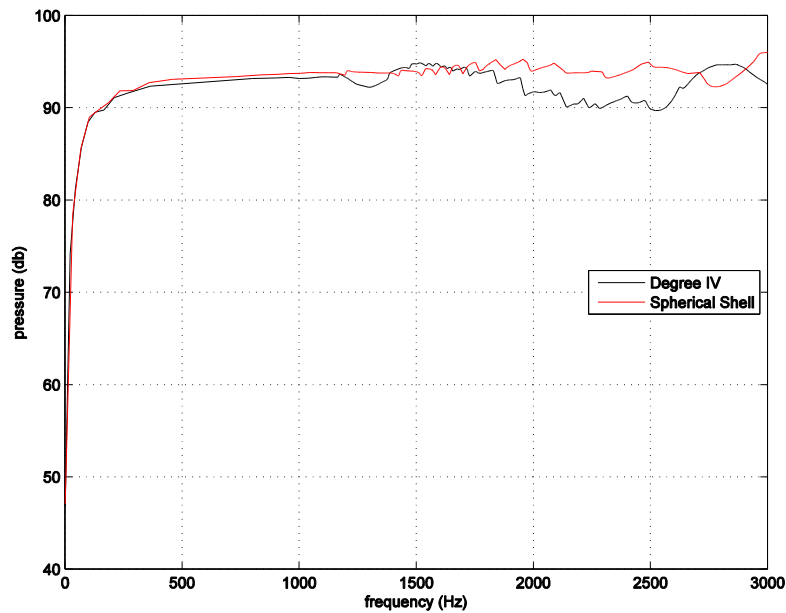
Figure 4-38 Scattering response of Degree IV in comparison to the spherical shell

.On similar lines as in 2-D, if the size of the facet can be determined by the ratio

$$\left(\frac{\lambda}{d_{avg}}\right) \approx 2$$

From , (4.30)we can approximate the similarity in the scattering response characteristics of the geodesic sphere up to a frequency of around 1200 Hz, which corresponds to a wavelength of

$$\lambda = \frac{c}{f} = \frac{343.996}{1338} = 0.28633 \text{ m}$$

Thus, from the ratio, $d_{avg} = 0.1433$m.

From the MATLAB code attached in the appendix 6.3, for a degree IV geodesic, the average diameter of the circumcircle is $d_{avg} = 0.1726$ m.

Thus, a close approximation to the diameter of the circumcircle is obtained.

4.13 Rigid body scattering - 2D

In this section, a layer of complexity is removed by performing a scattering analysis from a rigid body. This case is a reference for the scattering from an elastic body and is performed to validate the results obtained from the elastic body scattering. The resonance peaks will not be observed in the scattering response, as in the case of the elastic body scattering, but the trend is expected to be similar.

To simulate a rigid body condition, the inward normal derivative of pressure per unit density of the acoustic medium is zero. Hence in ABAQUS, if no boundary condition is specified on any boundary, it is treated as a rigid body.

4.13.1 Domain

As there is no boundary condition to be specified, no structural-acoustic coupling is required. Hence the elastic part is not modelled in this case. Thus the model has 2 parts. The Air domain and the acoustic domain. The domain size is kept the same as in the case of scattering by elastic body (section). The model and the properties are the same too.

4.13.2 Step

Same step is created, but instead of using the natural frequencies of the model as interval points, intervals of 200Hz are made.

4.13.3 Interaction Properties

The interaction properties remain the same too. But instead of defining properties for two surfaces, property for just the acoustic surface is defined as there is no elastic body present.
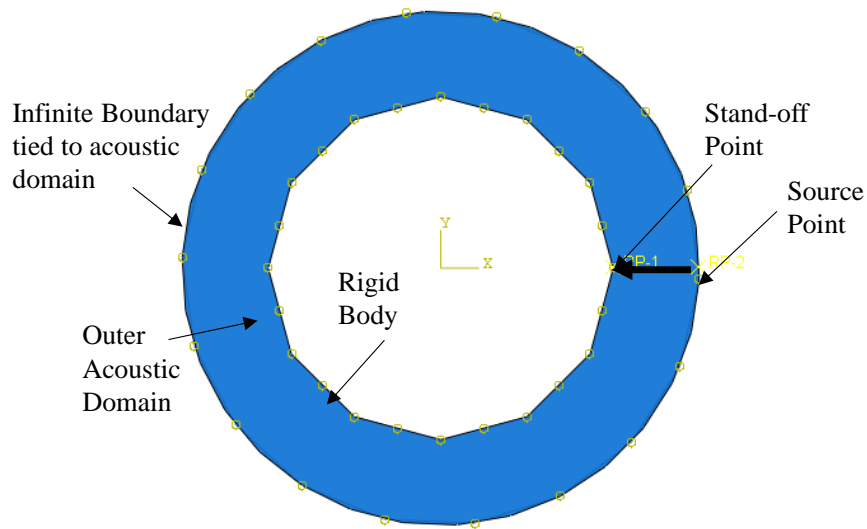
Figure 4-39 Interaction property definition.

4.13.4 Constraints

As there is no elastic body, there is only one TIE constraint between the acoustic domain and the infinite boundary.

4.13.5 Field Output Requests

Acoustic Pressure (POR) is requested at the same points as before.

4.13.6 Job

Job is submitted in the same way in the Palmetto Cluster.

4.14 2-D Rigid Body Scattering response

Figure 4-40 and Figure 4-41 show the scattering response from a rigid body at the front and back near nodes. The trend is similar to that of the scattering response from the elastic body.
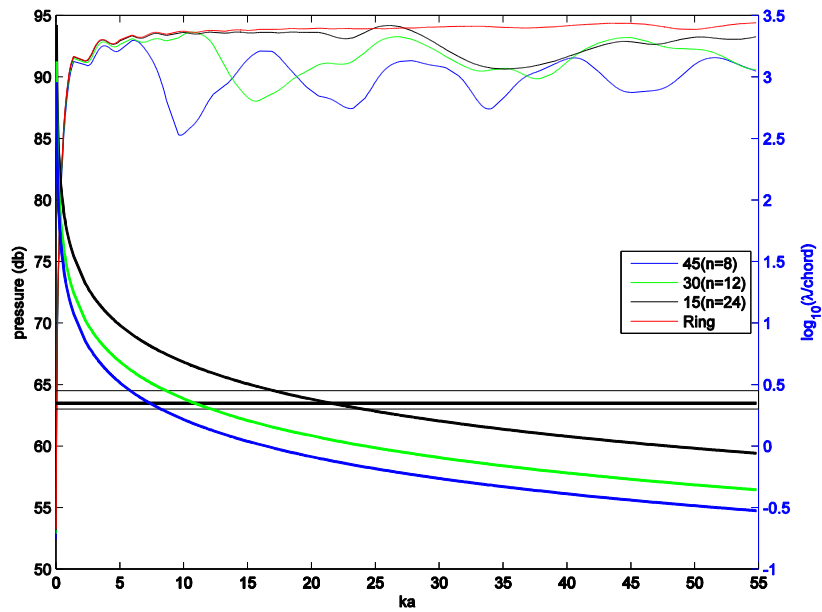
Figure 4-40Rigid body scattering response at front end for 2-D.
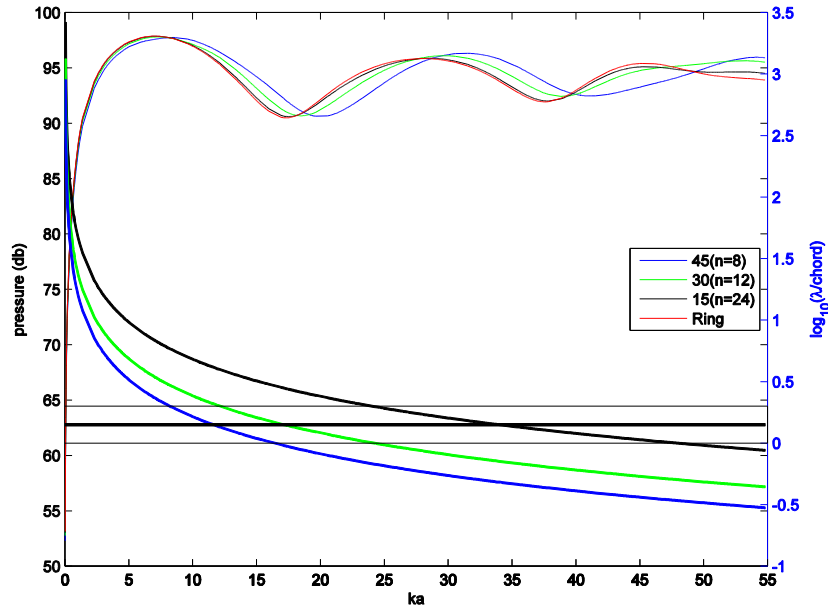
Figure 4-41 Rigid Body scattering response at back end for 2-D.

The major difference in the rigid and elastic scattering response plots is the peaks observed at resonance. This shows the importance in capturing the mode shapes and the natural frequencies of the coupled elastic body.

The bandwidth range falls on the same area in case of rigid body scattering too. The range of the threshold ratio for the near node can be given by $0.3 < \log_{10}(\lambda/L) < 0.45$, which gives

$$1.99 < (\lambda/L) < 2.82$$

And the mean threshold ratio is approximately the same as obtained in the scattering from elastic body.

$$\log_{10}\left(\frac{\lambda}{L}\right) \approx 0.35, \quad \Rightarrow \left(\frac{\lambda}{L}\right) \approx 2.24$$

116

For the back near node too, we can see no resonance peaks present. The threshold frequency can be given as,

$$\log_{10}\left(\frac{\lambda}{L}\right) \approx 0.15, \quad \Rightarrow \left(\frac{\lambda}{L}\right) \approx 1.41$$

And the bandwidth range for the back near node is given as $0 < \log_{10}(\lambda/L) < 0.3$ which can be written as

$$1 < (\lambda/L) < 1.99$$

As the plots follow the same trend, the values of the threshold ratio are approximately in the similar range as obtained in the elastic body scattering.

4.15 Rigid Body Scattering – 3D

This case also does not have an elastic body and there is an absence of structural-acoustic coupling

4.15.1 Domain

Only 2 parts are created in this case. The Acoustic Domain and the infinite boundary. The parts have the same properties and dimensions as in the elastic body scattering case.(Section 4.3.1.1)

4.15.2 Step

Step is the same as in Section 4.3.1.2

4.15.3 Interaction Properties

The properties remain the same, except just one interaction surface is defined.
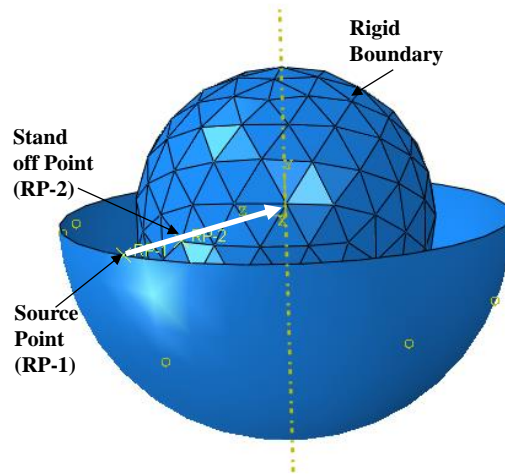
Figure 4-42 Interaction Properties for the rigid body scattering

4.15.4 Constraints

TIE constraint is applied only for the acoustic and infinite element.

4.15.5 Field Output Requests

Acoustic pressure (POR) is requested at the same points

4.15.6 Job

Job is submitted in Palmetto Cluster.

4.16 Rigid body scattering response for the 3-D geometry.

From Figure 4-43 and Figure 4-44, it can be seen that the scattering response at the front and back end follows a similar trend as seen in the elastic scattering response curves of 3-D geometries
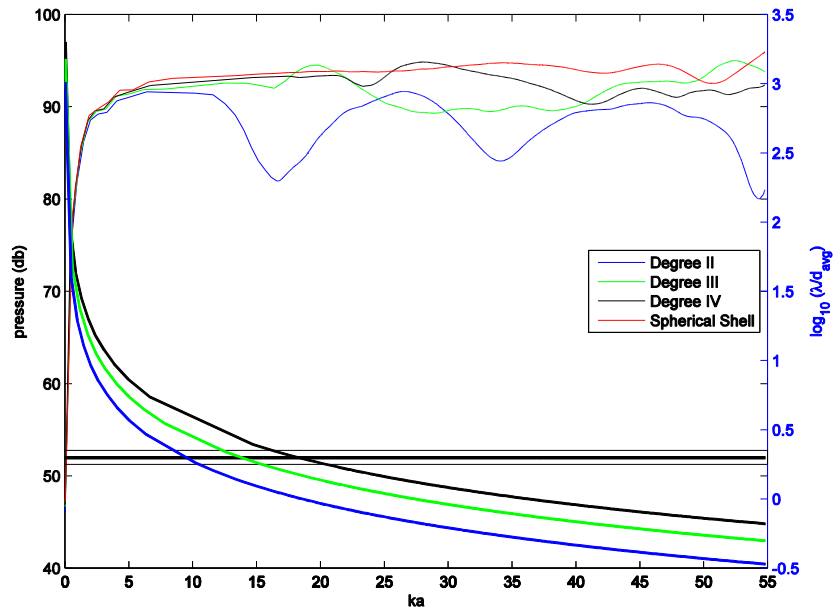
Figure 4-43 Rigid body scattering response at the front end for 3-D
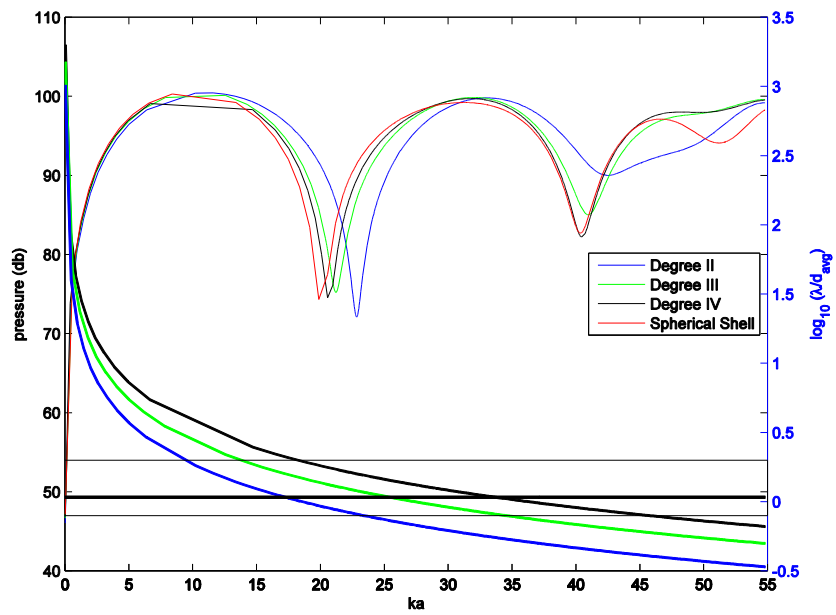
Figure 4-44 Rigid body scattering response at the back end for 3-D

119

A threshold ratio of λ / d_{avg} lies in the similar bandwidth as obtained in elastic scattering case. The ratio lies approximately between $0.25 < \log_{10}(\lambda / d_{avg}) < 0.35$, which gives

$$1.77 < (\lambda / d_{avg}) < 2.24$$

For a mean value of $\log_{10}\left(\dfrac{\lambda}{d_{avg}}\right) \approx 0.3, \Rightarrow \left(\dfrac{\lambda}{d_{avg}}\right) \approx 2$

This ratio is again a rule of thumb, and can be approximated depending upon the tolerance desired. This ratio is expectedly in approximately the same range as that obtained in the elastic body scattering response.

For the back end, the ratio of λ / d_{avg} lies in the similar range as in the elastic scattering, given by $-0.1 < \log_{10}(\lambda / d_{avg}) < 0.3$, which gives

$$0.79 < (\lambda / d_{avg}) < 1.99$$

The mean value at the back node is approximately around 0.03, which gives,

$$\log_{10}\left(\frac{\lambda}{d_{avg}}\right) \approx 0.03, \Rightarrow \left(\frac{\lambda}{d_{avg}}\right) \approx 1.07$$

The ratio thus obtained is similar to the one obtained in the elastic scattering response at the back end.

CHAPTER FIVE

5   CONCLUSIONS AND FUTURE WORK

Scattering response of different geometries both in 2-D and 3-D has been studied and presented in the thesis. The geometries which are being compared, have equal mass and the same diameter.

In Chapter 2, the geometry construction and calculation of the thickness has been discussed. The 3-D geometry was made with precision for proper meshing in ABAQUS and thickness was varied to keep the mass constant of all the models in case of 2-D and 3-D.

In Chapter 3, the Natural Frequency has been extracted in ABAQUS for a frequency range of 1-3000 Hz. The natural frequencies were compared in both 2-D and 3-D cases. It was observed that the natural frequencies are similar to the 2-D circular cylinder/spherical shell when the faceted geometries starts to approximate them. The natural frequencies extracted are then used in the acoustic scattering problem.

In Chapter 4, a full structure-acoustic coupling analysis has been done. Comparison of scattering response of the geometries (2-D and 3-D) is done with their respective canonical forms. Target strength at the front near and back near nodes are calculated and the threshold ratio is obtained as explained in the initial part of the section.

5.1   2-D Results

The 2-D circular cylinder is such that it circumscribes the 2-D regular polygonal structures. Target strength of 2-D regular polygon structures at the front near and back near

node has been calculated using finite elements analysis, and is compared to the Target strength of a 2-D circular cylindrical structure at the same nodes. A ratio of acoustic wavelength to polygon chord (facet) length (λ / L) is then obtained, which helps to quantify the comparison. Here λ is the wavelength and L is the facet length of the polygon. This ratio determines the threshold of a 2-D regular polygonal cylinder to behave like a 2-D circular cylinder in terms of acoustic scattering response. Conversely, if a known scattering response of a 2-D regular polygonal structure is compared to a 2-D circular cylinder, length of the facet of the polygon can be identified by this ratio.

The λ / L ratios obtained for elastic and rigid body scattering at front near and back near nodes are summarized in Table 5-1.

Table 5-1 Summary of the ratios obtained on front and back near node for 2-D geometry.

Ratio	2-D Elastic Body Scattering						2-D Rigid Body Scattering					
	Front near node			Back near node			Front near node			Back near node		
	Bandwidth Range	Mean Value of the threshold ratio of the geometries	Avg. value	Bandwidth Range	Mean Value of the threshold ratio of the geometries	Avg. Value	Bandwidth Range	Mean Value of the threshold ratio of the 3 geometries	Avg. value	Bandwidth Range	Mean Value of the threshold ratio of the geometries	Avg. Value
λ / L	1.78 - 2.82	2.24	2.3	1 - 2.5	1.6	1.75	1.99 - 2.82	2.24	2.4	1-1.99	1.41	1.49

5.2   3-D Results

An analogous study has been done for the 3-D geometries of geodesic spheres. Comparison of faceted geometries with spherical shells in 3-D has been done. In this case, geodesic spheres of different degrees are compared to a circumscribing spherical shell. The target strength at front near and back near nodes are obtained, and similar to 2-D scattering analysis, a threshold ratio is obtained. The ratio is wavelength to the average circumcircle diameter of the facets. The circumcircle diameter gives an overall idea of the surface area of the facet in the space, and these have been averaged out because the circumcircle

122

diameter is not equal for each facet of the geodesic sphere. This ratio determines the threshold of the faceted geodesic sphere to behave like a spherical shell in terms of acoustic scattering response.

Table 5-2 summarizes the ratios obtained for the 3-D case

Table 5-2 Summary of the ratios obtained on front and back near node for 3-D geometry.

Ratio	3-D Elastic Body Scattering						3-D Rigid Body Scattering					
	Front near node			Back near node			Front near node			Back near node		
	Bandwidth Range	Mean Value of the threshold ratio of the 3 geometries	Avg. value	Bandwidth Range	Mean Value of the threshold ratio of the 3 geometries	Avg. Value	Bandwidth Range	Mean Value of the threshold ratio of the 3 geometries	Avg. value	Bandwidth Range	Mean Value of the threshold ratio of the 3 geometries	Avg. Value
λ / d_{avg}	1.78-2.24	2.01	2	0.79 - 1.99	1.39	1.07	1.77-2.24	2.01	2	0.79-1.99	1.37	1.07

These ratios are a rule of thumb based on the desired tolerance level. As, the tolerance level decreases, the level approximation will also increase, hence the results obtained will have a higher error when compared to the exact values. The ratio of wavelength to local facet size used in this thesis also provides a novel and interesting way to compare geometries of other shapes with their canonical counterparts.

5.3 Future Work

1) The acoustic medium can be changed from air to water, to check the consistency of the ratio in different mediums. In water, the bulk modulus (K) and density (ρ) of the medium changes. The speed of sound in a medium is a function of K and ρ, given by $c_{medium} = \sqrt{K_{medium} / \rho_{medium}}$. The relation between the geometries considering the scattering effect may be different.

2) For 3-D, finer mesh and location of infinite boundary can be enlarged especially for accuracy at higher frequencies (ka>36.5; f = 2000Hz.) At this frequency, the

123

$\lambda / a = 0.1721$. This means the wavelength is 0.17 times smaller than the diameter of the scatterer.

3) The waves diffracted by the corners become more localized near corners especially at higher frequencies (ka>36.5; f = 2000 Hz). Hence, effect of variable meshing can be investigated. Mesh being fine at corners and edges, and coarse on the faces. The corner effects are expected to be more prominent at coarser models, as the corners are more prominent in those cases.

4) Higher degree of geodesic can be modelled and compared to the spherical shell. The variation in the bandwidth of the threshold ratio can be investigated and the shift in the mean value of the ratio can be calculated.

5) Thickness of the models can be increased. This will give a higher mass and stiffness to the models. For thick models, instead of using beam and shell elements, plain strain/3D - stress elements will have to be used.

REFERENCES

[1] H. C. Rhee, "Polygon-circle paradox in the finite element analysis of bending of a simply supported plate," *Comput. Struct.*

[2] N. W. Murray, "The polygon-circle paradox and convergence in thin plate theory," *Math. Proc. Cambridge Philos. Soc.*, vol. 73, no. 01, p. 279, 1973.

[3] K. Rajaiah and A. K. Rao, "On the Polygon-Circle Paradox," vol. 48, no. March 1981, pp. 1980–1981, 1981.

[4] H. Uberall, "Acoustic scattering from simple and complex submerged objects," vol. 4, 1994.

[5] L. M. Cureton and J. R. Kuttler, "Eigenvalues of the Laplacian on Regular Polygons and Polygons Resulting From Their Disection," *J. Sound Vib.*, vol. 220, pp. 83–98, 1999.

[6] N. Ari and J. R. Firth, "Acoustic inverse scattering problems of polygonal shape reconstruction," *Inverse Probl.*, vol. 6, no. 2, pp. 299–309, 1999.

[7] I. Dokmanić, Y. M. Lu, and M. Vetterli, "Can one hear the shape of a room: The 2-D polygonal case," *ICASSP, IEEE Int. Conf. Acoust. Speech Signal Process. - Proc.*, pp. 321–324, 2011.

[8] D. Colton and A. Kirsch, "A simple method for solving inverse scattering problems in the resonance region," *Inverse Probl.*, vol. 12, no. 4, pp. 383–393, 1999.

[9] X. Wang and T. J. Lu, "Optimized acoustic properties of cellular solids," *J. Acoust. Soc. Am.*, vol. 106, no. 2, p. 756, 1999.

[10] 6J. A. Fawcett, "Modeling of high-frequency scattering from objects using a hybrid Kirchhoff/diffraction approach," *J. Acoust. Soc. Am. 109, 1312–1319*, 2001.

[11] K. Lee and W. Seong, "Time-domain Kirchhoff model for acoustic scattering from an impedance polygon facet.," *J. Acoust. Soc. Am.*, vol. 126, no. 1, pp. EL14–L21, 2009.

[12] P. a. Chinnery, V. F. Humphrey, and J. Zhang, "Low-frequency acoustic scattering by a cube: Experimental measurements and theoretical predictions," *J. Acoust. Soc. Am.*, vol. 101, no. 5, p. 2571, 1997.

[13] S. N. Chandler-Wilde and S. Langdon, "A Galerkin boundary element method for high frequency scattering by convex polygons," vol. 45, no. 2, pp. 610–640, 2007.

[14] S. Langdon, "High frequency scattering by convex polygons," no. January 2008, pp. 1–12, 2007.

[15] E. Schmidtke, "Iteration Scheme," pp. 295–296, 2004.

[16] A. P. Lyons, "Scattering from Rock and Rock Outcrops," pp. 1–8.

[17] T. K. Stanton, D. Chu, P. H. Wiebe, R. L. Eastwood, and J. D. Warren, "Acoustic scattering by benthic and planktonic shelled animals.," *J. Acoust. Soc. Am.*, vol. 108, no. 2, pp. 535–550, 2000.

[18] C. S. Clay, "Scattering of Acoustic signals from the underside of sea ice," 94AD.

[19] Https://en.wikipedia.org/wiki/Geodesic_Sphere, "No Title." .

[20] 1895-1983. Fuller, R. Buckminster (Richard Buckminster), *Your private sky : R. Buckminster Fuller, the art of design science / edited by Joachim Krausse, Claude Lichtenstein ; [translation, Steven Lindberg, Julia Thorson]*. Baden : L. Müller, c1999.

[21] Http://science.howstuffworks.com/engineering/structural/geodesic-Sphere1.htm, "No Title." .

[22] T. Davis, "Geodesic Spheres," pp. 1–13, 2011.

[23] L. L. Thompson and P. M. Pinsky, "A space-time finite element method for structural acoustics in infinite domains part 2: Exact time-dependent non-reflecting boundary conditions," *Comput. Methods Appl. Mech. Eng.*, vol. 132, no. 3–4, pp. 229–258, 1996.

[24] T. D. Rossing, *Springer Handbook of Acoustics*. .

[25] L. L. T. and P. Pinsky, "Acoustics - Encyclopedia of computational mechanics."

[26] transmission and response. 1985. F. Fahy, Sound and Structural Vibration - radiation, "No Title."

[27] Y.-H. Kim, *Sound propagation, An Impedance Based Approach*. 2013.

[28] P. Davidsson, *Structure-acoustic analysis; finite element modelling and reduction methods*. 2004.

[29] Iyer V. (Clemson U.), "Acoustic scattering and radiation response of circular hexagonal and auxetic honeycomb shell structures," no. August, 2014.

6   APPENDIX

6.1   MATLAB code for thickness calculation of 2D polygons.

```matlab
clc;
clear;
d = 1;                    %depth = 1m.
rho = 2700;               % material density kg/m^3.
r_out = 0.5;              % outer raduis m.
alpha = 45;               % angle subtended at the centre.
chord = r_out*sqrt(2*(1-cosd(alpha)));  % length of the chord from
cosine law.
A_cir = 1e-2;             % surface area of the circular ring. (m^2)
P_cir = 2*pi*r_out;       % perimeter of the circle. (m)
vol_cir = P_cir*A_cir;    % volume of the circle. (m^3)
m_cir = rho*vol_cir;      % mass of the circle. (Kg)

P_poly = (360/alpha)*chord;  % perimeter of the polygon (m).
format long e
t_poly = m_cir/(rho*P_poly*d); % beam thickness of the polygon (m^2).
```

6.2   Infinite Boundary in 2D

To set up the infinite boundary elements in 2D, the section is defined in the input file of

ABAQUS. The script for the input file is given below.

*Solid Section, elset=_PickedSet6, material=Air

1., 0, 0, 0

Solid Section defines the section of the infinite boundary. The solid section cannot

be assigned to 2-D geometries in ABAQUS GUI, hence it is later assigned in the input

file.

elset is the element set of the infinite boundary. The created set is the outer

surface of the 2-D wireframe modelled for the infinite boundary. It should be noted that

the outer surface of the infinite boundary should be selected, as the direction of the

infinite elements is radially outwards.

In the second line, the first number 1, gives the depth of the boundary and the

other three numbers (0, 0, 0) gives the coordinate of the reference node.

6.3 MATLAB code for calculation of coordinates and the thickness of the Geodesic

Sphere.

```
n = 2;                    % degree of the geodesic.
[A_I] = geodesic(n);%calling the coordinates of the triangular surface.
A =zeros(n^2,3);
count = 0;
IEN =[];
c = n;
for j=1:n              % loop over the degree of geodesic sphere.
    A =[];
    c = c-1;
    k = 2*n -(2*j-1)-c; %pattern formula to set-up the IEN table
    count;
    for i=1:k
        count = count+1;
        A((2*i)-1,1) = count;
        A((2*i)-1,2) = count+1;
        A((2*i)-1,3) = A((2*i)-1,2)+k;
        A(2*i,1) = A(2*i-1,2);
        A(2*i,2) = A(2*i-1,2)+k+1;
        A(2*i,3) = A(2*i-1,2)+k;
        if i==k
            A(2*i,:)=[];
        end
    end
    count = count + 1;
    IEN = [IEN;A]; %IEN stored in a matrix.
end
T_all = [];
dia_all =[];
Area = 0;
dia = 0;
for i=1:n^2          % loop over the number of sub triangles of one
triangular surface.
    I = IEN(i,1);
    J = IEN(i,2);
    K = IEN(i,3);
    % picking the coordinates of the triangular surface from the IEN
table
    % and calculating the lengths of the sides of the sub-triangle.
```

```matlab
    a = sqrt((A_I(J,1)-A_I(I,1))^2 + (A_I(J,2)-A_I(I,2))^2 + (A_I(J,3)-
A_I(I,3))^2);
    b = sqrt((A_I(K,1)-A_I(J,1))^2 + (A_I(K,2)-A_I(J,2))^2 + (A_I(K,3)-
A_I(J,3))^2);
    c = sqrt((A_I(K,1)-A_I(I,1))^2 + (A_I(K,2)-A_I(I,2))^2 + (A_I(K,3)-
A_I(I,3))^2);
    s = (a+b+c)/2;   %semi-perimieter of the sub-triangle.
    T = sqrt(s*(s-a)*(s-b)*(s-c));   %Area of the triangle by heron's
formula.
    d = (a*b*c)/(2*T);   %diameter of the circumcircle.
    dia = dia+d;
    Area = Area+T;
    dia_all = [dia_all;d];
    T_all = [T_all;T];
end
dia = dia/n^2;           %averaging out the diameter.
A_t = Area/n^2;          %averaging out the area.
mass =84.82300166    ; %mass (Kg) of the spherical shell with thickness
0.01m
rho = 2700;              % density of the material (kg/m3)
thickness = mass/(20*Area*rho)   %thickness of the geodesic.
```

Function [A_I]

```matlab
% function to calculate the coordinates of the triangular surface. This
function also plots the triangular surface.
function[A_I] = geodesic(n)
L = 1;
phi = (1+ sqrt(1+4*L))/2;%golden ratio

% vertices of a triangular face of an icosahedron
A_1 = [0, L, phi];
I_1 = [L, phi, 0];
J_1 = [phi, 0, L];

r = 0.5; %radius of the enclosing sphere
A_I =[];
I_J =[];
J_A =[];
K = 0;
count = 1;
%Calculating the coordinates of the vertices of the smaller triangles
for j = 0:n
    for i = 0:n-K
        A_I(count,:) = (0+K)*J_1/n+(n-i-K)*A_1/n+i*I_1/n;
        count = count+1;
    end
    K = K+1;
end
%Radial direction
for i=1:size(A_I)
```

```
    A_I(i,:) = A_I(i,:)/norm(A_I(i,:));
end
A_I = A_I*r; %%coordinates lying on the surface of the sphere
K = 0;
% plotting the triangular surface of the Geodesic dome with vertices
lying on a sphere
for i=1:n+1
    plot3(A_I(i+K:n+1+K,1), A_I(i+K:n+1+K,2), A_I(i+K:n+1+K,3));
    I_J(i) = n+1+K;
    A_J(i) = i+K;
    hold on
    K = n+1+K-i;
end

plot3(A_I(I_J',1),A_I(I_J',2),A_I(I_J',3))
hold on
plot3(A_I(A_J',1),A_I(A_J',2),A_I(A_J',3))
hold on
K = 0;

for i = n:-1:1
    K = K+1;
    plot3(A_I((A_J(1:i)+K)',1), A_I((A_J(1:i)+K)',2),
A_I((A_J(1:i)+K)',3))
    hold on
    plot3(A_I((I_J(1:i)-K)',1), A_I((I_J(1:i)-K)',2), A_I((I_J(1:i)-
K)',3))
end
 hold off
 axis equal
 format longe
```

6.4   Infinite Boundary in 3-D

To set-up the infinite boundary in 3-D, the reference node of the infinite elements need to

be specified in the input file. ABAQUS GUI generates a reference node automatically

and the syntax looks like;

*Solid Section, elset=_PickedSet7, material=Air, ref node=Inf-RefPt_, order=10

1.,

The ref node is deleted from the syntax and the coordinates of the reference node are thus entered manually in the input file.

*Solid Section, elset=_PickedSet7, material=Air, order=10

1.,0,0,0.

Where, (0, 0, 0) are the coordinates of the reference node.

6.5 MATLAB code for calculation of Natural Frequency analytically by Dr. Thompson.

```
% The natural frequencies calculated are based on thin curved beam
bending theory
% Original: Lonny Thompson, Clemson University, March 2014
R = 0.5; %ring diameter at midline of thickness
t = 0.01; %ring thickness (meters)
Young_Modulus = 7.1*(10^10); %aluminum E = 71.9 GPa, Pa = N/m^2
rho = 2700; %mass density, kg/m^3
%unit depth b=1;
Area_Moment_Inertia = t^3/12;
EI = Young_Modulus * Area_Moment_Inertia;
Area = t;
coef = EI / (rho*Area*R^4);
N = 20;
omega = zeros(N+1,1);
for n=0:N
omega(n+1) = sqrt(coef*(n^2)*(n^2-1)^2 / (n^2+1) );
end
fn = omega/(2*pi) %Hz
frequencies = sort(fn) %kHz
```

6.6 Natural Frequencies extracted from ABAQUS of 2-D models.

Mode Number	15	30	45	Ring
1	25.5700	26.457	27.656	25.280
2	25.5700	26.457	27.656	25.280
3	72.2970	74.775	77.870	71.478

4	72.2970	74.775	77.870	71.478
5	138.550	143.19	138.71	136.99
6	138.550	143.19	160.82	136.99
7	223.920	231.02	239.81	221.40
8	223.920	231.02	239.81	221.40
9	328.220	327.46	337.99	324.55
10	328.220	350.18	337.99	324.55
11	451.310	464.94	357.98	446.30
12	451.310	464.94	398.02	446.30
13	593.070	606.55	398.02	586.55
14	593.070	606.55	651.74	586.55
15	753.350	731.18	694.69	745.17
16	753.350	758.50	694.69	745.17
17	931.970	758.50	879.73	922.03
18	931.970	889.18	879.73	922.03
19	1128.7	889.18	1102.0	1117.0
20	1128.7	895.33	1102.0	1117.0
21	1332.4	895.33	1271.9	1329.9
22	1355.2	1400.0	1432.7	1329.9
23	1481.4	1428.0	1603.3	1560.6
24	1576.6	1428.0	1603.3	1560.6
25	1576.6	1671.1	1763.6	1632.3
26	1826.3	1671.1	1805.2	1808.9
27	1826.3	1997.4	1805.2	1808.9
28	2077.6	1997.4	1854.0	2074.6
29	2077.6	2322.3	1854.0	2074.6
30	2092.9	2322.3	2538.4	2308.4
31	2092.9	2645.0	2558.8	2308.4
32	2375.6	2645.0	2558.8	2357.5
33	2375.6	2736.2	2836.1	2357.5
34	2673.2	2898.5	2836.1	2657.5
35	2673.2			2657.5
36	2982.8			2974.2
37	2982.8			2974.2

6.7   Natural Frequencies extracted from ABAQUS of 3-D models.

Mode Number	Degree II	Degree III	Degree IV	Shell
1	937.72	1121.6	1164.1	1191.2
2	938.03	1121.6	1164.2	1191.5
3	938.33	1121.6	1164.2	1191.6
4	938.44	1121.6	1164.2	1191.7
5	938.53	1121.7	1164.2	1192.2
6	966.11	1311.7	1373.5	1416.3
7	1006.7	1311.8	1373.5	1417.4
8	1006.8	1311.8	1373.5	1417.9
9	1006.9	1311.9	1373.6	1418.4
10	1031.5	1316.7	1376.9	1418.4
11	1032.0	1316.8	1376.9	1419.0
12	1032.1	1316.9	1377.0	1419.7
13	1032.5	1383.6	1451.0	1511.6
14	1079.3	1383.7	1451.0	1512.1
15	1079.3	1383.7	1451.1	1513.3
16	1079.5	1383.7	1451.1	1513.8
17	1079.5	1389.9	1467.9	1514.1
18	1079.7	1390.0	1468.0	1514.3
19	1081.5	1390.1	1468.0	1514.9
20	1081.7	1390.3	1468.1	1515.2
21	1081.9	1390.3	1468.2	1515.9
22	1081.9	1421.4	1497.7	1568.6
23	1082.1	1421.5	1497.8	1569.6
24	1110.5	1421.6	1497.8	1570.4
25	1110.7	1424.7	1509.9	1570.6
26	1110.8	1425.0	1510.0	1570.8
27	1110.9	1425.1	1510.1	1571.1
28	1111.1	1436.9	1510.1	1571.9
29	1132.7	1437.0	1510.2	1572.4
30	1132.9	1437.0	1534.5	1572.9
31	1133.0	1437.1	1534.8	1574.1
32	1185.2	1437.2	1534.9	1574.3
33	1185.6	1453.0	1541.8	1616.2
34	1185.9	1453.3	1541.8	1617.5
35	1186.2	1453.5	1541.9	1617.9
36	1201.3	1470.2	1542.0	1618.5
37	1201.5	1470.5	1561.4	1618.7

38	1201.6	1470.5	1561.6	1619.7
39	1201.7	1470.6	1561.6	1619.9
40	1226.5	1470.7	1561.8	1620.4
41	1226.5	1470.8	1561.8	1620.6
42	1226.7	1471.0	1577.8	1621.4
43	1263.2	1471.2	1577.9	1621.8
44	1263.4	1471.2	1578.2	1622.8
45	1263.8	1498.2	1589.3	1623.0
46	1282.6	1498.4	1589.4	1667.6
47	1282.8	1498.7	1589.4	1668.6
48	1283.0	1508.3	1589.5	1669.2
49	1283.1	1508.6	1592.7	1670.2
50	1382.3	1508.9	1618.6	1671.0
51	1382.4	1509.0	1619.1	1671.4
52	1382.7	1509.2	1619.2	1671.9
53	1383.0	1528.4	1622.1	1671.9
54	1383.1	1528.6	1622.2	1672.2
55	1448.3	1528.6	1622.5	1673.0
56	1448.6	1528.9	1622.6	1673.2
57	1449.1	1545.1	1622.7	1673.5
58	1449.4	1555.5	1639.4	1673.9
59	1487.0	1555.7	1639.4	1674.8
60	1487.3	1556.0	1639.7	1675.8
61	1487.4	1556.3	1663.5	1729.9
62	1487.6	1559.0	1663.5	1731.6
63	1505.7	1559.2	1663.7	1732.3
64	1505.8	1559.3	1663.8	1732.5
65	1506.0	1559.5	1664.0	1733.6
66	1506.1	1559.6	1669.1	1734.1
67	1506.3	1562.5	1669.4	1734.7
68	1510.8	1562.6	1669.4	1734.9
69	1511.4	1562.8	1694.9	1735.5
70	1511.9	1628.3	1695.1	1735.8
71	1583.9	1628.7	1695.4	1736.3
72	1584.2	1629.0	1695.7	1736.5
73	1584.7	1647.4	1702.3	1737.6
74	1587.6	1647.8	1702.3	1737.7
75	1587.9	1647.9	1702.6	1738.3
76	1588.4	1648.5	1703.0	1738.5

77	1592.6	1678.5	1703.2	1739.6
78	1592.9	1678.7	1738.0	1810.0
79	1593.3	1678.9	1738.1	1811.0
80	1593.5	1679.0	1738.2	1811.6
81	1593.6	1679.2	1761.4	1812.3
82	1641.2	1687.9	1761.8	1812.5
83	1641.6	1688.1	1761.8	1813.6
84	1641.7	1688.3	1762.1	1814.2
85	1660.5	1688.5	1762.2	1814.3
86	1661.1	1688.6	1762.4	1814.6
87	1661.8	1694.1	1762.5	1815.2
88	1662.0	1694.6	1762.6	1815.8
89	1662.3	1694.7	1762.7	1816.1
90	1822.4	1703.5	1776.5	1817.2
91	1823.9	1703.7	1776.6	1817.4
92	1824.9	1703.9	1776.9	1817.7
93	1879.3	1726.0	1777.3	1819.0
94	1880.0	1726.3	1806.4	1819.3
95	1880.9	1726.5	1806.6	1819.8
96	1881.3	1726.7	1806.8	1820.8
97	1881.7	1727.0	1816.1	1909.4
98	1894.8	1761.1	1861.2	1911.3
99	1894.9	1761.3	1861.3	1912.1
100	1895.3	1761.6	1861.6	1912.5
101	1896.0	1823.7	1866.2	1913.2
102	1913.6	1823.9	1866.7	1914.1
103	1914.4	1824.0	1866.7	1914.6
104	1914.6	1824.1	1866.7	1915.1
105	1941.4	1824.5	1866.8	1915.6
106	1942.3	1832.8	1869.1	1916.2
107	1943.8	1833.1	1869.4	1916.2
108	1984.7	1833.4	1869.5	1916.9
109	1985.4	1863.6	1869.8	1917.3
110	1985.7	1863.6	1873.2	1917.6
111	1986.1	1863.9	1873.2	1918.3
112	2029.9	1864.1	1873.3	1918.7
113	2070.0	1883.1	1910.2	1918.9
114	2070.7	1883.2	1910.5	1920.0
115	2071.0	1883.2	1910.8	1920.1

116	2071.2	1883.3	1911.1	1921.0
117	2108.0	1883.3	1911.2	1922.2
118	2108.6	1902.9	1964.1	2001.5
119	2109.2	1903.1	1964.4	2002.0
120	2109.4	1903.4	1964.5	2002.4
121	2110.2	1903.6	1967.4	2003.0
122	2150.1	1903.8	1967.4	2003.3
123	2150.3	1919.7	1967.4	2034.5
124	2151.3	1919.8	1967.4	2035.7
125	2213.5	1920.2	1967.6	2036.0
126	2214.5	1920.3	1990.3	2036.4
127	2215.0	1966.2	1990.6	2036.7
128	2216.1	1966.2	1990.8	2037.0
129	2216.6	1966.5	1991.4	2038.2
130	2291.9	1987.9	1991.6	2038.7
131	2292.1	1988.2	1998.1	2039.3
132	2292.8	1988.7	1998.2	2039.8
133	2293.1	2058.6	1998.5	2040.0
134	2293.5	2072.1	1998.7	2040.7
135	2293.7	2072.3	2000.6	2041.3
136	2294.4	2072.4	2000.7	2041.7
137	2294.7	2072.6	2000.9	2041.9
138	2360.3	2079.9	2001.0	2043.0
139	2360.9	2080.2	2001.3	2043.2
140	2361.4	2080.4	2037.2	2043.5
141	2362.4	2080.7	2037.6	2044.3
142	2415.2	2080.7	2037.7	2044.6
143	2463.5	2126.2	2070.2	2045.7
144	2465.5	2126.5	2070.7	2046.2
145	2465.8	2126.7	2071.2	2047.9
146	2500.8	2127.0	2116.2	2183.5
147	2500.9	2195.3	2116.3	2184.0
148	2502.3	2195.6	2116.6	2184.7
149	2516.1	2196.1	2118.2	2185.2
150	2516.3	2196.3	2118.3	2185.9
151	2516.8	2196.5	2118.3	2186.8
152	2517.3	2220.8	2118.5	2187.4
153	2517.6	2221.2	2118.6	2188.7
154	2619.4	2221.4	2148.4	2189.0

155	2620.1	2240.5	2148.6	2189.2
156	2620.5	2240.8	2148.8	2189.7
157	2620.6	2241.1	2149.0	2190.6
158	2621.7	2279.0	2149.3	2190.8
159	2701.7	2279.4	2162.4	2191.4
160	2702.6	2280.0	2162.8	2191.6
161	2703.2	2301.2	2163.3	2192.2
162	2703.8	2355.1	2163.5	2192.4
163	2785.3	2355.2	2195.9	2193.1
164	2785.9	2355.7	2214.5	2193.7
165	2786.5	2356.1	2214.9	2194.2
166	2801.8	2396.4	2215.4	2195.2
167	2802.8	2396.6	2215.6	2195.4
168	2803.8	2396.8	2239.4	2196.2
169	2805.5	2396.9	2239.7	2196.9
170	2806.4	2397.1	2239.8	2198.2
171	2829.4	2467.1	2240.3	2358.9
172	2829.7	2467.4	2243.1	2359.7
173	2830.6	2467.7	2243.3	2360.5
174	2831.4	2468.1	2243.8	2361.4
175	2864.4	2468.3	2313.9	2362.5
176	2864.8	2477.0	2314.1	2362.9
177	2864.8	2477.2	2314.6	2363.5
178	2865.7	2477.4	2314.7	2363.8
179	2865.9	2477.5	2314.9	2364.6
180	2866.4	2477.9	2318.1	2365.0
181	2867.1	2478.0	2318.4	2365.5
182	2867.7	2478.9	2318.4	2366.5
183	2926.7	2498.5	2377.3	2366.7
184	2928.0	2498.7	2377.4	2367.0
185	2928.5	2499.1	2378.0	2367.5
186	2947.9	2499.5	2378.1	2368.2
187	2949.8	2587.3	2398.3	2368.5
188	2950.4	2588.1	2398.5	2369.2
189	2950.8	2588.6	2399.1	2369.8
190	2950.9	2589.2	2399.5	2370.4
191	2952.1	2616.8	2400.2	2370.8
192	2952.5	2617.5	2400.7	2371.3
193		2617.9	2401.2	2371.8

194		2618.1	2401.9	2372.6
195		2640.2	2404.8	2372.7
196		2640.3	2405.0	2374.4
197		2640.8	2405.3	2376.2
198		2641.0	2415.9	2561.2
199		2641.5	2416.0	2563.0
200		2682.1	2416.1	2563.3
201		2682.5	2416.2	2564.2
202		2682.7	2496.2	2565.0
203		2682.9	2496.4	2565.8
204		2683.2	2496.5	2565.9
205		2721.0	2531.5	2566.4
206		2721.3	2531.6	2566.9
207		2722.4	2532.0	2567.5
208		2779.4	2532.2	2568.0
209		2779.8	2532.4	2568.6
210		2780.2	2570.1	2568.8
211		2822.9	2570.2	2569.7
212		2823.2	2570.9	2570.2
213		2823.5	2571.1	2570.2
214		2860.7	2598.7	2571.4
215		2861.5	2599.1	2571.9
216		2861.9	2599.5	2573.0
217		2862.3	2608.4	2573.2
218		2887.9	2608.7	2574.1
219		2888.6	2609.0	2574.5
220		2889.2	2609.3	2575.0
221		2889.5	2609.7	2575.8
222		2890.0	2621.0	2576.7
223		2905.2	2641.5	2577.3
224		2905.3	2733.0	2577.5
225		2905.6	2733.0	2578.6
226		2946.9	2733.5	2580.5
227		2947.2	2733.8	2789.3
228		2948.6	2734.1	2790.8
229		2948.9	2748.1	2792.3
230		2949.2	2748.3	2792.9
231		2963.1	2748.6	2794.5
232		2964.0	2759.3	2794.6

233		2964.6	2759.6	2795.1
234		2965.5	2760.3	2795.8
235		2971.5	2801.4	2796.6
236		2976.9	2802.0	2797.3
237		2977.3	2802.2	2797.5
238		2977.6	2802.6	2798.8
239		3002.7	2806.6	2799.2
240			2807.6	2799.6
241			2807.9	2800.1
242			2808.4	2800.4
243			2808.6	2800.9
244			2918.7	2802.0
245			2919.1	2802.8
246			2919.6	2803.3
247			2919.8	2803.5
248			2936.3	2804.0
249			2937.0	2804.3
250			2938.0	2805.2
251			2959.1	2806.0
252			2961.4	2806.5
253			2962.5	2807.4
254			2978.5	2808.6
255			2978.7	2809.6
256			2979.2	2810.0
257			2979.8	2812.2
258			2980.1	2822.1
259			2987.8	
260			2988.3	
261			2988.8	
262			2988.9	
263			2989.3	

6.8   MATLAB code for calculating the Target Strength from 2-D elastic body

scattering, plotting the target strength and the λ / L curves.

```matlab
load POR_Scatter_15_Pos.dat
load POR_Scatter_15_Neg.dat

load POR_Scatter_30_Pos.dat
load POR_Scatter_30_Neg.dat

load POR_Scatter_45_Pos.dat
load POR_Scatter_45_Neg.dat

load POR_Scatter_Ring_Pos.dat
load POR_Scatter_Ring_Neg.dat


P_ref = 2e-5;
c = 344;
a = 1;
%calculating nondimensional frequency ka
f_15 = (POR_Scatter_15_Pos(:,1).*(2*pi*a)/c);
f_30 = (POR_Scatter_30_Pos(:,1).*(2*pi*a)/c);
f_45 = (POR_Scatter_45_Pos(:,1).*(2*pi*a)/c);
f_ring = (POR_Scatter_Ring_Pos(:,1).*(2*pi*a)/c);
d = 1;    %m
% chord length calculation
l_15 = (d/2)*sqrt(2-2*cosd(15));
l_30 = (d/2)*sqrt(2-2*cosd(30));
l_45 = (d/2)*sqrt(2-2*cosd(45));
% target strength at front near node.
figure('name','Positive')
ax1 = gca;
plot(f_45,20*log10(POR_Scatter_45_Pos(:,2)/P_ref))
hold on
plot(f_30,20*log10(POR_Scatter_30_Pos(:,2)/P_ref),'g')
hold on
plot(f_15,20*log10(POR_Scatter_15_Pos(:,2)/P_ref),'k')
hold on
plot(f_ring,20*log10(POR_Scatter_Ring_Pos(:,2)/P_ref),'r')
legend('45','30','15','Ring','Location','east')
xlabel('ka')
ylabel('pressure(db)')
xlim([0 55])
hold on
%plotting the ratio on the other Y-axis on the right side
ax2 = axes('Position',get(ax1,'Position'),...
    'YAxisLocation','right',...
    'Color','none');
Y = 0.36*ones(size(f_15));
line(f_15,Y,'Parent',ax2,'Color','k','Linewidth',1.5)
hold on
x = [0,55,55,0];
y = [0.25,0.25,0.45,0.45];
line(x,y,'Parent',ax2,'Color','k')
hold on
line(f_45,log10(c./(POR_Scatter_45_Pos(:,1)*l_45)),'Parent',ax2,'Color',
'b','Linewidth',1.2)
```

```matlab
hold on
line(f_30,log10(c./(POR_Scatter_30_Pos(:,1)*l_30)),'Parent',ax2,'Color',...
'g','Linewidth',1.2)
hold on
line(f_15,log10(c./(POR_Scatter_15_Pos(:,1)*l_15)),'Parent',ax2,'Color',...
'k','Linewidth',1.2)
hold on
hold off
ylabel('log_{10}(\lambda/L)')
xlim([0 55])
set(ax2,'YColor','b')
hold off
print -depsc2 -tiff positive.eps
print -r300 -djpeg90 positive.jpg

%target strength at back near node
figure('name','Negative')
ax1 = gca;
plot(f_45,20*log10(POR_Scatter_45_Neg(:,2)/P_ref))
hold on
plot(f_30,20*log10(POR_Scatter_30_Neg(:,2)/P_ref),'g')
hold on
plot(f_15,20*log10(POR_Scatter_15_Neg(:,2)/P_ref),'k')
hold on
plot(f_ring,20*log10(POR_Scatter_Ring_Neg(:,2)/P_ref),'r')
legend('45','30','15','Ring','Location','east')
xlabel('ka')
ylabel('pressure(db)')
xlim([0 55])
hold on
%plotting the ratio on the other Y-axis on the right side
ax2 = axes('Position',get(ax1,'Position'),...
    'YAxisLocation','right',...
    'Color','none');
Y = 0.23*ones(size(f_15));
line(f_15,Y,'Parent',ax2,'Color','k','Linewidth',1.5)
hold on
x = [0,55,55,0];
y = [0,0,0.4,0.4];
line(x,y,'Parent',ax2,'Color','k')
hold on
line(f_45,log10(c./(POR_Scatter_45_Neg(:,1)*l_45)),'Parent',ax2,'Color',...
'b','Linewidth',1.2)
hold on
line(f_30,log10(c./(POR_Scatter_30_Neg(:,1)*l_30)),'Parent',ax2,'Color',...
'g','Linewidth',1.2)
hold on
line(f_15,log10(c./(POR_Scatter_15_Neg(:,1)*l_15)),'Parent',ax2,'Color',...
'k','Linewidth',1.2)
hold on
hold off
ylabel('log_{10}(\lambda/L)')
xlim([0 55])
```

```matlab
set(ax2,'YColor','b')
hold off
print -depsc2 -tiff negative.eps
print -r300 -djpeg90 negative.jpg
```

6.9 MATLAB code for calculating the target strength from 2-D elastic body scattering at the near inner surface and generating a polar plot.

```matlab
clc;
clear;
%load the data
load POR_Polar_15.dat
load nodes_15.dat
load coord_15.dat

load POR_Polar_Ring.dat
load nodes_ring.dat
load coord_ring.dat
n_15 = 596;
n_ring = 590;%row corresponding to the desired frequency

P_ref = 2e-5;
nodes_15 = nodes_15';
for i=1:size(nodes_15)
    A_2(i,1) = coord_15(nodes_15(i,1),2);
    A_2(i,2) = coord_15(nodes_15(i,1),3);
end
% Converting cartesian to polar.
[THETA,RHO] = cart2pol(A_2(:,1),A_2(:,2));
X_2(:,1) = THETA;
%Calculating target strength
for i=1:size(nodes_15)
    X_2(i,2) = 20*log10(POR_Polar_15(n_15,i+1)/P_ref);
end
[Y,I] = sort(X_2(:,1));
B_2 = X_2(I,:);
nodes_ring = nodes_ring';
%calculation for ring
for i=1:size(nodes_ring)
    A_S(i,1) = coord_ring(nodes_ring(i,1),2);
    A_S(i,2) = coord_ring(nodes_ring(i,1),3);
end
%converting cartesian to polar.
[THETA,RHO] = cart2pol(A_S(:,1),A_S(:,2));
X_S(:,1) = THETA;
%calculating target strength.
for i=1:size(nodes_ring)
    X_S(i,2) = 20*log10(POR_Polar_Ring(n_ring,i+1)/P_ref);
end
```

```
[Y,I] = sort(X_S(:,1));
B_S = X_S(I,:);

polar(B_2(:,1),B_2(:,2),'.b')
hold on
xlabel('node position (degrees)')
ylabel('pressure (db)')
h2=polar(B_S(:,1),B_S(:,2),'r');
set(h2,'LineWidth',1.2)
format short e
a= POR_Polar_Ring(n_ring,1);
b= POR_Polar_15(n_15,1);
legend(sprintf('15 @ %d (Hz)',b),sprintf('Ring @ %d (Hz)',a),
'Location','north')
hold off
print -depsc2 -tiff polar.eps
print -r300 -djpeg90 polar_geo.jpg
```

6.10 MATLAB code for calculating the Target Strength from 3-D elastic-body

scattering, plotting the target strength and the λ / d_{avg} curves.

```
clc;
clear;
%loading the data
load POR_Scatter_Geo2_Pos.dat
load POR_Scatter_Geo2_Neg.dat

load POR_Scatter_Geo3_Pos.dat
load POR_Scatter_Geo3_Neg.dat

load POR_Scatter_Geo4_Pos.dat
load POR_Scatter_Geo4_Neg.dat

load POR_Scatter_Shell_Pos.dat
load POR_Scatter_Shell_Neg.dat


a =1;
c = 343.996;
%calculating nondimensional frequency ka
f_4 = (POR_Scatter_Geo4_Pos(:,1).*(2*pi*a))/(c);
f_3 = (POR_Scatter_Geo3_Pos(:,1).*(2*pi*a))/(c);
f_2 = (POR_Scatter_Geo2_Pos(:,1).*(2*pi*a))/(c);
f_shell = (POR_Scatter_Shell_Pos(:,1).*(2*pi*a))/(c);
P_ref = 2e-5; %N/mm2
A_3 =  2.288737908239999e-01; %Surface Area of the triangle  (m)
A_2 = 3.376875231948716e-01;
A_4 =  1.726255088404506e-01;
```

```matlab
c = 344; %m/s
% target strength at front near node
figure('name','Positive')
ax1 = gca;
plot(f_2,20*log10(POR_Scatter_Geo2_Pos(:,2)/P_ref))
xlim([0 55])
xlabel('frequency (Hz)')
ylabel('pressure (db)')
hold on
plot(f_3,20*log10(POR_Scatter_Geo3_Pos(:,2)/P_ref),'g')
hold on
plot(f_4,20*log10(POR_Scatter_Geo4_Pos(:,2)/P_ref),'k')
hold on
plot(f_shell,20*log10(POR_Scatter_Shell_Pos(:,2)/P_ref),'r')
hold on
legend('Degree II','Degree III','Degree IV','Spherical
Shell','Location','east')
grid on
hold on
%plotting the ratio on the other Y-axis on the right side
ax2 = axes('Position',get(ax1,'Position'),...
    'YAxisLocation','right',...
    'Color','none');
Y = 0.3*ones(size(f_4));
line(f_4,Y,'Parent',ax2,'Color','k','Linewidth',1.5)
hold on
x = [0,55,55,0];
y = [0.25,0.25,0.35,0.35];
line(x,y,'Parent',ax2,'Color','k')
hold on
line(f_4,log10(c./(POR_Scatter_Geo4_Pos(:,1)*(A_4))),'Parent',ax2,'Color
','k','Linewidth',1.2)
xlim([0 55])
hold on
line(f_3,log10(c./(POR_Scatter_Geo3_Pos(:,1)*(A_3))),'Parent',ax2,'Color
','g','Linewidth',1.2)
hold on
line(f_2,log10(c./(POR_Scatter_Geo2_Pos(:,1)*(A_2))),'Parent',ax2,'Linew
idth',1.2)
xlabel('frequency')
ylabel('log_{10} (\lambda/d_{avg})')
set(ax2,'YColor','b')
hold on

hold off
print -depsc2 -tiff 3D_scatter_pos.eps
print -r300 -djpeg90 positive_rigid.jpg

%target strength at back near node
figure('name','Negative')
gca = ax1;
plot(f_2,20*log10(POR_Scatter_Geo2_Neg(:,2)/P_ref))
xlim([0 55])
```

145

```
xlabel('ka')
ylabel('pressure (db)')
hold on
plot(f_3,20*log10(POR_Scatter_Geo3_Neg(:,2)/P_ref),'g')
hold on
plot(f_4,20*log10(POR_Scatter_Geo4_Neg(:,2)/P_ref),'k')
hold on
plot(f_shell,20*log10(POR_Scatter_Shell_Neg(:,2)/P_ref),'r')
legend('Degree II','Degree III','Degree IV','Spherical
Shell','Location','east')
grid on
hold off
%plotting the ratio on the other Y-axis on the right side
ax2 = axes('Position',get(ax1,'Position'),...
    'YAxisLocation','right',...
    'Color','none');

line(f_4,log10(c./(POR_Scatter_Geo4_Pos(:,1)*(A_4))),'Parent',ax2,'Color
','k','Linewidth',1.2)
xlim([0 55])
hold on
line(f_3,log10(c./(POR_Scatter_Geo3_Pos(:,1)*(A_3))),'Parent',ax2,'Color
','g','Linewidth',1.2)
hold on
line(f_2,log10(c./(POR_Scatter_Geo2_Pos(:,1)*(A_2))),'Parent',ax2,'Linew
idth',1.2)
ylabel('log_{10}(\lambda/d_{avg}) ')
Y = 0.033*ones(size(f_4));
line(f_4,Y,'Parent',ax2,'Color','k','Linewidth',1.5)
hold on
x = [0,55,55,0];
y = [-0.1,-0.1,0.3,0.3];
line(x,y,'Parent',ax2,'Color','k')
set(ax2,'YColor','b')
hold on
print -depsc2 -tiff 3D_scatter_neg.eps
print -r300 -djpeg90 negative_rigid.jpg
```

6.11 MATLAB code for calculating the Target Strength of 2-D rigid bodies, plotting the

target strength and the λ/L curves.

```
load POR_15_pos.dat
load POR_15_neg.dat

load POR_30_pos.dat
load POR_30_neg.dat

load POR_45_pos.dat
load POR_45_neg.dat
```

146

```matlab
load POR_ring_pos.dat
load POR_ring_neg.dat

c = 344; %m/s
a = 1; %m
f_15 = (POR_15_pos(:,1).*(2*pi*a))/(c);
f_30 = (POR_30_pos(:,1).*(2*pi*a))/(c);
f_45 = (POR_45_pos(:,1).*(2*pi*a))/(c);
f_ring = (POR_ring_pos(:,1).*(2*pi*a))/(c);
l_15 = 2*(a/2)*sind(15/2);
l_30 = 2*(a/2)*sind(30/2);
l_45 = 2*(a/2)*sind(45/2);

P_ref = 2e-5;
figure('name','Positive')
ax1 = gca;
% plot(f_15,20*log10(POR_15_pos(:,2)/P_ref),'k')
plot(f_45,20*log10(POR_45_pos(:,2)/P_ref))
hold on
plot(f_30,20*log10(POR_30_pos(:,2)/P_ref),'g')
hold on
plot(f_15,20*log10(POR_15_pos(:,2)/P_ref),'k')
hold on
plot(f_ring,20*log10(POR_ring_pos(:,2)/P_ref),'r')
 xlim([0 55])
legend('45','30','15','Ring','Location','east')
xlabel('ka')
ylabel('pressure (db)')
hold on
ax2 = axes('Position',get(ax1,'Position'),...
    'YAxisLocation','right',...
    'Color','none');
Y = 0.36*ones(size(f_15));
line(f_15,Y,'Parent',ax2,'Color','k','Linewidth',1.5)
hold on
x = [0,55,55,0];
y = [0.25,0.25,0.45,0.45];
line(x,y,'Parent',ax2,'Color','k')
hold on
line(f_15,(log10(c./(POR_15_pos(:,1)*l_15))),'Parent',ax2,'Color','k','L
inewidth',1.2)
hold on
 xlim([0 55])
line(f_30,log10(c./(POR_30_pos(:,1)*l_30)),'Parent',ax2,'Color','g','Lin
ewidth',1.2)
hold on
line(f_45,log10(c./(POR_45_pos(:,1)*l_45)),'Parent',ax2,'Linewidth',1.2)
hold off
% xlabel('ka')
ylabel('log_{10}(\lambda/chord)')
set(ax2,'YColor','b')
print -depsc2 -tiff pos_rigid.eps
```

```
print -r300 -djpeg90 positive.jpg


figure('name','Negative')
ax1 = gca;
plot(f_45,20*log10(POR_45_neg(:,2)/P_ref))
hold on
plot(f_30,20*log10(POR_30_neg(:,2)/P_ref),'g')
hold on
plot(f_15,20*log10(POR_15_neg(:,2)/P_ref),'k')
hold on
plot(f_ring,20*log10(POR_ring_neg(:,2)/P_ref),'r')
legend('45','30','15','Ring','Location','east')
xlabel('ka')
ylabel('pressure (db)')
 xlim([0 55])
hold on
ax2 = axes('Position',get(ax1,'Position'),...
    'YAxisLocation','right',...
    'Color','none');
line(f_15,log10(c./(POR_15_neg(:,1)*l_15)),'Parent',ax2,'Color','k','Lin
ewidth',1.2)
hold on
 xlim([0 55])
line(f_30,log10(c./(POR_30_neg(:,1)*l_30)),'Parent',ax2,'Color','g','Lin
ewidth',1.2)
hold on
line(f_45,log10(c./(POR_45_neg(:,1)*l_45)),'Parent',ax2,'Linewidth',1.2)
hold off
ylabel('log_{10}(\lambda/chord)')
Y = 0.23*ones(size(f_15));
line(f_15,Y,'Parent',ax2,'Color','k','Linewidth',1.5)
hold on
x = [0,55,55,0];
y = [0,0,0.4,0.4];
line(x,y,'Parent',ax2,'Color','k')
set(ax2,'YColor','b')
print -depsc2 -tiff neg_rigid.eps
print -r300 -djpeg90 negative.jpg
```

6.12 MATLAB code for calculating the Target Strength for 3-D rigid body scattering,

plotting the target strength and the λ/d_{avg} curves.

```
load POR_Geo2_Pos.dat
load POR_Geo2_Neg.dat

load POR_Shell_Pos.dat
load POR_Shell_Neg.dat
```

```matlab
load POR_Geo3_Pos.dat
load POR_Geo3_Neg.dat

load POR_Geo4_Pos.dat
load POR_Geo4_Neg.dat

figure('name','Positive')
plot(POR_Geo2_Pos(:,1),POR_Geo2_Pos(:,2))
xlabel('frequency')
ylabel('pressure')
hold on
plot(POR_Geo3_Pos(:,1),POR_Geo3_Pos(:,2),'g')
hold on
plot(POR_Geo4_Pos(:,1),POR_Geo4_Pos(:,2),'k')
hold on
plot(POR_Shell_Pos(:,1),POR_Shell_Pos(:,2),'r')
legend('Geo_2','Geo_3','Geo_4','Shell','Location','northwest')
hold off
print -r300 -djpeg90 positive_geo.jpg

figure('name','Negative')
plot(POR_Geo2_Neg(:,1),POR_Geo2_Neg(:,2))
xlabel('frequency')
ylabel('pressure')
hold on
plot(POR_Geo3_Neg(:,1),POR_Geo3_Neg(:,2),'g')
hold on
plot(POR_Geo4_Neg(:,1),POR_Geo4_Neg(:,2),'k')
hold on
plot(POR_Shell_Neg(:,1),POR_Shell_Neg(:,2),'r')
legend('Geo_2','Geo_3','Geo_4','Shell','Location','northwest')
hold off
print -r300 -djpeg90 negative_geo.jpg
```